**Josef Dobiecki-Davies**

# ESTABLISHING A STRUCTURE-ACTIVITY-RELATIONSHIP FOR SMALL MOLECULE NON-SUGAR GLYCOMIMETICS

## Table of contents:

## List of abbreviations:

CS – Chondroitin sulfate

DCM – Dichloromethane

DMF – Dimethylformamide

DMSO – Dimethylsulfoxide

DS – Dermatan sulfate

EGFR – Epidermal growth factor receptor

EMA – European medicines authority

ESI – Electrospray ionisation

GAB2 -GRB2-assosiated binding protein 2

GRB2 - Growth factor receptor-bound protein 2

HGF/SF – Hepatocyte growth factor/scatter factor

HSPG – Heparan sulfate proteoglycan

ICP-OES – Inductively coupled plasma-optical emission spectroscopy

LC – Liquid chromatography

MB – Medulloblastoma

MS – Mass spectrometry

NMR – Nuclear magnetic resonance

PI3K – Phosphoinositide 3-kinase

PTC – Phenylthiocarbamide

RTK – Receptor tyrosine kinase

SAR – Structure-activity-relationship

SHH – Sonic hedgehog

SPE – Solid phase extraction

STAT3 – Signal transducer and activator of transcription 3

TBSAB – Tributylsulfoammonium betaine

TKI – Tyrosine kinase inhibitor

TYR - Tyrosine

WNT – Wingless

ZFP -Zinc finger protein

## List of figures and schemes:

(red).

## List of tables:

## Acknowledgments:

**Statement of originality:**

I declare that, with the exception of any statements to the contrary, the contents of this report/dissertation are my own work, that the data presented herein has been obtained by experimentation and that no part of the report has been copied from previous reports/dissertations, books, manuscripts, research papers or the internet.

Signed....JOSEF DOBIECKI-DAVIES.......

Print name....JOSEF DOBIECKI-DAVIES.............

Date....31/03/2021................................

x

## 1.0 - Abstract:

DAOY Medullablastoma cells are highly invasive, mobile and can cause severe neurological and physical illness in patients affected by this cancer. Previous work by Wilkinson & Co-workers (2017) showed that some small-molecule non-sugar glycomimetic drugs were able to prevent wound healing in DAOY cells. Therefore establishing a SAR for these molecules was of interest.

A number of mono, di, tri, tetra & poly-sulfated drug molecules were synthesised from easily available starting materials and reagents and tested for potency against wound healing in DAOY cells in a scratch assay against human growth factor/scatter factor (HGF/SF) as a control. Compounds trialled in scratch assays did not show any reasonable biological activity. HGF/SF has been shown to activate downstream signalling of the oncogene product c-Met which is a biomarker for cancer(s) and can be associated with poorer outcomes for patients.

## 1.1 - Introduction:

Glycosaminoglycans (GAGs) are highly-sulfated, anionic linear polysaccharide glycans found in many mammalian tissues (Medeiros *et al.*, 2000). Functions of these ubiquitous GAGs within the body are extensive and the functions can generally be related to their differing molecular structure, as seen with different GAGs such as heparin, heparan sulfate & chondroitin sulfate. The differing pattern in the molecular structures of GAGs (such as sulfation position, number of anionic sulfate groups & linkages between monosaccharide units) give much structural complexity to these molecules in their function (Morla, 2019). Interestingly, average molecular weight of reference preparations of heparin were seen to be around 14-19 kDa with an mean of 18 kDa (Mulloy, Gray & Barrowcliffe, 2000). The variable lengths and molecular structure within different heparin fractions may play a part in binding to different proteins and biological materials within the body.

GAGs are made up of repeat saccharide units of uronic acid linked to a hexosamines such as α-D-glucosamine. The general disaccharide backbone structure of GAGs consisting of either 1->3 linkages or 1->4 linkages is shown below in figure 1.
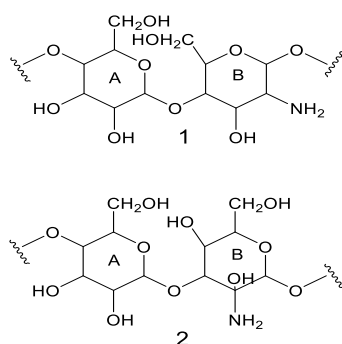


Figure 1: General disaccharide backbone structure of GAGs. Reproduced from figure 1 of (Page, 2013). (A = Hexuronic acid & B = Hexosamine)
Top: 1->4 linkage
Bottom: 1->3 linkage

Heparan sulfate proteoglycans (HSPG) are a group of GAG proteins that have received a vast amount of attention from the scientific community over the past 30 years (Sarrazin, Lamanna & Esko, 2011). Due to the increase in high-resolution analytical instrumentation such as LC-MS/MS, GC-MS/MS & ICP-OES, structure elucidation and corresponding structure & function analysis has been a well-documented topic in the wider literature. What make these HSPG molecules so interesting is that the covalently attached sidechains are that of heparan sulfate. Heparin is a GAG and so it is a highly sulfated & polyanionic side chain. Heparan sulfate has been used as an affinity matrix for the purification of proteins via "heparin affinity chromatography" due to the anionic character of heparin. Many growth factors have been isolated using heparin affinity chromatography since the 1970s (Bolten, Rinas & Scheper, 2018).  Interactions of HSPG molecules with their protein ligands are usually through the heparan sulfate side chains due to the high negative charge interacting with protein residues, but the core molecule could also play a part (Bishop, Schuksz & Esko, 2007). The figure below (2) outlines the activities and pathways in cells that HSPG molecules play a part in. This includes ligand-receptor downstream signalling, cell-cell crosstalk and molecular adhesion leading to downstream signalling and activation of other signalling cascades and pathways.
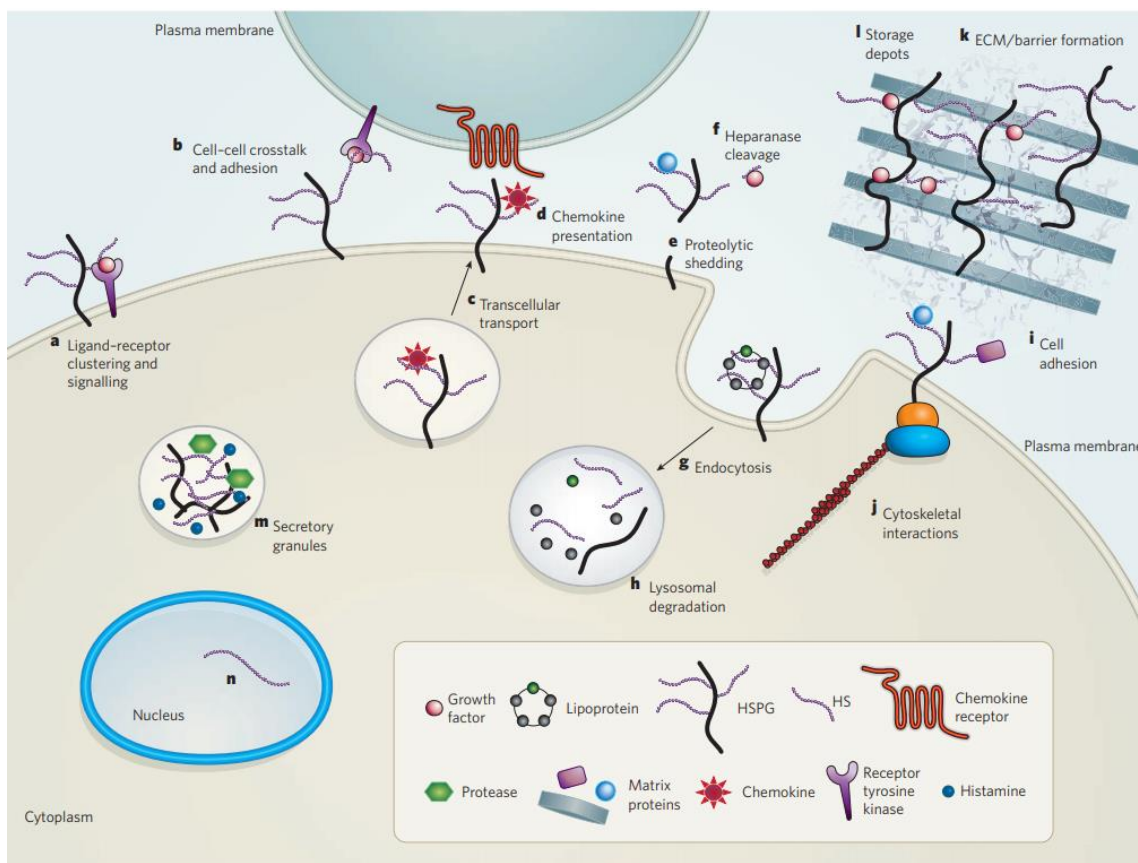


Figure 2: HSPG interactions and activities inside cells. Reproduced from Bishop, Schuksz & Esko, 2007.

As heparan sulfate and HSPG molecules can be regarded as "informationally rich" due to differing backbone structure and highly specific sulfation patterns, studies to determine the biosynthesis of heparan sulfate and associated GAGs have been conducted (Lidholt,

1997)(For review please see: Sugahara & Kitagawa, 2020).

Assembly of the core backbone of the HS molecule occurs via formation of the tetrasaccharide linkage "GlcAβ1-3Galβ1-3Galβ1-4Xylβ" on serine residues of core proteins (Aikawa, Grobe, Tsujimoto & Esko, 2000)(Sugahara & Kitagawa, 2002). The synthesis of the backbone appears to be initiated by the addition of Xyl to the serine residue and the remaining sugar units are added stepwise. Phosphorylation of the first xylose sugar unit has been implicated as a molecular switch mechanism to regulate the biosynthesis of GAGs (Wen *et al.*, 2014). Addition of sugar units are catalysed by xylosyltransferase (XylT), galactosyltransferase-I (GalT-I), galactosyltransferase-II (GalT-II), & glucuronyltransferase-I (GlcST-I)(Sugahara & Kitagawa, 2002). This region is the GAG-protein linker region.

From this point, the tetrasaccharide linker region can become differentiated to form either chondroitin sulfate (CS), dermatan sulfate (DS) or Heparin/HS GAGs based on the next sugar unit attached. Attachment of a GlcNAc sugar (*N*-acetylglucosamine) "commits" the growing chain to become a heparin/HS GAG. Attachment of the GalNAc (*N*-acetylgalactosamine) sugar rather than the GlcNAc sugar will commit the chain to become a CS/DS GAG (Kusche-Gullberg & Kjellén, 2003)(Ritelli *et al.*, 2019). An example of this can be seen in figure 3. From this point, repeating disaccharide units of either GlcA & GlcNAc (for HS biosynthesis) or GlcA & GalNAc (for CS/DS biosynthesis) are added via EXT1 and EXT2 glycostrasferases (Busse *et al.*, 2007).
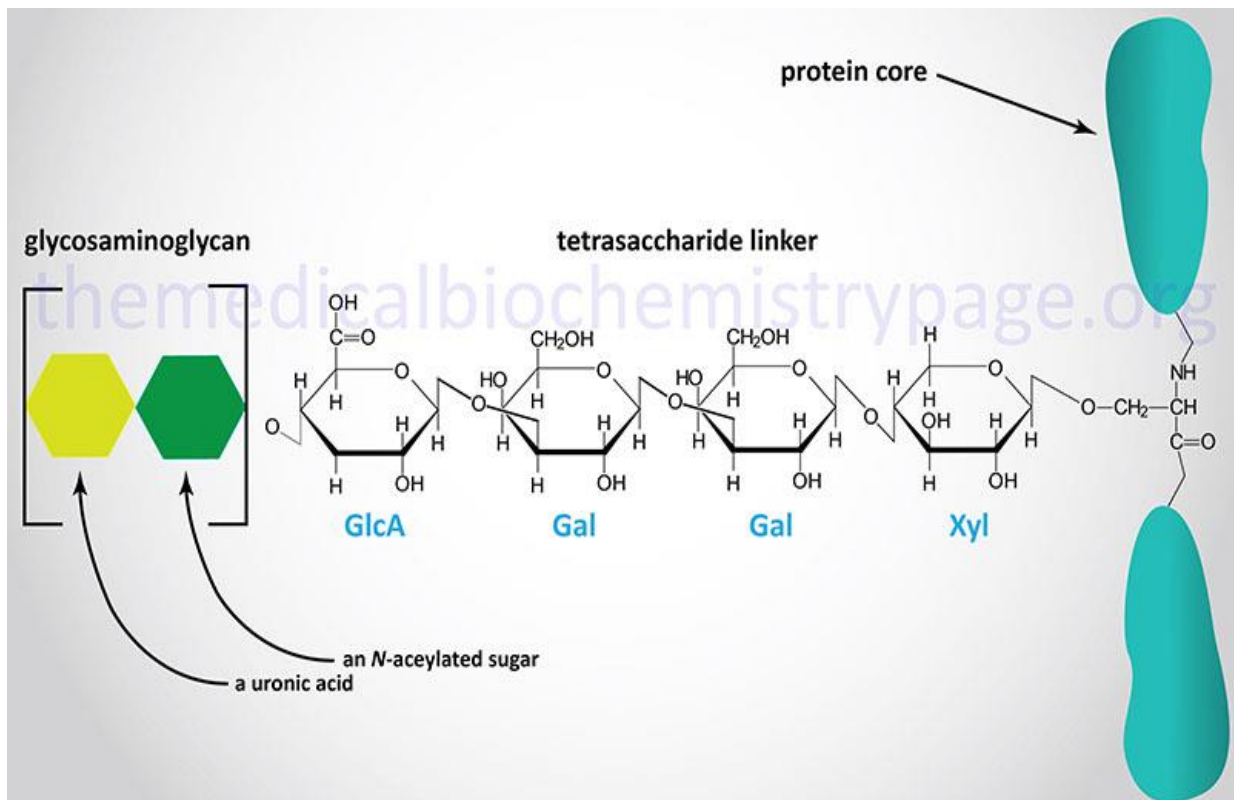


Figure 3: GAG attachment to the GlcAβ1-3Galβ1-3Galβ1-4Xylβ tetrasaccharide linker. Linkage of the tetrasaccharide to the serine residue is seen with the -O-CH$_2$- bond at the end (The Medical Biochemistry Page, 2020).

## 1.2 - HGF/c-Met:

The HGF/c-Met cascade is a biochemical signalling pathway which has been studied extensively for its effect on cancer growth and progression in biological systems. c-Met is a proto oncogene found on chromosome 7 band 7q21-31 (Dean *et al.*, 1985) which encodes a tyrosine kinase receptor (RTK) which binds hepatocyte growth factor/scatter factor (HGF/SF) as a ligand. Downstream signalling of the c-Met pathway has been shown to be involved in cancer growth and progression in different cancers (Sierra & Tsao, 2011)(Chakraborty *et al.*, 2019).

c-Met is made up of an extracellular domain, transmembrane domain and an intracellular tyrosine kinase domain which is flanked by a carboxy-tail domain and a "juxtamembrane" (Organ & Tsao, 2011). When the endogenous HGF/SF ligand binds with the c-Met RTK, the RTK dimerises and causes a *trans*-phosphorylation cascade at two tyrosine residues (TYR-1234 & TYR-1235 in the intracellular catalytical binding domain of the RTK protein. It is suspected that HSPG interactions on the extracellular surface could be involved with the downstream activation of c-Met in certain cancers, as Wielenga & co-workers (2000) found that CD44 isoforms containing HSPG side chains activated c-Met signalling in colorectal cancer cell lines. The phosphorylation cascade then causes two more tyrosine residues to autophosphorylate (TYR-1349 & TYR-1356) within the intracellular domain that forms another "Multifunctional docking site"(Faria, Smith & Rutka, 2011)(Lam, Dai & Qin, 2016)(Zhang *et al.*, 2018). This Multifunctional docking site has a variety of different kinase substrates such as growth factor receptor-bound protein 2 (Grb2), Grb-2-assosiated adaptor protein 2 (Gab2), phosphatidylinositol-3-kinase (PI3K) & signal transducer and activator of transcription 3 (STAT3) (Faria, Smith & Rutka, 2011) (Cecchi, Rabe & Bottaro, 2012) (Organ & Tsao, 2011).

## 1.3 - c-Met activation and cancer:

HGF/SF was identified as a novel growth factor in 1984 from the serum of hepatectomized rats (Nakamura, Nawa & Ichihara, 1984). Studies have shown that HGF is responsible for cell proliferation, survival, scattering, invasion and motility (invasion and motility in this context refers to metastasis) in certain cancers (Organ & Tsao, 2011) (Basilico, Arnesano, Galluzzo, Comoglio & Michieli, 2008)(Rong, Segal, Anver, Resau & Woude, 1994). Downstream signalling of c-Met leading to activation of the PI3K, STAT3, AKT & GRB2 (GRB2 activates the RAS/RAF/ERK/MAPK pathway) pathway leads to cancer metastasis as outlined above through gene expression changes, transcription activation and cell cycle progression. This downstream signalling pathway is commonly seen in other RTKs which bind endogenous growth factor ligands such as epidermal growth factor (EGF) (Olayioye, Neve, Lane & Hynes, 2000) (Purba, Saita & Maruyama, 2017) & fibroblast growth factor (FGF) (Korc & Friesel, 2009). An overview of the HGF/c-Met signalling cascade can be seen in figure 4 below. MET amplification has also been shown to confer EGFR-Tyrosine Kinase Inhibitor resistance to non-small cell lung cancer cells bearing the EGFR mutation (HCC827) through activation of ErbB3 signalling complex which activates PI3K/AKT signalling which prevents apoptosis in these cells ((Engelman *et al.*, 2007).)
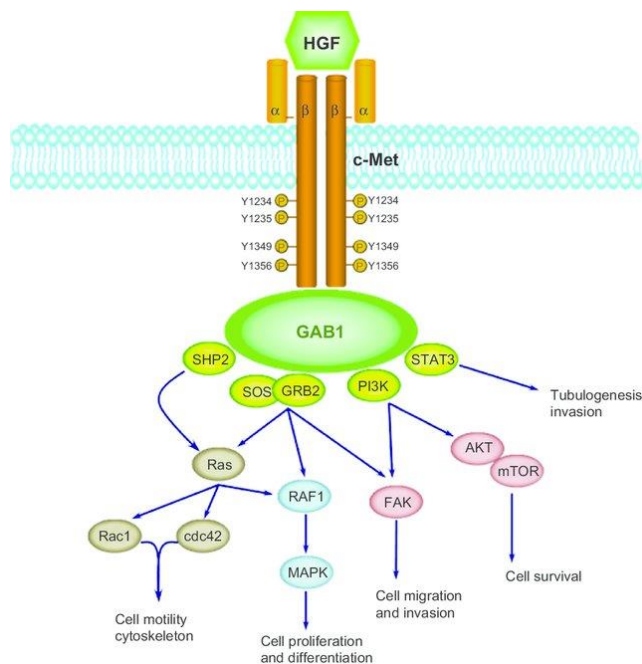


Figure 4: An overview of the HGF/c-MET downstream signalling cascade. The autophosphorylated residues can be seen (Y1234, Y1235, Y1349 & Y1356) leading to the downstream activation of Ras, RAF1, FAK, Pl3K/AKT/mTOR. Figure 4 reproduced from Lee, Sung, Ahn, An, Huh & You (2015).

c-Met is a druggable target by both monoclonal antibodies (both anti-c-met and anti-HGF) and small molecule tyrosine kinase inhibitors (both ATP-competitive and non-competitive). Capmatinib is an ATP-competitive small molecule TKI for patients with NSCLC with an exon-14 mutation in MET which has been approved for human use in May 2020 by the FDA (Food and drug administration, 2020). The ATP binding site on the c-met receptor is the target for ATP-competitive TKIs which prevents autophosphorylation at the tyrosine residues and

prevents further downstream signalling and eventually the gene expression and transcriptional changes that help to progress tumour growth. Important interactions in both the hinge region (at Pro1158, Tyr1159 & Met1160) and the activation loop is important for biological activity (Yuan *et al.*, 2018).

There are currently only three small-molecule c-Met TKI's available that have passed all licencing and regulatory approval and are available on the market for patients. These drugs are capmatinib and two multiple-target oral TKI's: cabozantinib (Exelixis Inc.) & crizotinib (Pfizer). Capmatinib (Norvartis) has been approved for use by the FDA but not by the European medical authority (EMA). These drugs are summarized in table 1 below:

Table 1: A table summarizing the current approved c-Met inhibitors on the market. Reproduced from table 1 of Puccini *et al.*, 2019.

| Compound | Indicated for use in | EMA authorization citation |
|---|---|---|
| Cabozantinib | Metastatic medullary thyroid cancer<br>Advanced renal cell carcinoma with previous VEGF inhibitor therapy<br>Hepatocellular carcinomas | (European medicines agency, 2020) (https://www.ema.europa.eu/en/medicines/human/EPAR/cometriq) (https://www.ema.europa.eu/en/medicines/human/EPAR/cabometyx) |
| Crizotinib | Metastatic ALK-fusion positive Non-small cell lung cancer (NSCLC)<br>Metastatic ROS1-positive NSCLC | (European medicines agency, 2020)( https://www.ema.europa.eu/en/medicines/human/EPAR/xalkori) |
| Capmatinib[1] | Met Exon-14-mutated NSCLC | N/A |

[1] – Not currently approved for use in Europe by the EMA.

A review in the literature of the safety, efficacy, and tolerability profiles of carozantinib and crizotinib (Puccini *et al.*, 2019) found that these compounds were generally well tolerated in adult patients with mainly mild/moderate adverse reactions. However, life-threatening adverse reactions such as hepatotoxicity and QT interval prolongation were documented. The authors stress the importance of patient monitoring during use of these compounds. Crizotinib is also primarily metabolized by the CYP3A4 enzyme. This makes it important to not administer crizotinib with other drugs that are metabolized by CPY3A4 enzyme as this could lead to increased plasma concentrations of drug for longer, potentially leading to more adverse reactions and potentially life-threatening adverse reactions.

## 1.4 – HGF/c-Met axis in Medulloblastoma:

Medulloblastoma (MB) cancers are solid tumours found in the brain. They are the second most common brain tumour in children (Cancer Research UK, 2019). Medulloblastoma tumours are highly aggressive, malignant neoplasms that form in the posterior fossa area of the brain (Lanier & Abrams, 2016). Although the five-year survival rate appears to be between 60-70% depending on progression (Children with cancer UK, 2021), current oncological strategies for treatment in children can have devastating impacts on the physical & mental wellbeing of the patient. Although more targeted approaches to surgical resection, radiotherapy and chemotherapy exist, serious short-term and long-term side effects are still abundant post-treatment, especially for children (Fossati, Ricardi & Orecchia, 2008). Current regimes for postoperative care in children with standard risk medulloblastoma consists of craniospinal radiotherapy including a tumour bed boost followed by radiotherapy directly to the posterior fossa (Khatua, Song, Sridhar & Mack, 2018). Reduced craniospinal radiotherapy with low tumour bed boost volume combined with cytotoxic chemotherapy appeared to provide stable intelligence trajectories without worsening survival rates for patients (Moxon-Emre *et al.*, 2014). Ensuring IQ trajectories remain stable throughout treatment is important in paediatric treatments as the brain is still developing & radiotherapy combined with chemotherapy as a standard adjuvant treatment could disrupt neurodevelopment in children. Although children can "bounce back" from chemotherapy faster than some adults, the long-term effect on neurocognitive development could have a less favourable outcome than in adults.

Postoperative adjuvant chemotherapy is generally a combination of cytotoxic agents with differing mechanisms of action. In the case of standard risk medulloblastoma, the drugs of choice appear to be vincristine, cisplatin & cyclophosphamide, however cyclophosphamide can be switched for lomustine (Packer *et al.*, 2006)(Mueller & Chang, 2009)(Khatua, Song, Sridhar & Mack, 2018).

Currently, MB tumours are split in to four categories: Wingless (WNT), Sonic Hedgehog (SHH), group 3 & group 4 (Taylor *et al.*, 2012). An overview of the four major molecular subgroups can be seen below in figure 5. These four subcategories of MB tumours have distinct genetic alterations between them which leads to a differing prognosis for the patient based on the MB tumour group (Taylor *et al.*, 2012). WNT & SHH MB subgroups were named based on the signalling pathways that have been implicated in tumorigenesis. A study in 1997 identified the PTC gene to be involved in tumourigenesis via the sonic hedgehog signalling pathway (Goodrich, Milenkovic, Higgins & Scott, 1997). Dysregulation of the sonic hedgehog pathway appears to lead to unregulated tumour suppression and neural cell development & is apparent in SHH MB tumours (Goodrich, Milenkovic, Higgins & Scott, 1997).

| Subgroup | | WNT | SHH | Group 3 | Group 4 |
|---|---|---|---|---|---|
| **Clinical Characteristics** | % of Cases | 10 | 30 | 25 | 35 |
| | Age at Diagnosis | Child, Adult | Infant, Child, Adult | Infant, Child | Child |
| | Gender Ratio (M:F) | 1:1 | 1:1 | 2:1 | 3:1 |
| | Anatomic Location |  |  |  |  |
| | Histology | Classic, Rarely LCA | Desmoplastic, Classic, LCA | Classic, LCA | Classic, LCA |
| | Metastasis at Diagnosis (%) | 5-10 | 15-20 | 40-45 | 35-40 |
| | Recurrence Pattern | Rare; Local or metastatic | Local | Metastatic | Metastatic |
| | Prognosis | Very good | Infants good, others intermediate | Poor | Intermediate |
| **Molecular Characteristics** | Proposed Cell of Origin | Progenitor cells in the lower rhombic lip | Granule precursors of the external granule layer | Neural stem cells | Unipolar brush cells |
| | Recurrent Gene Amplifications | - | MYCN GLI1 or GLI2 | MYC MYCN OTX2 | SNCAIP MYCN OTX2 CDK6 |
| | Recurrent SNVs | CTNNB1 DDX3X SMARCA4 TP53 | PTCH1 TERT SUFU SMO TP53 | SMARCA4 KBTBD4 CTDNEP1 KMT2D | KDM6A ZMYM3 KTM2C KBTBD4 |
| | Cytogenetic Events ■ Gain ■ Loss | 6 | 3q, 9p 9q, 10q, 17p | 1q, 7, 18 8, 10q, 11, 16q i17q | 7, 18q 8, 11p, X i17q |
| | Other Recurrent Genetic Events | - | - | GFI1 and GFI1B enhancer hijacking | PRDM6, GFI1, and GFI1B enhancer hijacking |

Age: Infant  Child  Adult

Figure 5: The four major molecular subgroups for MB. Reproduced from Figure 2 of Juraschka & Taylor, 2019 (data can be found in references 36,37,61 of Juraschka & Taylor, 2019).

The HGF/c-met proto-oncogene product has been implicated in tumorigenesis of MB tumours and remains a novel strategy for treatment as the HGF/c-met pathway is a druggable target for preventing tumour pathogenesis. The first research showing an involvement of HGF/SF in MB tumour progression was in 2005. The authors showed that high expression levels of HGF/SF in human MB cell lines has been associated with poor clinical outcomes when compared with MB cell lines with low expression levels of HGF/SF (Li *et al.*, 2005). The same authors also found that HGF/SF in MB cell lines is responsible for cell proliferation, cell cycle progression and interestingly, protects MB cells from chemotherapeutic drug-induced cell death via the PI3K pathway. However, pre-treatment of

cells with a PI3K inhibitor (without MAPK inhibitors) preventing the cytoprotective properties of PI3K activation by HGF/SF.

Further research on the topic of activation of the HGF/c-Met pathway in MB cells has shown that high levels of circulating tissue factors in DAOY MB cells are directly related to activation of the HGF/c-Met pathway. In the same work, the authors showed that tissue factor expression in DAOY MB cells stimulated with HGF enhanced cell migration and locomotion (Provençal *et al.*, 2009). In 2010, work done by Kongkham *et al.* showed that small-molecule MET inhibitors are effective at preventing closure of artificial wounds in MB cell lines (Kongkham, Onvani, Smith & Rutka, 2010), furthering evidence that the HGF/c-Met pathway may be responsible for cell migration and invasion of MB cells.

## 2.0 – Synthesis of glycomimetics:

The term "glycomimetic" refers to small drug-like molecules that mimic the biological activity of endogenous carbohydrates. Glycomimetics can be highly sulfonated molecules designed to mimic the activity of their endogenous ligand, such as heparin sulfate. Although not all glycomimetic drug compounds require the sulfate moiety for activity, compounds have been developed to exploit the highly polar properties of sulfates.

One drug that has successfully reached the market as a small-molecule glycomimetic is the influenza drug oseltamivir (Tamiflu), an orally active competitive inhibitor of the neurominidase enzyme responsible for the cleavage of Sialic acid glycoproteins on cell surfaces to release mature influenza virions in to the host during influenza infection. The structures of Sialic acid and Tamiflu are below in figure 6:



Sialic Acid
3

Oseltamivir (Tamiflu)
4
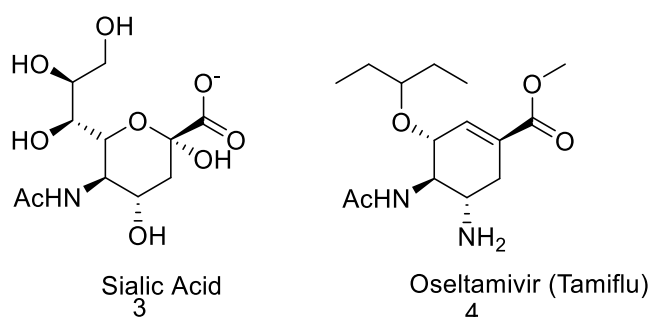
Figure 6: The structures of sialic acid and oseltamivir (Tamiflu). In Tamiflu, the ester is cleaved *in vivo* to form the carboxylate ion and the active drug.

As a competitive inhibitor of neurominidase, the active drug form of Tamiflu must bind to the neurominidase enzyme with a higher affinity than the endogenous ligand (sialic acid). Due to this, rational drug design used the carbohydrate backbone of sialic acid to design a ligand and keep the important ligand-protein interactions needed for binding. This structure-based design of Tamiflu resulted in a successful drug candidate which entered the market.

Rational design of glycomimetics involves some of the usual transformations and bioisosteric atom replacement that is generally involved in the design of small-molecule drug compounds (Hevey, 2019). Bioisosteres can be defined as atoms or functional groups that have similar biological and electronic properties as the atom or functional group(s) being replaced. In medicinal chemistry (bio)isosteric replacement can improve drug-like

compounds pharmacodynamic and pharmacokinetic properties such as drug-ligand binding affinity, water solubility, drug absorption, elimination, distribution, metabolism & off-target side effects. In the case of Tamiflu, the isopentyl group improved drug potency and water solubility, meaning that Tamiflu could be used as the phosphate salt in an oral delivery system in the form of tablets. Although Tamiflu successfully entered the market and showed very good efficacy, the synthesis of glycomimetics such as Tamiflu (although a simple molecule) are fraught with synthetic issues such as stereochemical and regiochemical control during synthesis. Although the Tamiflu synthesis starts with chiral starting materials, the retention of stereochemistry must be kept during the total synthesis. Keeping chirality intact during a multistep synthesis can be a challenge, especially with reactions such as an $SN_2$ which can invert stereochemistry at a chiral centre. As ligand binding in a biological system is in a chiral environment, stereochemistry is extremely important when designing drug compounds.

As the glycomimetics produced in our laboratory for this paper are small molecule heparin/heparan sulfate mimics, the -$SO_3H$ group was essential. It was decided that establishing a SAR for the sulfation pattern of the molecule was of interest as unpublished results by Wilkinson & co-workers showed that some non-sugar glycomimetics (figure 7) can prevent HGF/SF-induced MET activation in DAOY cells which are known to cause cancer cell proliferation, progression, motility, invasion, and wound healing. Results from a DAOY scratch assay showed that these molecules prevent an artificial wound (made with a pipette tip) in the cell monolayer from closing. A scratch assay can be used to quantify the rate of cell migration & wound closure time using real-time measurements such as time-lapse microscopy or live-cell imaging for the assay. An example scratch assay performed on DAOY cells to inspect migratory potential can be seen in figure 8.
Although our GAG mimetics are being trialled as agents to prevent wound healing & neovascularisation, GAG mimetics such as OTR4120 have been studied as agents to induce wound healing & neovascularisation in a mouse model (Tong *et al.*, 2009).
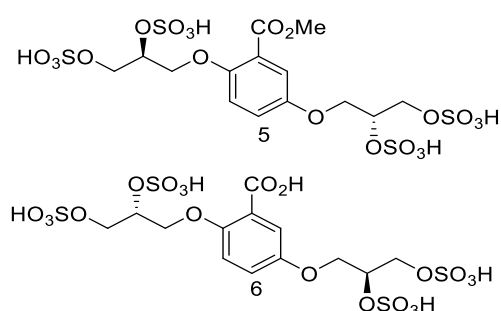


Figure 7: Two compounds synthesised and tested by Wilkinson & co-workers for potency against HGF/SF induced c-Met activation in DAOY cells using a scratch assay.
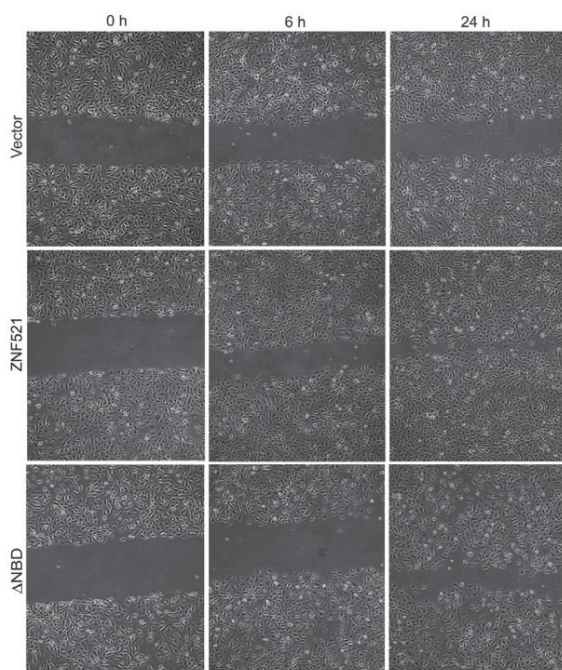
Figure 8: An example of a scratch assay performed on DAOY cells. Vector (top) is the control. Zinc finger protein (ZFP) 521 (middle) shows that ZFP521 increases migratory potential for DAOY cells. This can be seen as the scratch made in the cell monolayer begins to close as the DAOY cells migrate. Figure from figure 4 of Spina *et al.*, 2013.

DAOY cells for *in vitro* testing of the glycomimetic molecules produced are an immortal cell line collected from a 4-year-old Caucasian boy who suffered a MB tumour in his posterior fossa in 1985 (Jacobsen, Jenkyn & Papadimitriou, 1985). It is regarded as a primary cell line for MB. DAOY cells had the highest migratory potential (vs UW402, UW472 & ONS-76 MB cell lines) *in vitro* & DAOY cells also shows tumorigenic potential when cells were implanted in nude mice (Bonfim-Silva *et al.*, 2019). DAOY cells are subcategorized as SHH-type MB with a TP53 mutation (Ivanov, Coyle, Walker & Grabowska, 2016). SHH-type MB with a TP53 mutation is regarded as clinically high risk and carries a generally unfavourable diagnosis for the patient. Due to this, Kidscan laboratories decided to use these cells for trialling compounds on, as current treatments for SHH-TP53 MB are very few and mostly cytotoxic.

Addition of sulfur trioxide to the hydroxyl and amine groups will proceed via an $S_N2$ nucleophilic addition reaction between sulfur trioxide and the heteroatom. Attack of the nucleophile onto the sulfur trioxide yields the adduct and oxonium intermediate & proton abstraction by the negatively charged oxygen through intermolecular proton transfer will form the neutral sulfate ester and return the oxonium ion to a neutral state. *N*-sulfation would appear to undergo the same mechanism, however N-sulfation requires base for the reaction to proceed. Does this mean that the reaction uses basic conditions to form the deprotonated amine & are basic conditions vital to reaction completion? The secondary amine would appear on paper to be as reactive (if not a little more) to $SO_3$ as the hydroxyl group, as these two groups have pKa values of around 12 & 16, respectively.
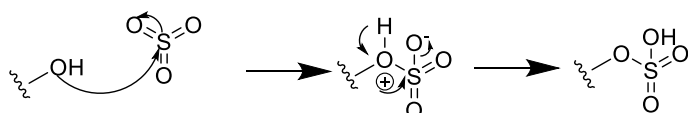
Figure 9: *O*-Sulfation reaction mechanism

Due to the electronics of the sulfate group being highly electron withdrawing, purification and isolation of products can be difficult (mainly due to the increase in aqueous solubility of the product), although not impossible. *O*-Sulfation techniques have been widely reported and are generally carried out with an $SO_3$ complex such as $SO_3.NMe_3$ in a polar aprotic solvent such as DMF or acetonitrile. Some Non-commercially available $SO_3$ complexes can simply be made by the reaction of the lewis base with $SO_3HCl$ or gaseous $SO_3$ under inert conditions at sub-zero temperatures (Gill, Male & Jones, 2019). Raiber & Co-workers (2007) used commercially available $SO_3$ complexes ($SO_3.NMe_3$) with substrates in dimethylformamide (DMF) to construct glycomimetic molecules bearing *O*-sulfation for use in testing for preventing HGF/SF-induced MET activation in wildtype Chinese hamster ovary cells. Their method is simple, and purification was via normal-phase flash column chromatography to yield the pure product. Many other papers have used different commercially available $SO_3$ complexes ($SO_3.NMe_3$/$SO_3.NEt_3$/$SO_3.Py$) to achieve chemical *O*-sulfation of hydroxyl groups on organic molecules (Lubineau & Lemoine, 1994)(Correia, Lin, Aria, Jain & Globisch, 2020)(Waller & McLeod, 2014)(Mahmoud *et al.*, 2017)(Afosah, Al-Horani, Sankaranarayanan & Desai, 2016)(Tully, Mabon, Gama, Tsai, Liu & Hsieh-Wilson, 2004). Reactions involving $SO_3$ complexes generally require the use of super-stoichiometric amounts of reagent to achieve reaction completion (2-5eq/reactive site). These reactions require purification to remove any unreacted reagent.

However, *N*-sulfation is less reported and very few articles are available in the wider literature regarding chemical methods for *N*-sulfation. Even fewer articles are available regarding chemical methods for simultaneous sulfonation of both hydroxyl and amine groups in one pot (Xu, Laval, Guo & Yu, 2016). The ability to perform a single-step sulfation and have both available sulfation sites (-OH & -NHR) successfully converted to the sulfates was highly desirable and advantageous to the author as a structure-activity-relationship (SAR) for compounds containing both *O* & *N*-sulfates could be constructed very quickly. As nitrogen-containing scaffolds are popular for drug discovery in medicinal chemistry due to the highly-polar surface area & electronics of the nitrogen atoms being able to form interactions with the drug target(s), nitrogen-containing sulfates were of great interest. Commercial heparin fractions and low weight heparin sulfate both contain *N*-sulfates in the core sugar ring, so working on the biological activity of *N*-sulfates and their synthesis and biological activity was highly desirable.

Therefore it was decided to create a model compound with both *O* & *N*-sulfonation sites on which it was possible to perform method development to design a synthesis that could provide the desired product(s) in a single-step without the need for column chromatography or other purification techniques that can be incompatible with highly sulfonated, polar molecules. As it was expected that molecules would have multiple *O* & *N*-sulfate groups,

column chromatography would get increasingly difficult as the number of sulfate groups increase due to the extremely polar nature of the molecules.

Classical reactions for the sulfation or introduction of a sulfate into a molecule include the use of sulfuric acid for sulfating benzene rings. Reaction conditions are harsh (gaseous $SO_3$ bubbled into conc. Sulfuric acid generates the activated $SO_3$ (known as "fuming sulfuric acid") used in the reaction. Reaction conditions like these should be avoided if possible & more bench stable and less toxic reagents should be used where possible. As detailed above, commercially available $SO_3$ complexes are available to buy and are bench-stable solids that are less toxic than gaseous $SO_3$ and easier to handle & work with.

### 3.0 – Results & Discussion:

Originally, it was decided to use phenyl glycidyl ether as the starting material to investigate epoxide openings and the conditions required (scheme 1). Table 2 (in results) shows reactions of phenyl glycidyl ether with different nucleophiles.
 Once a methodology for the opening of epoxides with nucleophiles was established, the same methods were used for the opening of the 1,3-epoxide resorcinol diglycidyl ether (scheme 2) as it was expected that the *mono* compounds would not be active (previous work done by Wilkinson & co-workers (unreported) showed that the 1,3-phenoxy compounds were much more active).
These commercially available epoxides were readily available and cheap enough to be used for our method development. The precursor price and amount of synthetic steps needed to produce the potentially biologically active *bis*-compounds bearing aromatic functionality such as a carboxylic acid group (such as the compounds in figure 7) are both high, it was decided to only make the compounds bearing these aromatic functional groups once a sufficient method for both *O*- & *N*-sulfation had been established.
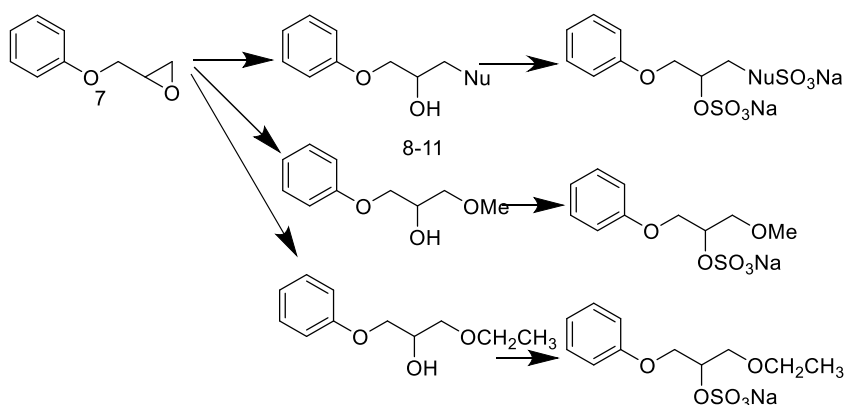


Scheme 1: General scheme for the synthesis of sulfated compounds starting from Phenyl glycidyl ether. Nu (in final product) = NH, iPrNH. Final products bearing -OMe & -OCH$_2$CH$_3$ groups have been drawn separately on the same scheme for the purposes of disambiguation.
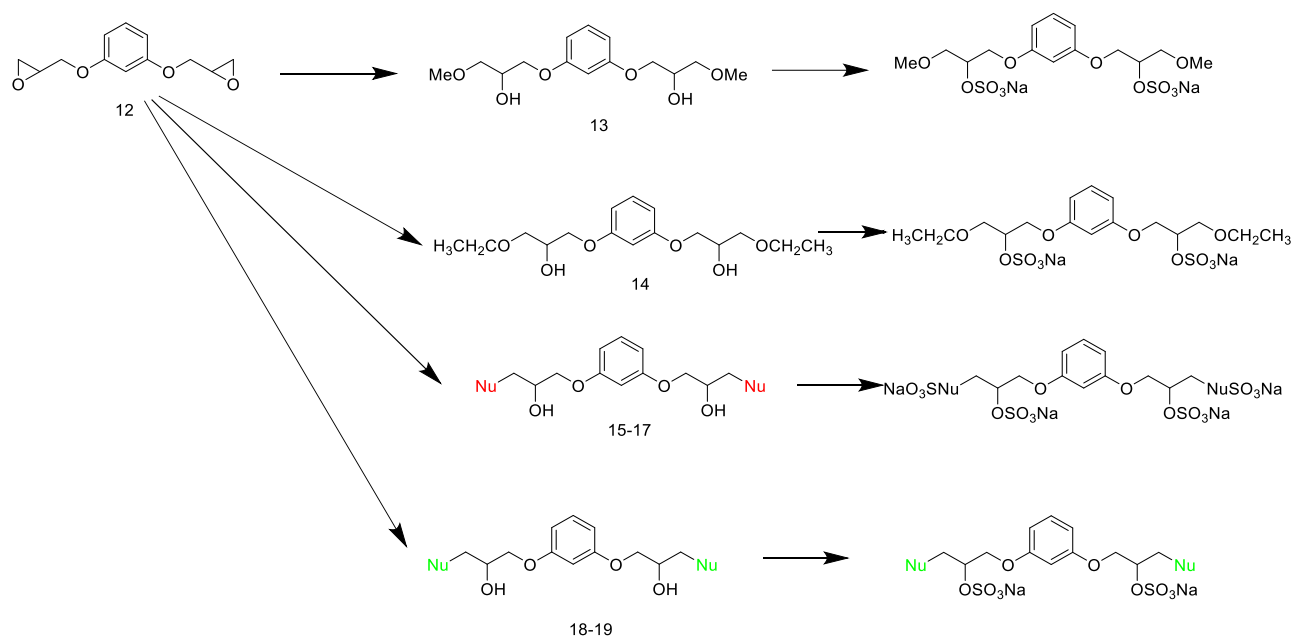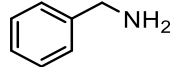
Scheme 2: General scheme for the synthesis of sulfated compounds starting from resorcinol diglycidyl ether. Nu (red) (in final product) = NH, iPrNH. Nu (green) (in final product) = iPr$_2$N, N(CH$_2$CH$_3$)$_2$. Final products bearing -OMe & -OCH$_2$CH$_3$ groups have been drawn separately on the same scheme for the purposes of disambiguation.
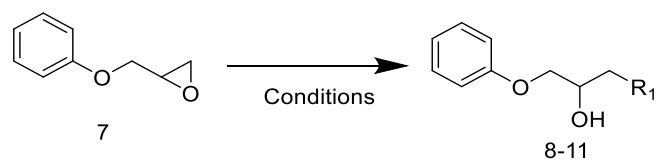


Scheme 3: The Nucleophilic opening of phenyl glycidyl ether

Table 2: Nucleophilic openings of phenyl glycidyl ether.

| R$_1$ | Conditions | Yield (%) | Compound |
|---|---|---|---|
| NH$_2$ | NH$_4$OH | 40 | **8** |
| CH$_3$ | Dry THF, MeLi (In Et$_2$O) | 0 | **9** |
| iPrNH | iPrNH$_2$, Propan-2-ol | 99 | **10** |

| | | | |
|---|---|---|---|
| NH$_2$ | C$_7$H$_9$N, Propan-2-ol | 0 | **11** |
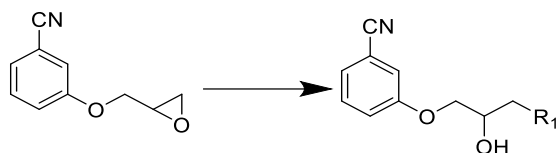
Scheme 4: Nucleophilic opening of 3-Cyano-phenyl glycidyl ether

Table 3: Nucleophilic opening of 3-Cyano-phenyl glycidyl ether

| R$_1$ | Conditions | Yield (%) | Compound |
|---|---|---|---|
| iPrNH | iPrNH, Propan-2-ol | 0 | **12** |

$^a$ – Starting material was produced by the author. Procedure on page 22.

Scheme 5: Nucleophilic openings of resorcinol diglycidyl ether

Table 4: Nucleophilic openings of resorcinol diglycidyl ether
$^a$ – Reaction done in microwave

| R | Conditions | Yield (%) | Compound |
|---|---|---|---|
| OCH$_3$ | NaOCH$_3$, MeOH | 70 | **13** |
| OCH$_2$CH$_3$ | NaOCH$_2$CH$_3$, EtOH | 82 | **14** |
| NH$_2$ | NH$_4$OH | 0 | |
| NH$_2$ | NH$_4$OH$^a$ | 98 | **15** |
| CH$_3$ | Dry THF, MeLi (In Et$_2$O) | 0 | **16** |
| (CH$_3$)$_2$CHNH | (CH$_3$)$_2$CHNH$_2$, Propan-2-ol | 97 | **17** |
| Diisopropylamine | Diisopropylamine, Propan-2-ol | 92 | **18** |
| Diethylamine | Diethylamine, Propan-2-ol | 88 | **19** |

### 3.1 – Material and methods - general:

All reagents were commercially available and used without further purification unless specifically noted. $^1$H-NMR and $^{13}$C-NMR spectra were recorded on a Bruker 400MHz ultrashield and all chemical shift data is given in δ (ppm) relative to TMS as in internal standard. (s = singlet, d = doublet, t = triplet, q = quartet, dd = doublet doublet, & m=multiplet). FT-IR spectra were recorded on a Bruker ALPHA II Diamond-ATR FT-IR spectrometer (Source: MIR, Beamsplitter: KBr, Resolution 4.0+ cm$^{-1}$, Background scans: 16, Sample scans: 16, Data recorded: 4000cm$^{-1}$-400cm$^{-1}$, Peak picking at 5%.).
LC-MS analysis was recorded on an Agilent 1260 Infinity II LC system with an Agilent 6120 quadrupole MS unit using either +ESI or -ESI mode. The column used was a Phenomenex Synergi 4u Hydro-RP 80A (150 x 4 60mm 4 micron) with water and acetonitrile as the mobile phase with 0.1% formic acid (unless specified). Melting point was recorded using a Stuart Scientific model SMP20 (Maximum temperature 300°C) and all values are uncorrected. NMR Spectra were processed using Bruker Topspin 4.1.0 & converted to .JPG image files (300dpi). LC-MS data was processed with Openchrom software & scan tables were converted to .JPG image files. Chemical literature searching was done with both Reaxys and ScienceDirect.

### 3.1.1 - 1-Amino-3-phenoxypropan-2-ol (8):
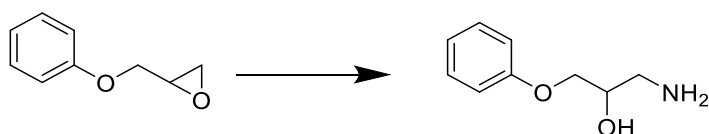


Scheme 8: Synthesis of *1-Amino-3-phenoxypropan-2-ol*

Phenyl glycidyl ether (0.150g, 1.0 mmol) was added to concentrated NH$_4$OH (37%)(5mL) & stirred overnight at room temperature. The solution was extracted with CHCl$_3$ (3x25mL), dried with MgSO$_4$, filtered, and the solvent was removed *in vacuo* to yield the crude product as white crystals. Purification was carried out on a flash column with normal phase silica using CHCl$_3$:MeOH:NH$_4$OH 10:1:0.1 as the solvent system. Fractions containing product were concentrated *in vacuo* to yield *1-amino-3-phenoxyisopropanol* as a white solid. Yield: (0.070g, 40%). $^1$H-NMR (CDCl$_3$): 7.21-7.15 (m, 2H), 6.89-6.78 (m, 3H), 4.09-4.01 (m, 1H), 3.90-3.82 (m, 2H), 2.84-2.68 (m, 2H). FT-IR: 3362.78, 2919.17, 2849.78, 2722.57, 1596.49, 1584.52, 1495.81, 1449.38, 1365.78, 1291.52, 1238.48, 1192.24, 1172.20, 1159.19, 1122.19, 1077.49, 1056.36, 1027.54, 1005.47, 990.48, 917.46, 882.51, 859.87, 827.05, 806.92, 751.11, 688.80, 616.64, 537.72, 509.10, 462.68. M.P.: 98-100°C (Consistent with Stankevichene, Vizas, Kost, Stankevichyus & Smailene, 1977).

### 3.1.2 - 1-Isopropylamino-3-phenoxypropan-2-ol (10):
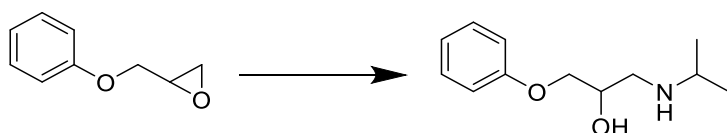


Scheme 9: Synthesis of *1-Isopropylamino-3-phenoxypropan-2-ol*

Phenyl glycidyl ether (0.150g, 1.0 mmol) was added to propan-2-ol (25mL) containing isopropylamine (10eq)(10.0 mmol) & the solution was heated under refluxfor 18 hours. The solvent was removed *in vacuo* to yield the crude product as a colourless oil which spontaneously crystallised overnight. The powder was then stirred in pentane and dried *in vacuo* to yield *1-isopropylamino-3-phenoxypropan-2-ol* as a white solid. Yield: (0.207g, 99%).

$^{1}$H-NMR (CDCl$_3$): 7.27 (t, J=7.95), 6.94 (dd, J=17.81Hz, 8.49Hz), 4.10 (m, 1H), 3.95 (m, 2H), 2.85 (m, 2H), 2.69 (dd, 1H, J=8.50Hz, 3.30Hz), 1.10 (d, 6H, J=6.44Hz). FT-IR: 3315.74, 2968.71, 2925.61, 2836.82, 1597.71, 1490.94, 1446.79, 1380.41, 1332.79, 1295.64, 1240.40, 1172.79, 1147.11, 1109.13, 1084.55, 1033.39, 1019.00, 977.02, 926.38, 892.85, 847.86, 813.44, 759.97, 697.09, 621.54, 549.71, 531.14, 514.33, 490.55, 369.83. M.P.: 95°C.

Data was consistent with literature (Apparu, Tiba, Léo, Hamman & Coulombeau, 2000).

### 3.1.3 – 3-Cyanophenyl glycidyl ether (7a):
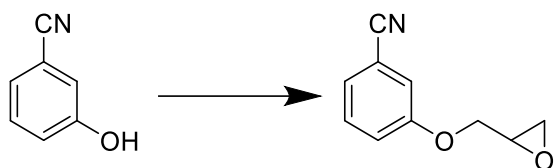


Scheme 10: Synthesis of *3-Cyanophenyl glycidyl ether*

3-Cyanophenol (0.119g, 1.0mmol) was added to anhydrous acetonitrile (25mL) containing potassium carbonate (3.0 mmol). Once the starting material had dissolved, epichlorohydrin (2.0 mmol) was added dropwise. The solution was stirred overnight at 75°C, Once the starting material was used up (monitored via TLC), the solvent was removed *in vacuo*, quenched with water (10mL) & extracted with EtOAc (3x30mL). The organic layer was dried with MgSO4, filtered & the solvent removed *in vacuo*. The resulting oil was purified by flash column chromatography (Hexane:Ethyl acetate 7:3) to *yield 3-Cyanophenyl glycidyl ether* as a white crystalline solid. Yield: (0.130g, 74%). ^{1}H-NMR (CDCl$_3$): 7.43-7.36 (m, 1H), 7.31-7.25 (m, 1H), 7.21-7.15 (m, 2H), 4.31 (dd, 1H, J= 8.37Hz, 2.71Hz), 3.94 (dd, 1H, J=5.06Hz, 5.95Hz), 3.40-3.35 (m, 1H), 2.95 (t, 1H, J=4.47Hz), 2.78 (dd, 1H, J=4.98Hz, 2.68Hz). M.P.: 88°C (No comparison data available).

### 3.1.4 - 1,3-Bis-(3-methoxy-2-hydroxypropyloxy)benzol (13):
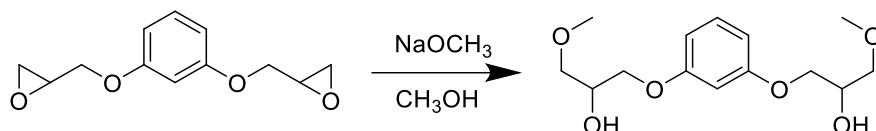


Scheme 12: Synthesis of *1,3-Bis-(3-methoxy-2-hydroxypropyloxy)benzol*

Resorcinol diglycidyl ether (0.222g, 1.0mmol) was added to absolute methanol (15mL) containing sodium methoxide (2.0 mmol) & the solution was heated under reflux for 18 hours. The solvent was evaporated *in vacuo* and the resulting oil diluted in water (10mL) and extracted with EtOAC (3x25mL). The organic layer was dried with $MgSO_4$ & the solvent evaporated *in vacuo* to yield *1,3-Bis-(3-methoxy-2-hydroxypropyloxy)benzol* as a yellow oil. Yield: (0.201g, 70%). $^1$H-NMR (CDCl$_3$): 7.11 (m, 1H), 6.49 (m, 3H), 4.15-4.04 (m, 2H), 3.99-3.89 (m, 4H), 3.57-3.45 (m, 4H), 3.36 (s, 6H), 3.27 (b, 2 O**H**). FT-IR: 3397.22, 2926.28, 1591.16, 1491.69, 1451.57, 1286.99, 1181.80, 1154.75, 1083.91, 1040.34, 965.85, 860.065, 760.89, 685.56, 604.52. LRMS: (+ESI): Expected: [M+H]: 287.32. Found: [M]: 286.20.

### 3.1.5 - 1,3-Bis-(3-ethoxy-2-hydroxypropyloxy)benzol (14):
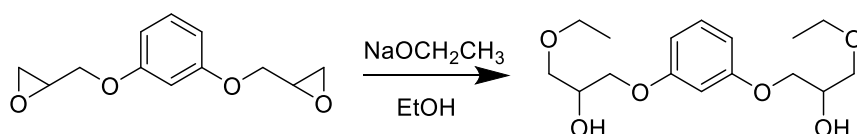


Scheme 13: Synthesis of *1,3-Bis-(3-ethoxy-2-hydroxypropyloxy)benzol*

Resorcinol diglycidyl ether (0.222g, 1.0 mmol) was added to absolute ethanol (15mL) containing sodium ethoxide (2.0 mmol) & the solution was heated under reflux for 18 hours. The solvent was evaporated *in vacuo* and the resulting oil diluted in water (10mL) and extracted with EtOAC (3x25mL). The organic layer was dried with $MgSO_4$ & the solvent evaporated *in vacuo* to yield *1,3-Bis-(3-ethoxy-2-hydroxypropyloxy)benzol* as an orange oil. Yield: (0.256g, 82%). $^1$H-NMR (CDCl$_3$): 7.07 (m, 1H), 6.48-6.39 (m, 3H), 4.11-4.01 (m, 2H),

3.95-3.86 (m, 2H), 3.55-3.43 (m, 8H) 2.81 (b, 2xO**H**), 1.13 (t, 6H, J=7.01Hz) ^{13}C-NMR: 159.83, 129.94, 107.20, 101.69, 71.32, 69.09, 69.04, 66.95, 15.10. FT-IR: 3398.41, 2974.09, 2871.72, 1591.84, 1491.51, 1452.36, 1379.77, 1287.09, 1263.49, 1182.12, 1099.58, 1041.65, 854.33, 760.72, 685.64, 604.25, 455.51.

### 3.1.6 - 1,3-Bis-(3-amino-2-hydroxypropyloxy)benzol (15):



Scheme 14: Synthesis of *1,3-Bis-(3-amino-2-hydroxy-propyloxy)-benzol*

Resorcinol diglycidyl ether (0.222g, 1.0 mmol) was added to absolute ethanol (2.5mL) containing concentrated (30%) NH4OH (5mL). The solution was stirred until the starting material had dissolved & then irradiated in a microwave (140°C, Avg power 80W, 50psi) for 5 minutes. The solution was concentrated *in vacuo* to yield *1,3-Bis-(3-amino-2-hydroxypropyloxy)benzol* as a colourless oil. Yield: (0.251g, 98%). ^{1}H-NMR (CDCl$_3$): 7.19 (m, 1H), 6.58-6.50 (m, 3H), 4.02-3.92 (m, 6H), 2.98 (dd, 2H, J=13.46Hz, 9.01Hz), 2.86 (dd, 2H, J=12.76Hz, 6.31Hz), 1.60 (b, 6H). ^{13}C-NMR: 159.86, 130.02, 107.20, 101.64, 70.37, 70.09, 43.96. FT-IR: 3074.04, 1600.34, 1524.09, 1495.00, 1455.51, 1291.74, 1255.94, 1219.05, 1193.34, 1094.97, 1059.19, 1035.88, 999.64, 927.74, 865.11, 808.64, 754.99, 680.71, 619.78, 585.90, 566.83, 456.27. LRMS: (+ESI): Expected: [M+H]: 257.30. Found: [M+H]: 257.05.

### 3.1.7 - 1,3-Bis-(3-isopropylamino-2-hydroxypropyloxy)benzol (17):



Scheme 15: Synthesis of *1,3-Bis-(3-isopropylamino-2-hydroxypropyloxy)benzol*

Resorcinol diglycidyl ether (0.222g, 1.0 mmol) was added to propan-2-ol (25mL) containing isopropylamine (10eq/epoxide)(20.0 mmol) & the solution was heated under reflux for 18 hours. The solvent was removed *in vacuo* to yield *1,3-Bis-(3-isopropylamino-2-hydroxypropyloxy)benzol* as a colourless oil. No further purification was needed. Yield: (0.331g, 97%). $^1$H-NMR (CDCl$_3$): 7.11 (m, 1H), 6.48 (m, 3H), 4.12-4.03 (m, 2H), 3.95-3.82 (m, 4H), 2.86-2.74 (m, 4H), 2.70-2.58 (dd, 2H, J=12.17Hz, 2.97Hz), 1.08 (dd, 12H, J=12.11Hz, 6.44Hz). FT-IR: 3280.72, 3085.62, 2963.86, 2916.37, 2869.34, 1594.70, 1492.69, 1450.42, 1369.18, 1334.27, 1290.81, 1264.59, 1179.68, 1156.24, 1121.38, 1080.82, 1037.20, 987.45, 945.20, 903.63, 888.88, 848.28, 832.03, 757.11, 685.20, 629.63, 596.69, 540.30, 454.42.

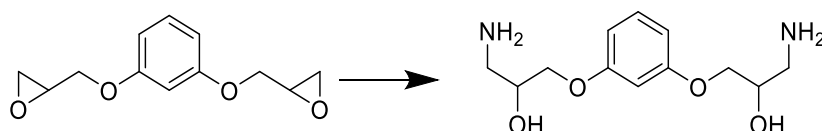### 3.1.8 - 1,3-Bis-(3-diisopropylamino-2-hydroxypropyloxy)benzol (18):



Scheme 16: Synthesis of *1,3-Bis-(3-diisopropylamino-2-hydroxypropyloxy)benzol*

Resorcinol diglycidyl ether (0.222g, 1.0 mmol) was added to propan-2-ol (25mL) containing diisopropylamine (10eq/epoxide)(20.0 mmol) & the solution was heated under reflux for 18 hours. The solvent was removed *in vacuo* to yield *1,3-Bis-(3-diisopropylamino-2-hydroxypropyloxy)benzol* as a dark brown oil. No further purification was needed. Yield: (0.386g, 91%). $^1$H-NMR (CDCl$_3$): 7.14 (m, 1H), 6.53 (m, 3H), 4.01-3.84 (m, 6H), 3.11-2.99 (m,

4H), 2.69 (dd, 2H, J=13.43Hz, 9.03Hz), 2.46 (dd, 2H, J=13.56Hz, 4.14Hz), 1.04 (dd, 24H, J=18.93Hz, 12.00Hz). $^{13}$C-NMR: 160.11, 129.76, 107.00, 101.60, 70.83, 65.41, 48.35, 47.11, 22.24. FT-IR: 3323.97, 2964.39, 1592.21, 1491.76, 1452.24, 1385.39, 1364.35, 1286.99, 1262.98, 1179.44, 1153.65, 1110.04, 1043.80, 927.09, 832.89, 759.49, 685.63, 607.26, 455.87. LRMS: +ESI: Expected [M+H]: 425.63. Found: [M+H]: 425.25.
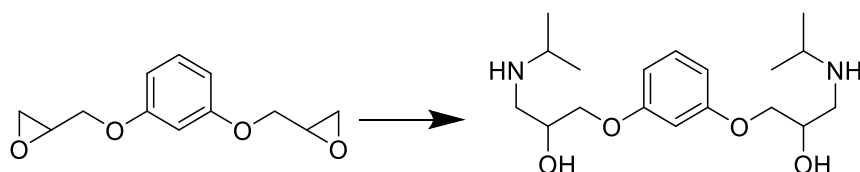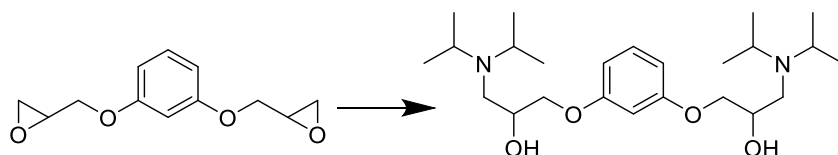
### 3.1.9 – 1,3-Bis-(3-diethylamino-2-hydroxypropyloxy)benzol (19):
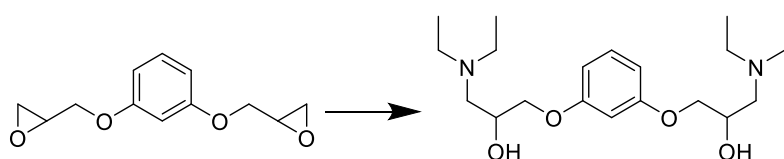


Scheme 17: Synthesis of *1,3-Bis-(3-diethylamino-2-hydroxypropyloxy)benzol*

Resorcinol diglycidyl ether (0.222g, 1.0 mmol) was added to propan-2-ol (25mL) containing diethylamine (10eq/epoxide)(20.0 mmol) & the solution was heated under reflux for 18 hours. The solvent was removed *in vacuo* to yield *1,3-Bis-(3-diethylamino-2-hydroxypropyloxy)benzol* as a pale yellow oil. Yield: (0.324g, 88%). $^{1}$H-NMR (CDCl$_3$): 7.16 (m, 1H), 6.56-6.50 (m, 3H), 4.04-3.90 (m, 6H), 2.74-2.48 (m, 12H), 1.05 (t, 12H, J=7.10Hz). FT-IR: 3398.82, 2967.95, 2932.67, 1591.29, 1491.63, 1451.16, 1384.21, 1333.15, 1286.83, 1262.80, 1182.06, 1153.36, 1040.00, 994.91, 832.97, 759.82, 685.59, 605.63, 456.85.

Once the optimal conditions for epoxide opening were in hand, sulfation was attempted on a variety of different substrates. Whilst there are many papers currently out in the literature regarding *O*-Sulfation (Lubineau & Lemoine, 1994)(Correia *et al.*, 2020)(Waller & McLeod, 2014)(Mahmoud *et al.*, 2017)(Afosah *et al.*, 2016)(Tully *et al.*, 2004), there are very few on the subject of *N*-sulfation and even less reporting simultaneous *O,N*-sulfation. Due to this, ease of synthesis and the molecule provided a suitable scaffold of the hydroxy and secondary amine for developing a method for sulfonation of both the hydroxy and amine groups.

Most epoxide opening reactions provided the desired compound in excellent yields with only minor impurities from residual solvent present. Reactions were telescoped to the next step as method development of the sulfation reaction on different scaffolds was time

critical due to the project only having a 12-month time constraint and covid-19 made lab work increasingly difficult.

The first sulfation reactions started with a method for *O*-sulfation using commercially available $SO_3.NMe_3$ complex in DMF. However this method did not provide any purified product or any structural information on which site(s) had been sulfonated. It was decided not to explore the scope of this reaction on our substrates and instead focused on exploring the possibilities for simultaneous *O,N*-sulfation using other commercially available $SO_3$ complexes.

Next, $SO_3.Pyridine$ complex using pyridine as a solvent with 1:10 $Et_3N$:Pyridine additive. Xu & co-workers (2015) describe using this method for simultaneous *O,N*-sulfation under microwave conditions & that $Et_3N$ was integral for reaction completion of both sulfation sites. Unfortunately, this procedure was not compatible with any purification techniques used and produced NMR spectra with large impurities in. This reaction was abandoned early on.

Gill & Co-workers (2019) reported a new sulfur trioxide complex using tributylamine as the lewis base for sulfur trioxide via the reaction of tributylamine with chlorosulfonic acid. As luck would have it, some of this complex had been pre-prepared by a former postgraduate student at The University of Salford. Due to the increased lipophilicity of the sulfate ester intermediate generated using this reagent, Gill & co-workers theorized that subsequent work-up and purification of the sulfate ester product would be easier due to increased solubility in organic solvents. Their purification method included a sodium-salt exchange from the $Bu_3N^+$ salt to the $Na^+$ salt using sodium-2-ethylhexanoate as the sodium atom donor. During the time of the experimental work there had been no reports of anybody using this reagent to sulfate amine groups or provide simultaneous *O,N*-sulfation to small molecules. As purification is a challenging step of chemical sulfation, this method was of interest to us.
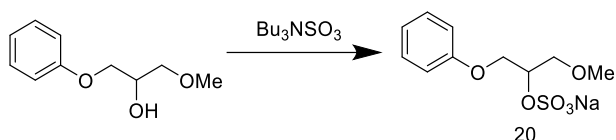
Scheme 18: Synthesis of *Sodium 1-(methoxy)-3-phenoxypropan-2-yl sulfate* using TBSAB as the sulfating reagent

Table 5: Yield table for *Sodium 1-(methoxy)-3-phenoxypropan-2-yl sulfate* using TBSAB as the sulfating reagent

| Yield (%)[a] | Compound |
|---|---|
| 0 | **20** |

a – Yield after salt exchange
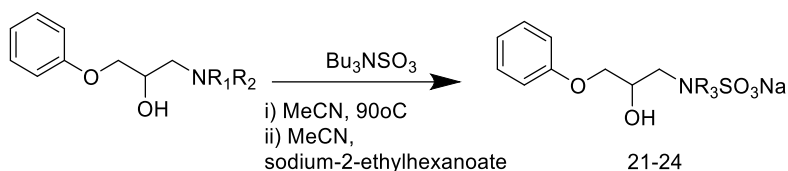


Scheme 19: General scheme for the sulfation of *mono-β-aminols* using TBSAB as a sulfating reagent

Table 6: Yield table for the sulfation of *mono-β-aminols* using TBSAB as a sulfating reagent

| R$_1$ | R$_2$ | R$_3$ | Yield (%)[a] | Compound |
|---|---|---|---|---|
| H | H | H | 0 | **21** |
| iPr | H | iPr | 34 | **22** |
| iPr | iPr | iPr | 0 | **23** |
| CH$_3$CH$_2$ | CH$_3$CH$_2$ | CH$_3$CH$_2$ | 0 | **24** |

Table 5: Sulfation reactions of various b-aminol compounds.
[a] – Yield after salt exchange

For compound **22**, sulfated using TBSAB & sodium-2-ethylhexanoate as the sodium atom donor, the spectrum was generally free of impurities seen with other sulfating methods (SO$_3$HCl, SO$_3$.Py). The spectra for the starting material and the product can be seen below (figure 9):
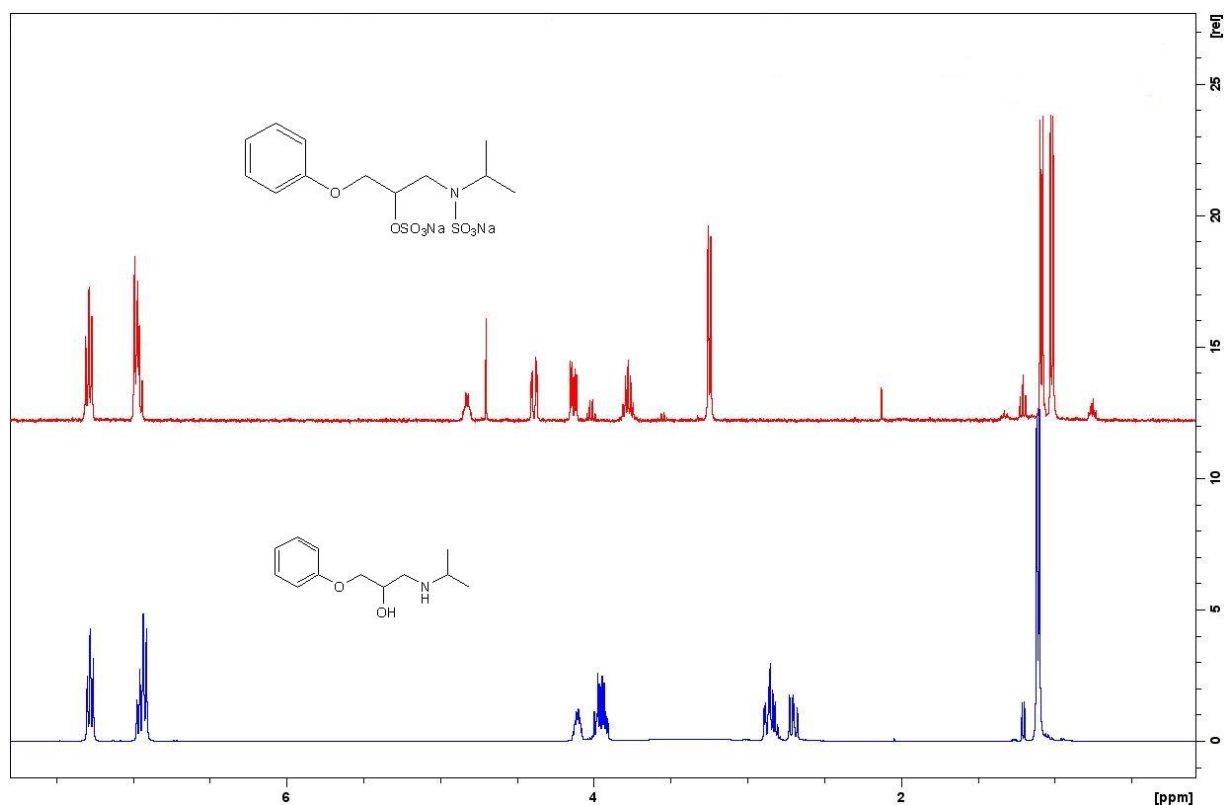
Figure 9: NMR spectrums from the starting material (blue) & the final product 3a (red).

Downfield shifting of the proton adjacent to the -OH in the starting material can be seen from 4.11 in the blue spectrum to 4.82 in the red spectrum. The 4 alkyl protons in the phenoxypropyl side chain have also moved downfield. 2 protons now show doublet-doublet splitting and the peaks have unmerged. The protons adjacent to the isopropylamine group have also moved from 2.87 to 3.79. Impurity is still present in this sample, presumably it is $Bu_3NSO_3$ still left in the sample after washing.

FT-IR spectrums from before and after sulfation also confirmed the loss of the -NH & -OH functional groups via the loss of broad spectrum at around ~2986cm$^{-1}$. Peaks at around 1450cm$^{-1}$ & 1288cm$^{-1}$ could be attributed to sulfate group attachment, indicating reaction completion. This can be seen in figure 10:

Figure 10: FT-IR spectrums from the starting material (left) & the product (right) after sulfation & sodium salt exchange.

Next, the author attempted to synthesise a variety of glycomimetics from the 1,3-epoxide using the same reagent (TBSAB) starting from the 1,3-β-aminol compounds.
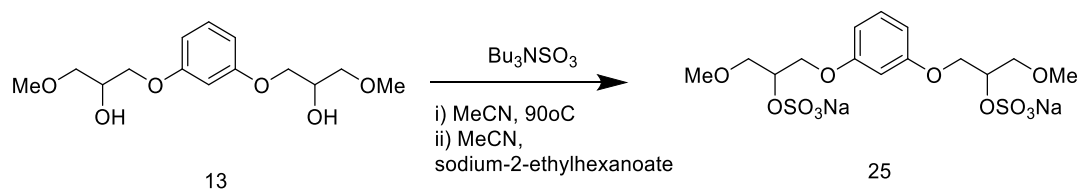


Scheme 20: Sulfation of *Sodium (1,3-phenylenebis(oxy))bis(3-methoxypropane-1,2-diyl) bis(sulfate)* using TBSAB as the sulfating reagent

Table 7: Yield table of *Sodium (1,3-phenylenebis(oxy))bis(3-methoxypropane-1,2-diyl) bis(sulfate)* using TBSAB as the sulfating reagent

| Yield (%)[a] | Compound |
|---|---|
| 28 | **25** |

a – Yield after salt exchange

Compound 25 was sulfated the same way as the compound above, using TBSAB followed by a salt exchange. This molecule only contained two reactive sites (both -OH) & the best route for simple O-sulfation at the time was by using TBSAB. The NMR spectrums for before and after sulfation can be seen in figure 11:
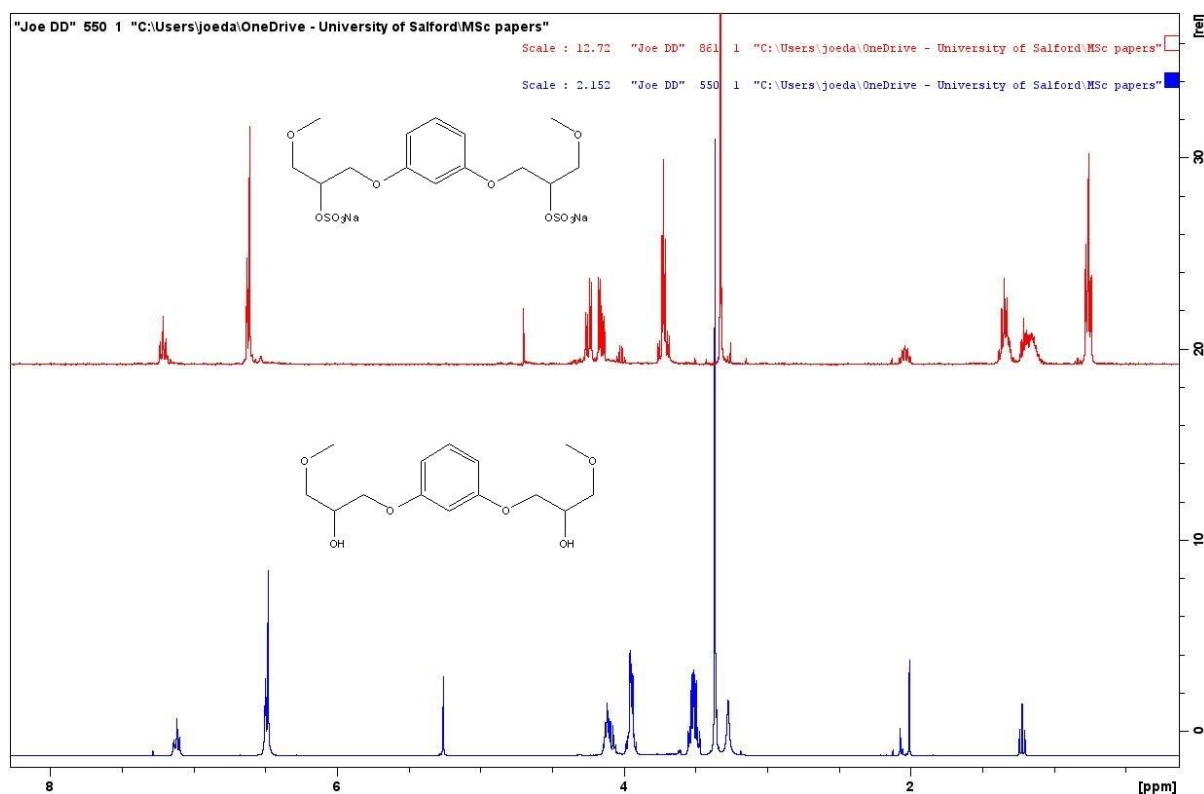
Figure 11: NMR spectrums from the starting material (blue) & the final product 3b (red).

The spectrum for after sulfation was cleaner than reactions done with $SO_3HCl$ & $SO_3.Py$, however a small amount of TBSAB (presumably as $Bu_3N$) is still visible in the reaction, as seen with the triplet and multiplets from 0.7-2.1ppm on the red spectrum ($Bu_3NSO_3$ spectrum shown below in figure 12. Two protons adjacent to the sulfation site are missing from the spectrum for the product. Carbon NMR was used to deduce more information about this molecule, however the NMR is messy with many peaks which can't be assigned to either the compound or potential impurity (NMR not shown, supporting info).
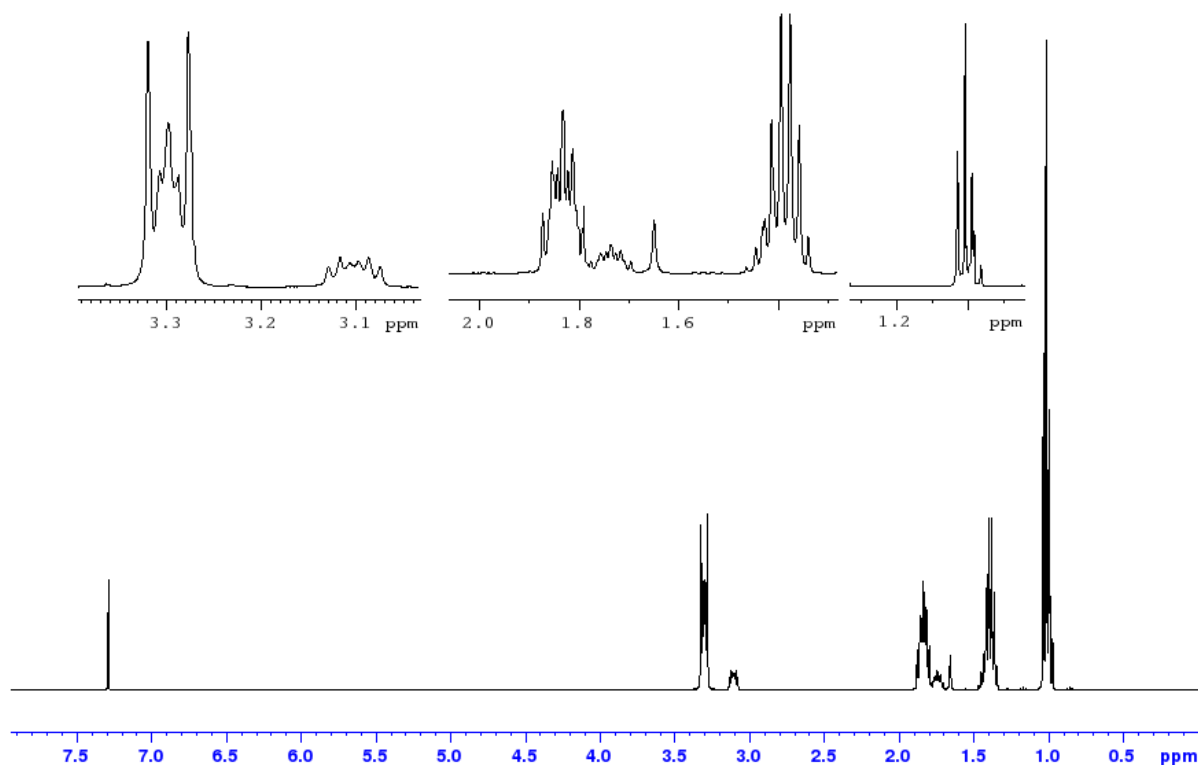
Figure 12: An unintegrated $^1$H-NMR spectrum of $Bu_3NSO_3$

FT-IR spectrums for *sodium (1,3-phenylenebis(oxy))bis(3-methoxypropane-1,2-diyl) bis(sulfate)* still showed some broad peaks at 3465cm$^{-1}$, however the absorbance was much less than in the starting material spectrum (~97% & ~75%, respectively). This is shown in figure 13:
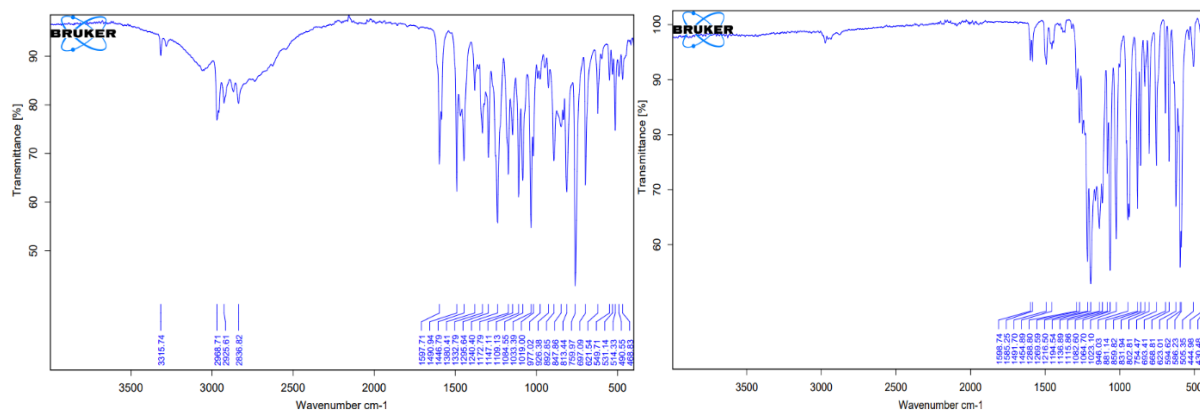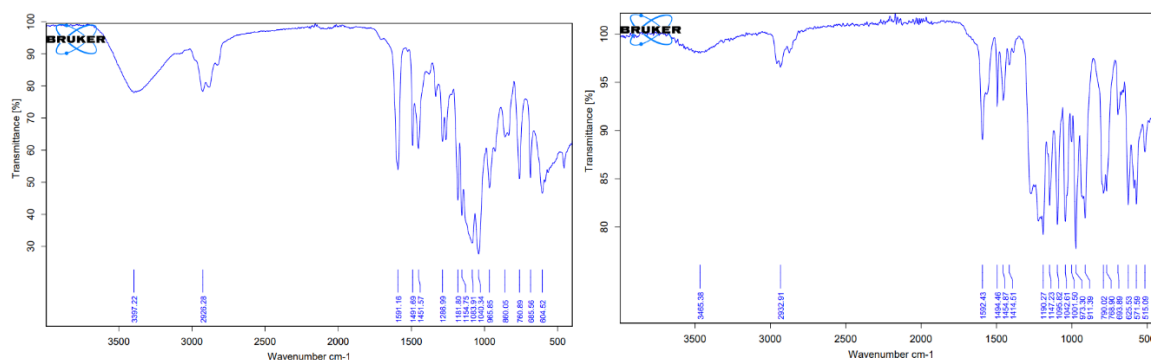


Figure 13: The FT-IR spectrum for the starting material (left) & the product (right) after sulfation & sodium salt exchange.

This methodology was applied to other *1,3-β-aminol* compounds produced by the author. The general scheme and results table can be seen below (scheme 24 & table 8):
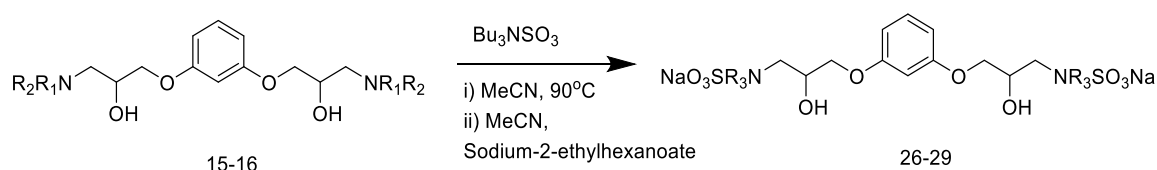


Scheme 21: General scheme for sulfation of various *1,3-β-aminol* compounds using TBSAB as the sulfating reagent

Table 8: Yield table for the sulfation of various *1,3-β-aminol* compounds using TBSAB as the sulfating reagent

| $R_1$ | $R_2$ | $R_3$ | Yield (%) [a] | Compound |
|-------|-------|-------|---------------|----------|
| H | H | H | 0 | 26 |
| iPr | H | iPr | 0 | 27 |
| iPr | iPr | iPr | 0 | 28 |
| $CH_3CH_2$ | $CH_3CH_2$ | $CH_3CH_2$ | 0 | 29 |

a – Yield after salt exchange

Salt exchange reactions for the compounds of interest did not occur and no product formed as the sodium salt apart from the reaction bearing a methoxy group on both positions (compound **25**). This was unexpected but not entirely as the reactions from the mono-compounds also did not work as we had hoped apart from one compound.

The use of Gills & co-workers $SO_3.Bu_3N$ complex produced *O*-sulfation (NMR analysis showed the proton next to the sulfated oxygen moved downfield by around 0.2-0.5ppm) but not *N*-sulfation. The purification step using sodium-2-ethylhexanoate as a sodium atom donor did not work as expected. No precipitate of the product formed in any reaction other than one reaction. The exact reason for this result is still unknown. NMRs of compounds using this methodology showed residue of the sulfating reagent, presumably as the compounds salt form ($Bu_3NH^+$) which could not be removed from the reaction mixture. This form was not suitable for the purposes of testing as a $Bu_3NH^+$ salt rather than $Na^+$ may impact the assay.

In 2020, during the writeup of this project, Alshehri & Co-workers (2020) reported a study in

which SO₃.Bu₃N complex was used to access sulfated molecules and scaffolds. Although in their previous works they had reported the synthesis of both *O*-& *N*-sulfates (Benedetti, Gill, Tsang & Jones, 2019) with their TBSAB reagent, this work focused on the formation of *in situ* lipophilic cation intermediates (Bu₃NH⁺) rather than preparing the TBSAB reagent before sulfation (Scheme 23).
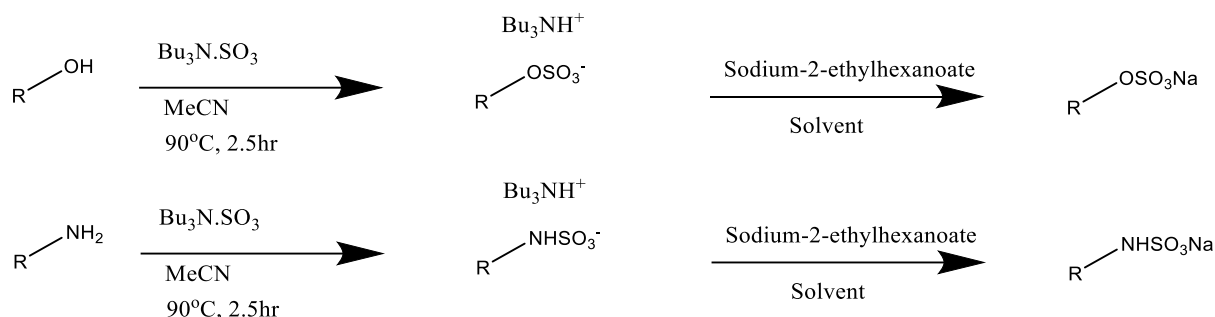


Scheme 22: Previous work on sulfation using the TBSAB reagent. Top: Gill, Male & Jones (2019). Bottom: Benedetti, Gill, Tsang & Jones (2020). Reproduced from figure 1 of Alshehri, Benedetti & Jones, 2020.
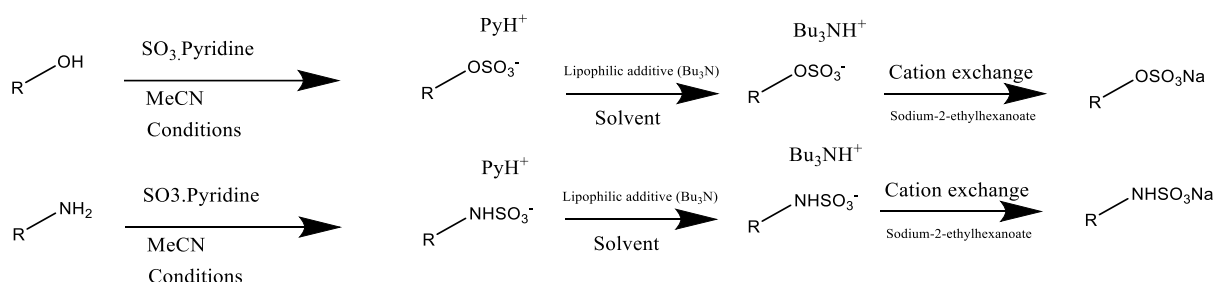


Scheme 23: Current work utilising the generation of the *in situ* Bu₃NH⁺ salt for accessing sodium salts of sulfate esters and sulfamates. Reproduced from Figure 1 of Alshehri, Benedetti & Jones, 2020.

The group managed to access both sulfate ester sodium salts and sulfamate sodium salts through the generation of the lipophilic sulfate intermediates *in situ* by using Bu₃N as a lipophilic cation exchange agent rather than the pre-prepared TBSAB reagent, which can be tricky, long to produce & uses highly toxic and acidic reagents to introduce the -SO₃⁻ moiety. However,Gill & co-workers (2019) found that some *O*-containing scaffolds could not be converted from the Bu₃NH⁺ to the Na⁺ salt and had to be isolated as the tributylammonium salt. The exact reason for this is unknown, but the authors do say that the issue appears to be with the precipitation of the Na⁺ salt rather than the conversion of the ammonium salt itself. This was also apparent in the 2020 paper by Benedetti & co-workers (2020) in which TBSAB was used to sulfate both *O* & *N*-containing scaffolds. Unfortunately, no explanation for this phenomenon could be given. During the author's experiments, all available workup

procedures given in the papers (Gill & co-workers, 2019)(Benedetti & co-workers, 2020) were trialled. These procedures used differing solvents (MeCN, EtOH or EtOAc) for the salt exchange and precipitation step. No difference in product formation was seen with other solvents. The theory that differing electronics of solvents could effect salt precipitation has been published in the wider literature, as acetonitrile can supress salt precipitation via interaction with the Na$^+$ cations in solution to change solvation structures (Sun *et al.*, 2020).

It was then decided to move onto a more classical method of sulfation using chlorosulfonic acid with the hope that an improved protocol for sulfation followed by cation-exchange could help to provide more information on sulfation through the use of a hard sulfation reagent which could be easily removed from the reaction (without the use of column chromatography) once the reaction had completed.
Spectral data from the reactions involving chlorosulfonic acid & subsequent ion-exchange chromatography showed considerably more impurities and peak mixing than using the TBSAB reagent.
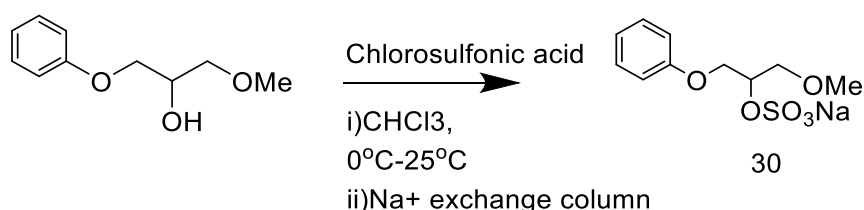


Scheme 24: Synthesis of *Sodium 1-(methoxy)-3-phenoxypropan-2-yl sulfate* using chlorosulfonic acid as the sulfating reagent

Table 9: Yield table for *Sodium 1-(methoxy)-3-phenoxypropan-2-yl sulfate* using chlorosulfonic acid as the sulfating reagent

| Yield (%)[a] | Compound |
|---|---|
| 0 | **30** |

a – Yield after salt exchange
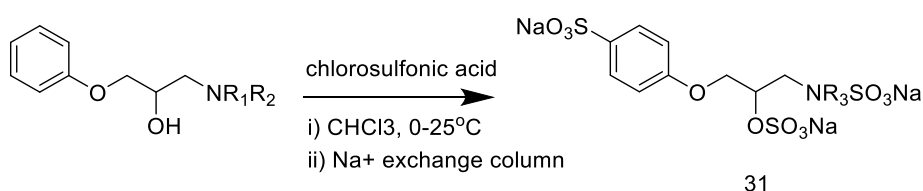


Scheme 25: Synthesis *of Sodium 1-(sulfonatoamino)-3-(4-sulfonatophenoxy)propan-2-yl sulfate* using chlorosulfonic acid as the sulfating reagent

Table 10: Yield table for *Sodium 1-(sulfonatoamino)-3-(4-sulfonatophenoxy)propan-2-yl sulfate* using chlorosulfonic acid as the sulfating reagent

| R1 | R2 | R3 | Yield (%)[a] | Compound |
|----|----|----|----------|----------|
| H | H | H | 35 | **31** |
| iPr | H | iPr | 0 | **32** |

a – Yield after salt exchange

For compound **31**, the sulfation conditions were changed to SO$_3$HCl followed by a non-aqueous workup (removal of solvent & wash) & elution through a column of Amberlite IR-120 Na$^+$ cation-exchange resin. This reaction showed how aggressive of a sulfating reagent SO$_3$HCl can be, as -*para* aromatic sulfation occurred. The NMR spectrums are shown below in figure 14:
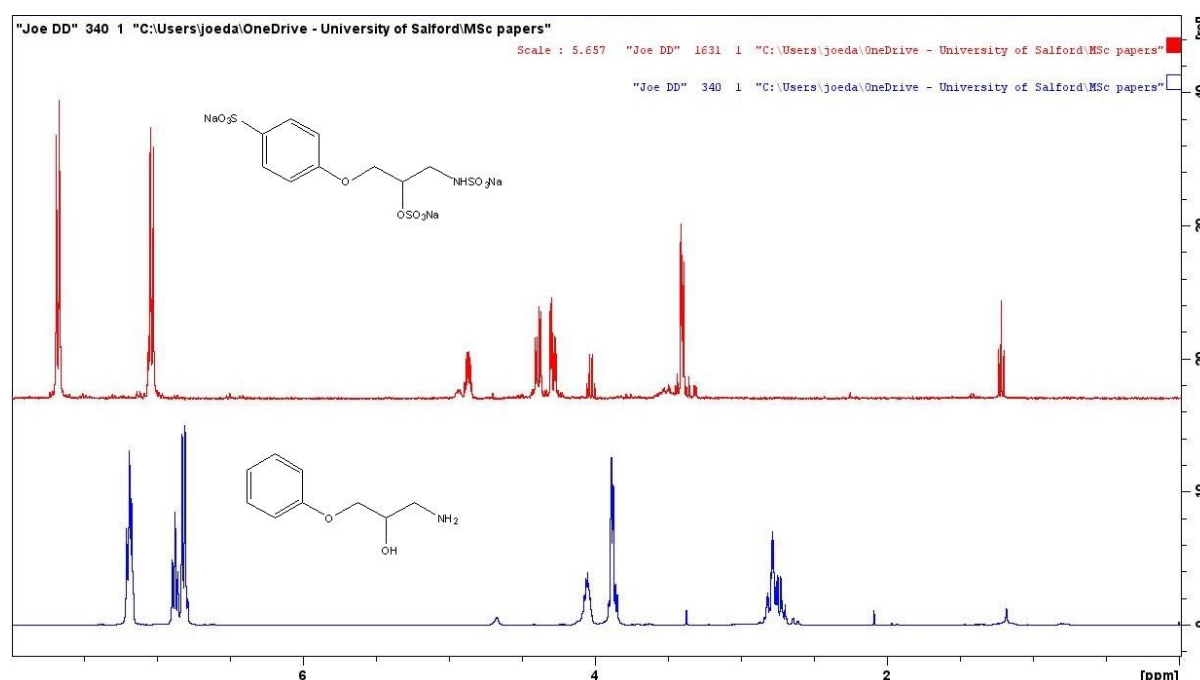


Figure 14: NMR spectrums from the starting material (blue) & the final product *sodium 1-(sulfonatoamino)-3-(4-sulfonatophenoxy)propan-2-yl sulfate* (red).

FT-IR spectrums showed removal of the broad peaks from 2919-2722cm$^{-1}$ (-NH & -OH groups) however a small broad peak at 3434cm$^{-1}$ was still present in the sample, but the absorbance was much less than the starting material (~96% & ~80% respectively). A large broad stretch at 1120cm$^{-1}$ was present in the final compound spectrum. Spectrums are in figure 15:
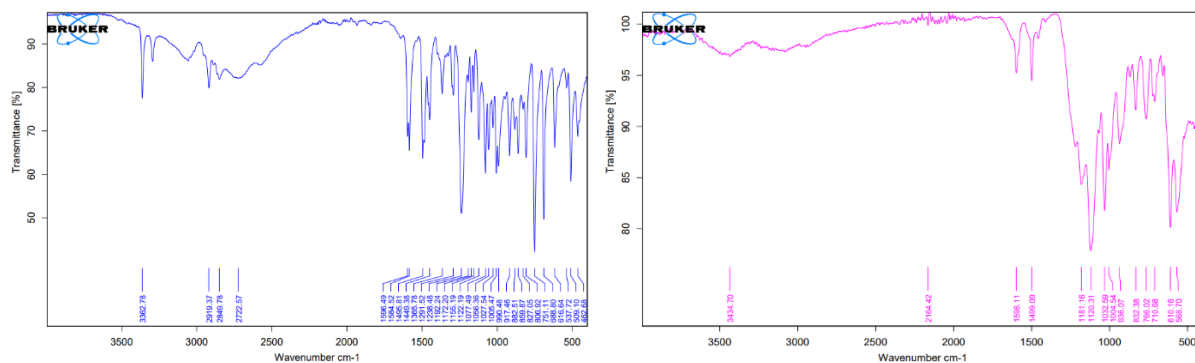
Figure 15: FT-IR spectrums for the starting material (left) & the sulfated product (right) after elution through a Na+ exchange column.

LC-MS (-ESI) showed m/z peaks at 246.0 & 325.85. 246.0 could be attributed to the [M-2Na-CN-$SO_3H$] adduct, with 325.85 being the [M-2Na-CN] adduct. Interestingly, an [M+$SO_3H$] adduct at m/z 475.90 was seen in the (-)ESI chromatogram. Again, this evidence is tentative to assign compounds as the adducts and peaks are not what would be expected. Unfortunately high-resolution MS was not available at the time of this project.

Compound **31** was not soluble in $D_2O$ or MeOD like many of the other compounds. It was only slightly soluble in DMSO so the solution was filtered through a pipette containing cotton. At the time of this compound being made, our bruker NMR was being repaired. The starting material has no NMR for it and only has LRMS for product confirmation. The LRMS of the starting material is included in the supporting information.

Originally it was thought that the $SO_3HCl$ may have aromatically sulfated the ring -*ortho* to the -CN group, however upon examination of the ^{1}H-NMR, 4 aromatic protons seemed to be the most likely predominating product in the mixture.
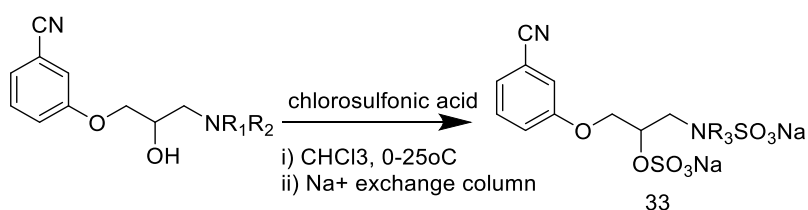


Scheme 26: Sulfation of *mono-β-aminol* compounds bearing a 3-Cyano moiety on the ring

Table 11: Yield table for *mono-β-aminol* compounds bearing a 3-Cyano moiety on the ring

| R1 | R2 | R3 | Yield (%)[a] | Compound |
|----|----|----|----------|----------|
| H | H | H | 41 | **33** |
| iPr | H | iPr | 0 | **34** |

a – Yield after salt exchange
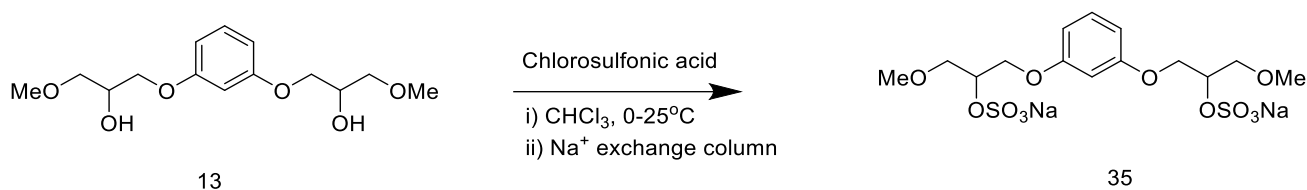


Scheme 27: Synthesis of *Sodium (1,3-phenylenebis(oxy))bis(3-methoxypropane-1,2-diyl) bis(sulfate)* using chlorosulfonic acid as the sulfating reagent

Table 12: Yield table for *Sodium (1,3-phenylenebis(oxy))bis(3-methoxypropane-1,2-diyl) bis(sulfate)* using chlorosulfonic acid as the sulfating reagent

| Yield (%)[a] | Compound |
|----------|----------|
| 0 | **35** |

a – Yield after salt exchange
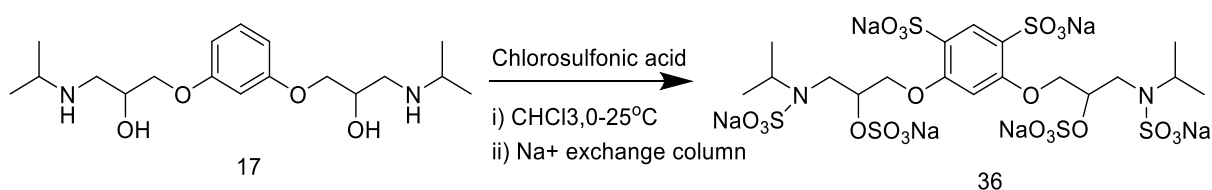


Scheme 28: Synthesis of *sodium ((4,6-disulfonato-1,3-phenylene)bis(oxy))bis(3-(isopropyl(sulfonato)amino)propane-1,2-diyl) bis(sulfate)* using chlorosulfonic acid as a sulfating reagent

Table 13: Yield table for *sodium ((4,6-disulfonato-1,3-phenylene)bis(oxy))bis(3-(isopropyl(sulfonato)amino)propane-1,2-diyl) bis(sulfate)* using chlorosulfonic acid as a sulfating reagent

| Yield (%)[a] | Compound |
|---|---|
| 39 | **36** |

a – Yield after salt exchange

For compound **36**, the 4.0-5.0 ppm region was filled with peak merging and resulted in a very messy NMR sample. This can be seen below in figure 16:
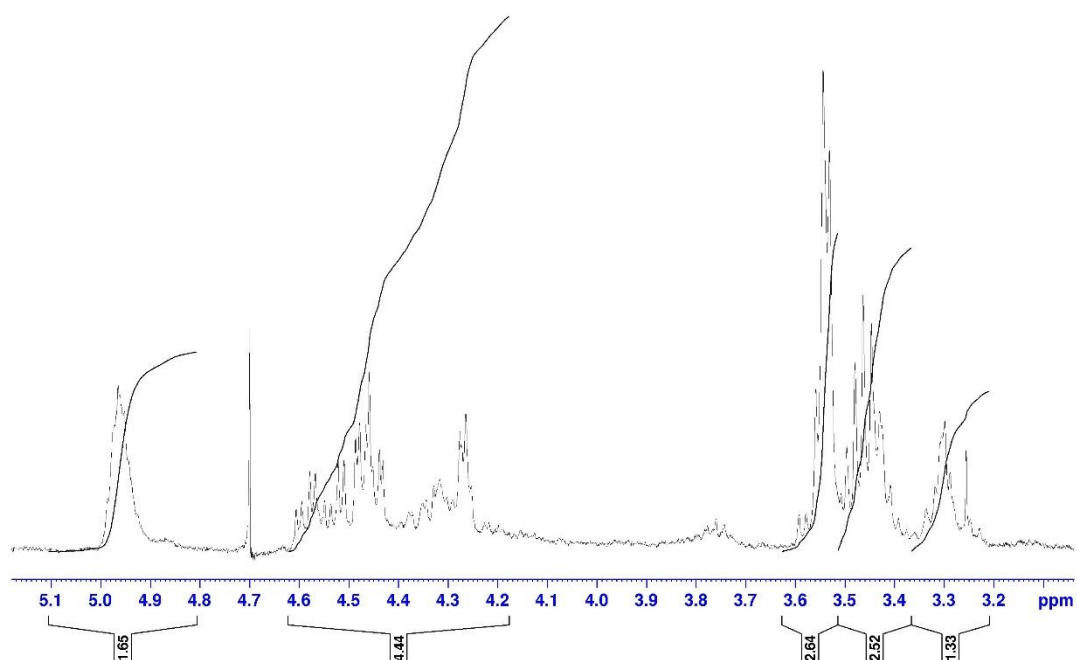


Figure 16: Expanded region of compound 36. The 2 protons at 5.00-4.90 ppm are much further downfield than the starting material (around 1.00ppm).

This is tentative evidence for a sulfation at the hydroxyl site, however the proton integrations and unclear peaks from the NMR lead the author to believe that multiple sulfated products were present in the reaction mixture. The feature of the NMR that stood out the most was the aromatic region. A singlet and a doublet each integrating to one proton each seemed to show that 2 aromatic sulfations had occurred *ortho* to the phenoxy side chains. This means that if we include *N*-sulfation too, a molecule with six potential sulfations could be in the reaction mixture. Although peak merging and splitting within

other NMR spectrums of the final compounds were seen, compound **36** had the most side-products in. From the preliminary analysis, it was decided to tentatively assign the compound. Figure 17 shows the two spectrums overlayed in topspin processing mode.
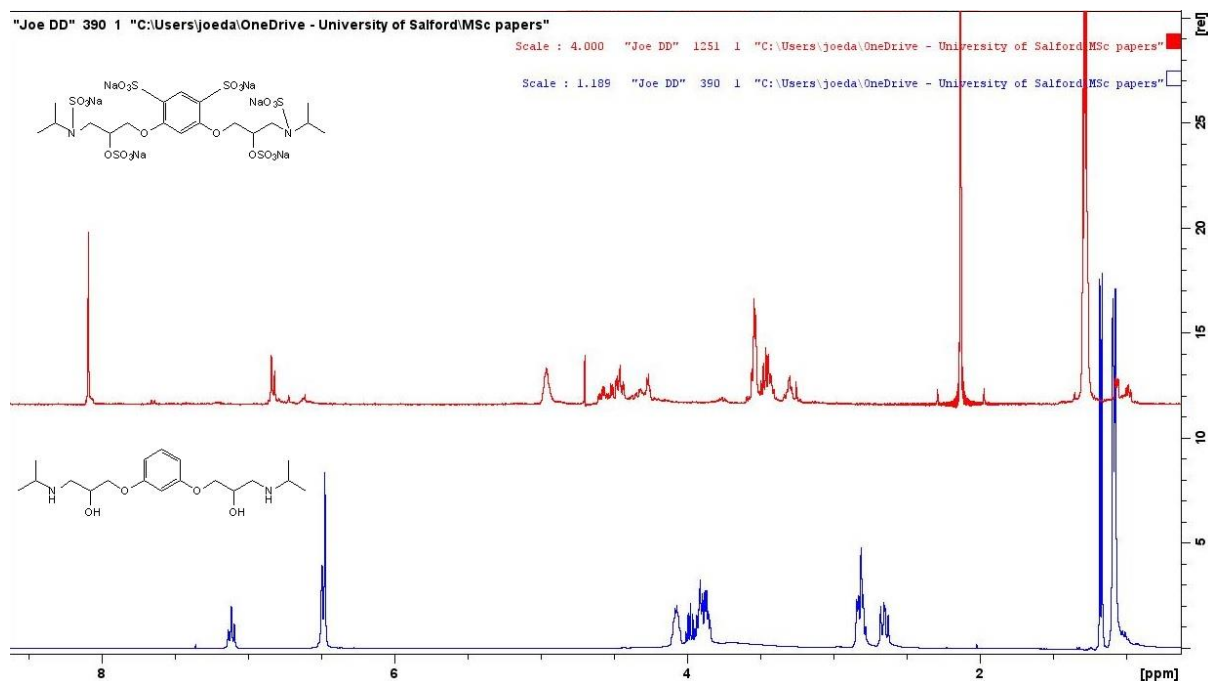


Figure 17: NMR spectrums from the starting material (blue) & the final product (red).

Downfield shifting of the aromatic and alkyl protons attached next to O & N heteroatoms can be seen in the NMR spectrums above. The -CH in the isopropylamine group has shifted downfield too.

Unfortunately due to time constraints, an FT-IR spectrum for JD-4 was not available.
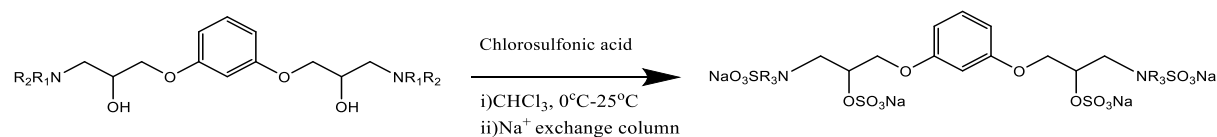


Scheme 29: Sulfation of 1,3-*β-aminol* compounds using chlorosulfonic acid as the sulfating reagent

Table 14: Yield table for sulfation reactions of 1,3-*β-aminol* compounds using chlorosulfonic acid as the sulfating reagent

| R₁ | R₂ | R₃ | Yield (%)ᵃ | Compound |
|----|----|----|-----------|----------|
| H | H | H | 22 | **37** |
| iPr | iPr | iPr | 0 | **38** |
| CH₃CH₂ | CH₃CH₂ | CH₃CH₂ | 0 | **39** |

a – Yield after salt exchange

### 3.1.10 - Sodium 1-(isopropyl(sulfonato)amino)-3-phenoxypropan-2-yl sulfate (22):
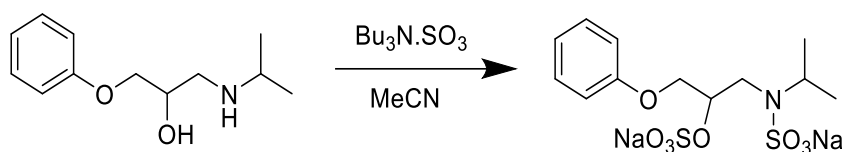


Scheme 30: Synthesis of *Sodium 1-(isopropyl(sulfonato)amino)-3-phenoxypropan-2-yl sulfate*

*1-isopropylamino-3-phenoxypropan-2-ol* (0.50 mmol) was added to an oven-dried flask under argon containing anhydrous acetonitrile (2.5mL). Bu₃NSO₃ (2.5eq per reactive site)(5.0 mmol) was added & the reaction mixture was stirred for 30 minutes at 30°C and heating was increased to 90°C for 60 minutes. The solvent was evaporated *in vacuo* and water (20mL) was added & extracted with EtOAc (3x40mL). The organic later was dried with MgSO₄, filtered, and the solvent evaporated *in vacuo*. The resulting oil was taken up in absolute ethanol (30mL) and sodium-2-ethylhexanoate (5.0 mmol) (in 5mL anhydrous acetonitrile) was added dropwise & the solution was stirred vigorously overnight. The solid was allowed to settle and was collected by filtration & washed with absolute ethanol (3x10mL) & air-dried to yield *sodium 1-(isopropyl(sulfonato)amino)-3-phenoxypropan-2-yl sulfate* as a white solid. Yield: (0.063g, 34%). ¹H-NMR (D₂O): 7.29 (t, 2H, J=7.31Hz, Ar **H**), 6.98 (m, 3H, Ar **H**), 4.86-4.79 (m, 1H, C**H**(CH3)₂) 4.39 (dd, 1H, J=12.77Hz, 2.92Hz, CH₂C**H**CH₂), 4.14 (dd, 1H, J=11.41Hz, 4.58Hz, NC**H**₂), 3.25 (d, 2H, J=7.07Hz, OC**H**₂), 1.06 (dd, 6H, J=26.84Hz, 6.81Hz, NCH(C**H**3)₂). FT-IR: 1204.35,1187.00, 1121.99, 1068.17, 1023.05, 942.01, 886.71, 872.62, 798.68, 750.43, 676.61, 664.77,626.33, 588.43. LC-MS: (-ESI): Retention time: 14.70 minutes. Found: 288.0 [M-2Na-SO₃⁻]. M.P.: 268-270°C.

### 3.1.11 - Sodium (1,3-phenylenebis(oxy))bis(3-methoxypropane-1,2-diyl) bis(sulfate) (25):
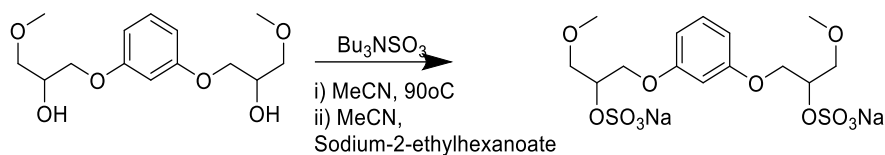


Scheme 31: Synthesis of *Sodium (1,3-phenylenebis(oxy))bis(3-methoxypropane-1,2-diyl) bis(sulfate)*

*1,3-Bis-(3-methoxy-2-hydroxypropyloxy)-benzol* (0.143g, 0.50 mmol) was added to an oven-dried flask under argon containing anhydrous acetonitrile (2mL). $Bu_3NSO_3$ (2eq per reactive site)(2.0 mmol) was added & the reaction mixture was stirred for 30 minutes at 30°C and heating was increased to 90°C for 60 minutes. The solvent was evaporated *in vacuo* and water (20mL) was added & extracted with EtOAc (3x40ml). The organic layer was dried with $MgSO_4$, filtered, and the solvent evaporated *in vacuo*. The resulting oil was taken up in absolute ethanol (15mL) and sodium-2-ethylhexanoate (5eq/site)(5.0 mmol) in anhydrous acetonitrile (5mL) was added dropwise & the solution was stirred vigorously overnight. The solid was allowed to settle and was collected by filtration & was washed with absolute ethanol (3x10mL) & air-dried to yield *sodium (1,3-phenylenebis(oxy))bis(3-methoxypropane-1,2-diyl) bis(sulfate)* as a white solid. Yield: (0.070g, 28%). $^1$H-NMR ($D_2O$): 7.21 (m, 1H, Ar **H**), 6.62 (m, 3H, Ar **H**), 4.24 (dd, 2H, OC**H**$_2$, J=11.15Hz, 4.71Hz), 4.15 (dd, 2H, J=11.22Hz, 4.95Hz, $_3$HCOC**H**2), 3.76-3.66 (m, 4H, OC**H**$_2$), 3.32 (s, 6H, OC**H**$_3$). FT-IR: 3465.38, 2932.91, 1592.43, 1494.46, 1454.87, 1414.51, 1190.27, 1147.23, 1095.82, 1042.61, 1001.50, 973.30, 911.39, 790.02, 768.90, 693.89, 625.53, 571.59, 515.09, 431.60. LR-MS (-ESI): Retention time: 14.3 minutes. Found: 364.9 [M-2Na-$SO_3^-$]. M.P.: 282-285°C.

### 3.1.12 - Sodium 1-(sulfonatoamino)-3-(4-sulfonatophenoxy)propan-2-yl sulfate (31):
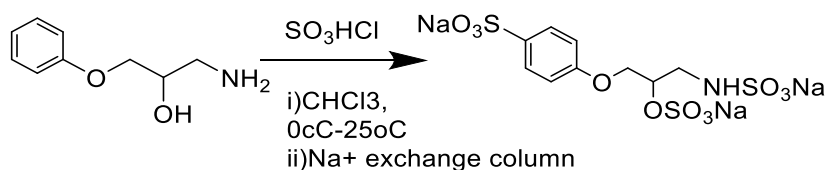


Scheme 32: Synthesis *of Sodium 1-(sulfonatoamino)-3-(4-sulfonatophenoxy)propan-2-yl sulfate*

*1-Amino-3-phenoxypropan-2-ol* (0.50 mmol) was added to an ice-cooled flask containing chloroform (5mL) at $0^oC$. Once the material had dissolved & the solution temperature was at $0^oC$, $SO_3HCl$ (0.132mL, 2.0 mmol) was added dropwise over 10 minutes to the solution. The solution was stirred at $0^oC$ for 1 hour and then slowly warmed to room temperature over 1 hour. The solvent was removed *in vacuo* & the resulting powder was washed with $CHCl_3$ (3x10mL) and dried *in vacuo*. The resulting powder was immediately dissolved in water and ran through a column containing amberlite IR-120 $Na^+$. The resulting water was removed *in vacuo* using toluene as an azeotrope solvent to yield *sodium 1-(sulfonatoamino)-3-(4-sulfonatophenoxy)propan-2-yl sulfate* as a white solid. Yield: 182mg (35%). $^1$H-NMR ($D_2O$): 7.67 (d, 2H, J=8.86Hz, Ar **H**), 7.03 (d, 2H, J=8.94Hz, Ar **H**), 4.86 (s, 1H, $CH_2C$**H**$CH_2$), 4.38 (dd, 1H, J=11.05Hz, 6.61Hz, NC**H**$_2$), 4.28 (dd, 1H, J=11.14Hz, 7.42Hz, OC**H**$_2$), 3.40 (dd, 2H, J=5.79Hz, 2.70Hz, $CH_2C$**H**$CH_2$). $^{13}$C-NMR ($D_2O$): 159.90, 135.45, 127.39, 114.79, 73.31, 67.42, 40.59. FT-IR: 3434.70, 2164.42, 1598.11, 1499.09, 1181.16, 1120.31, 1032.59, 1004.54, 936.07, 832.38, 766.02, 710.68, 610.16, 568.70, 420.17. LRMS (-ESI): Retention time: 3.86 minutes. Found: 246.00 [M-3Na-2SO$_3^-$]. M.P.: >$300^oC$.

### 3.1.13 - Sodium 1-(3-cyanophenoxy)-3-(sulfatoamino)propan-2-yl sulfate (33):
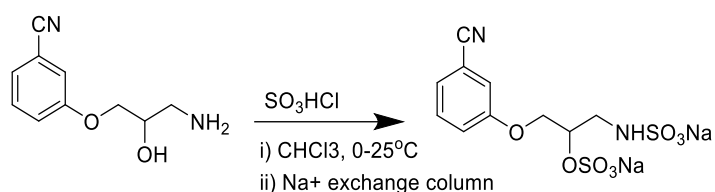


Scheme 33: Synthesis *of Sodium 1-(3-cyanophenoxy)-3-(sulfatoamino)propan-2-yl sulfate*

*1-(3-Cyanophenoxy)-2-hydroxy-3-amino propane* (0.096g, 0.50 mmol) was added to an ice-cooled flask containing chloroform (5mL) at 0°C. Once the starting material had dissolved & the solution temperature was at 0°C, $SO_3HCl$ (0.132ml, 2.0 mmol) was added dropwise over 10 minutes. The solution was stirred at 0°C for 1 hour and then slowly warmed to room temperature over 1 hour. The solvent was removed *in vacuo* & the resulting powder was washed with $CHCl_3$ (3x10mL) & dried *in vacuo*. The resulting power was dissolved in water and immediately ran through a column of amberlite IR-120 $Na^+$. The resulting water was removed *in vacuo* using toluene as an azeotrope solvent to yield *Sodium 1-(3-cyanophenoxy)-3-(sulfatoamino)propan-2-yl sulfate* as a white solid. Yield: (41%, 50mg). ^{1}H-NMR (d6-DMSO): 7.53-7.29 (m, 4H, Ar **H**), 4.22 (m, 1H, C**H**), 4.23 (d, 2H, J=4.71Hz, NC**H**$_2$), 3.12 (d, 2H, J=8.78Hz, OC**H**$_2$). FT-IR: 3073.20, 2233.26, 1582.18, 1526.81, 1483.80, 1437.57, 1289.51, 1256.38, 1215.25, 1108.39, 1062.42, 1037.76, 998.78, 927.47, 868.22, 769.83, 681.67, 617.04, 588.42, 565.17, 474.50. LRMS: Found: 246.0 [M-$SO_3$-CN]. M.P.: >300°C.

## 3.1.14 - Sodium ((4,6-disulfonato-1,3-phenylene)bis(oxy))bis(3-(isopropyl(sulfonato)amino)propane-1,2-diyl) bis(sulfate) (36):
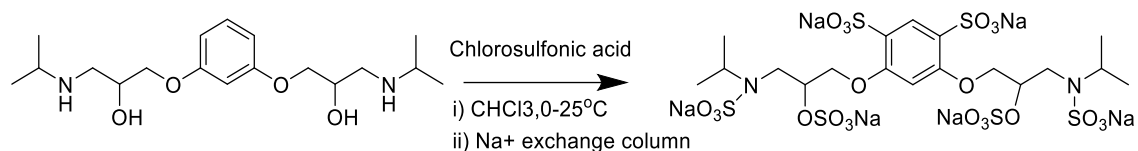


Scheme 34: Synthesis *of Sodium ((4,6-disulfonato-1,3-phenylene)bis(oxy))bis(3-(isopropyl(sulfonato)amino)propane-1,2-diyl) bis(sulfate)*

*1,3-Bis-(3-isopropylamino-2-hydroxypropyloxy)benzol* (0.50 mmol) was added to an ice-cooled flask containing chloroform (5mL) at 0°C. Once the material had dissolved & the solution temperature was at 0°C, $SO_3HCl$ (0.264ml, 4.0 mmol) was added dropwise over 10 minutes to the solution. The solution was stirred at 0°C for 1 hour and then slowly warmed to room temperature over 1 hour. The solvent was removed *in vacuo* & the resulting powder was washed with $CHCl_3$ (3x10mL) and dried *in vacuo*. The resulting powder was immediately dissolved in water and ran through a column containing amberlite IR-120 Na^{+}. The resulting water was removed *in vacuo* using toluene as an azeotrope solvent to yield *Sodium ((4,6-disulfonato-1,3-phenylene)bis(oxy))bis(3-(isopropyl(sulfonato)amino)propane-1,2-diyl) bis(sulfate)* as a white solid. Yield: (0.186g, 39%). ^{1}H-NMR ($CDCl_3$): 8.09 (s, 1H, Ar **H**), 6.83 (s, 1H, Ar **H**), 5.00-4.90 (m, 2H, $CH_2C$**H**$CH_2$), 4.62-4.23 (m, 4H, C**H**$_2$N), 3.60-3.38 (m, 4H, OC**H**$_2$), 1.28 (m, 12H, CH(C**H**$_3$)$_2$). M.P.: >300°C.

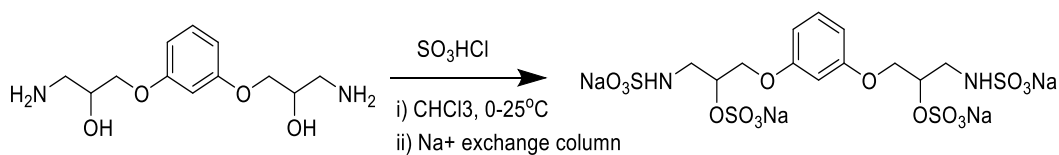### 3.1.15 - Sodium (1,3-phenylenebis(oxy))bis(3-(sulfonatoamino)propane-1,2-diyl) bis(sulfate) (37):



Scheme 35: Synthesis of *Sodium (1,3-phenylenebis(oxy))bis(3-(sulfonatoamino)propane-1,2-diyl) bis(sulfate)*

*1,3-Bis-(3-amino-2-hydroxypropyloxy)benzol* (0.50 mmol) was added to an ice-cooled flask containing chloroform (5mL) at 0°C. Once the starting material had dissolved & the solution temperature was at 0°C, SO$_3$HCl (0.264ml, 4.0 mmol) was added dropwise over 10 minutes. The solution was stirred at 0°C for 1 hour and then slowly warmed to room temperature over 1 hour. The solvent was removed *in vacuo* & the resulting powder was washed with CHCl$_3$ (3x10mL) & dried *in vacuo*. The resulting power was dissolved in water and immediately ran through a column of amberlite IR-120 Na$^+$. The resulting water was removed *in vacuo* using toluene as an azeotrope solvent to yield *Sodium (1,3-phenylenebis(oxy))bis(3-(sulfonatoamino)propane-1,2-diyl) bis(sulfate)* as a white solid. Yield: (0.105g ,22%). No NMR data could be recorded for this compound. LRMS: Found: 334.90 [M-4Na-3SO$_3^-$]. M.P.: >300°C.

A number of compounds were successfully sulfated however purification remained the biggest challenge of the synthesis. Organosulfate synthesis and purification has been regarded as a "synthetic nightmare" due to high net negative charge density (Raghuraman, Riaz, Hindle & Desai, 2007). Normal-phase silica gel chromatography did not afford products once sulfation had been completed. Many polar solvent systems were trialled (hexane:ethyl acetate, methanol:chloroform, dichloromethane:methanol & Methanol:water to name a few) and used but none provided the pure compounds in either the -$SO_3H$ or free -$SO_3^-$ form. Subsequent ion-exchange chromatography using a $Na^+$ exchange resin also failed to purify the compound to high purity but provided the compounds as their sodium salts. Papers describing the synthesis of highly-sulfated molecules made by chemical sulfation have used reverse-phase TLC and column chromatography to separate reactions products and reactants after reaction completion. Although this purification technique is well described and yields pure products (Raghuraman *et al.*, 2007), this technique is much more expensive to use than normal-phase TLC and column chromatography. Whilst this may remain the best way to purify highly polar molecules, the level of funding to this project did not allow for the purchase of reverse-phase TLC plates or silica to allow for experimentation into this method of purification.

Solid phase extraction (SPE) has successfully been used to purify *per*sulfated molecules such as heparin and sulfated steroids using SPE cartridges loaded with a stationary phase much like in flash column chromatography. Pre-packed SPE cartridges can easily be used as a "washing" step to purify compounds by pushing mobile phase through the cartridge under vacuum. The compound of interest can be eluted from the column much like in flash column chromatography. GAGs from cartilage tissue have been successfully purified by SPE extraction and then derivatised for online LC-MS analysis in negative ESI mode (Hitchcock, Yates, Shortkroff, Costello & Zaia, 2006).

Another possible purification route for organosulfates that are incompatible with normal-phase column chromatography is dialysis (Nguyen *et al.*, 2016)(Strätz, Liedmann, Heinze, Fischer & Groth, 2019). Dialysis to remove excess sulfation reagent has been reported in the literature due to commercially available amine complexes such as $SO_3.Py$ are soluble in water. Dialysing using dialysis tubing with a specific molecular weight cut-off point is used

for purification of proteins and DNA samples. Lyophilization of samples after dialysis is usually done to concentrate the sample and remove water.

The use of chlorosulfonic acid (ClSO$_3$H) as a sulfating reagent proved to be quite tricky. Not only does the reagent fume HCl and H$_2$SO$_4$ upon contact with air, but it is also a superacid with a pKa of approximately -6.0 and must be handled with extreme care. Chlorosulfonic acid is a powerful electrophile capable of both *O*-& *N*-sulfation reactions (Li, Chen & Xu, 2010)(Li, Qiu, Shi & Li, 2016). As chlorosulfonic acid is soluble in chloroform it was decided to use chloroform as the solvent for the reaction, as chloroform and other aprotic solvents such as DCM, DMF & acetonitrile are commonly used for sulfation reaction involving chlorosulfonic acid. As the procedure and work-up was simple and removed any excess chlorosulfonic acid easily, we tried this sulfation strategy for both hydroxyl and amine groups. However purification of the compound after work-up was not possible and flash column chromatography did not produce the compound with any more considerable purity than before purification. The compounds were also subjected to ion-exchange chromatography with a Na$^+$ exchange resin but this also did not purify the compound. Sulfation did occur but in a much more "aggressive" manner than thought. The chlorosulfonic acid produced aromatic sulfation at the *ortho* position to the alkoxy side chains as well as sulfation of the hydroxyl and amine groups in the 1,3-*bis* opened epoxides. *Para* sulfation in the *mono*-opened epoxides occurred exclusively (classic AB doublet splitting was observed in the NMR specta). This wasn't expected to begin with but chlorosulfonic acid is a powerful enough electrophile to sulfate aromatic rings at mild to moderate reaction conditions (Horner, Holman & Ward, 2007)(Pearce, Jotterand & Imperiali, 2001). The use of stoichiometric amounts of chlorosulfonic acid (1eq/reactive site) did produce two compounds with two sulfates (*O* & *N*) but also with aromatic sulfation. Chlorosulfonic acid is difficult to dispense by hand without the use of an auto-injection system. This may have led to inconsistencies when dispensing the reagent over the ten minute time period, leading to increased chlorosulfonic acid concentrations which may have influenced the sulfation pattern.

Microwave heating for sulfation reactions has been reported in recent years (Raghuraman, Riaz, Hindle & Desai, 2007)(Umrigar, Chakraborty & Parikh, 2007) and is useful for decreasing reaction times, increasing yields and reaction completion. Work by Xu *et al.*

(2015) showed simultaneous *O*-&*N*-sulfation with the use of commercially available SO₃.Py complex & Et₃N as an additive under microwave heating. Triethylamine was shown by the authors to be important for the *N*-sulfation to occur. As simultaneous sulfation was of interest to the author, this method was tested on our substrates. The reaction time was short at 15 minutes; however purification encountered the same issues as our other synthetic procedures. Normal-phase flash column chromatography and Na⁺ ion-exchange chromatography did not successfully purify the compound and the spectral data showed a large amount of residue of the sulfation reagent and salts were still present in the mixture.
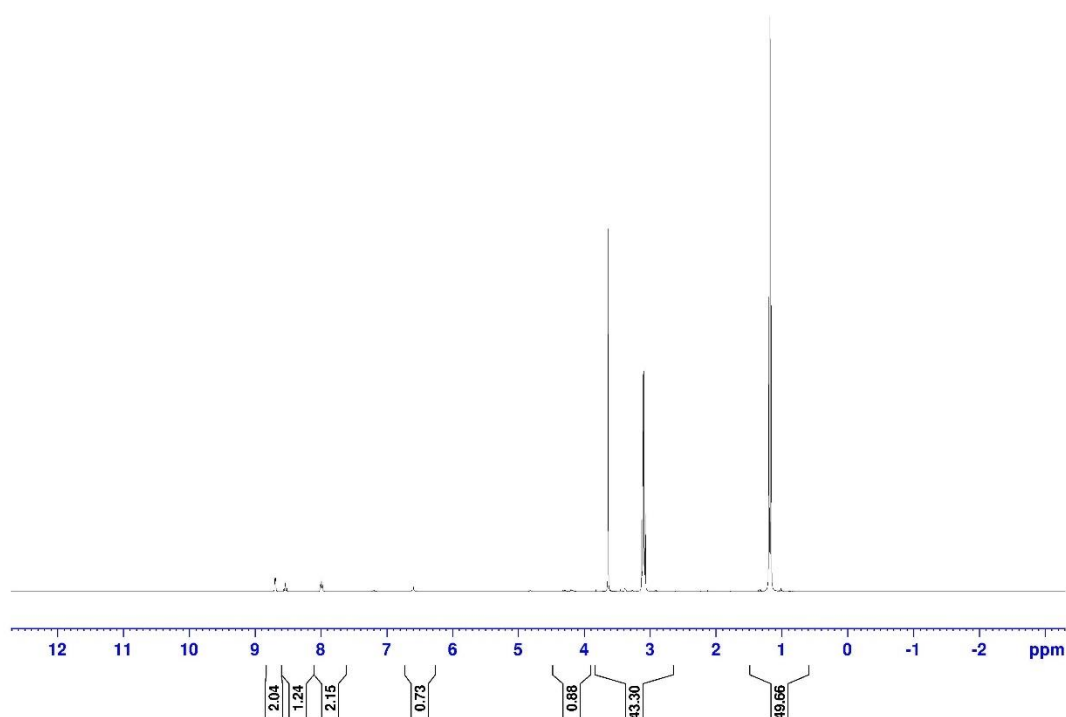


Figure 18: An NMR spectrum from using SO₃.Py as the sulfating reagent with Et₃N as a base.

A massive impurity of Et₃N can instantly be seen in the spectrum in figure 18. The figure below it shows the expanded aromatic region, with a large amount of pyridine (either as the pyridinium salt or as the free pyridine) present, which can be seen from the peaks at 8.00, 8.54 & 8.69 ppm. Although the spectrum showed some indications of a small amount of product in the NMR, purification was not possible. Although the author performed this reaction on multiple substrates, the samples could not be successfully purified. This was a

shame as simultaneous O,N-sulfation under microwave irradiation was quite exciting at first.
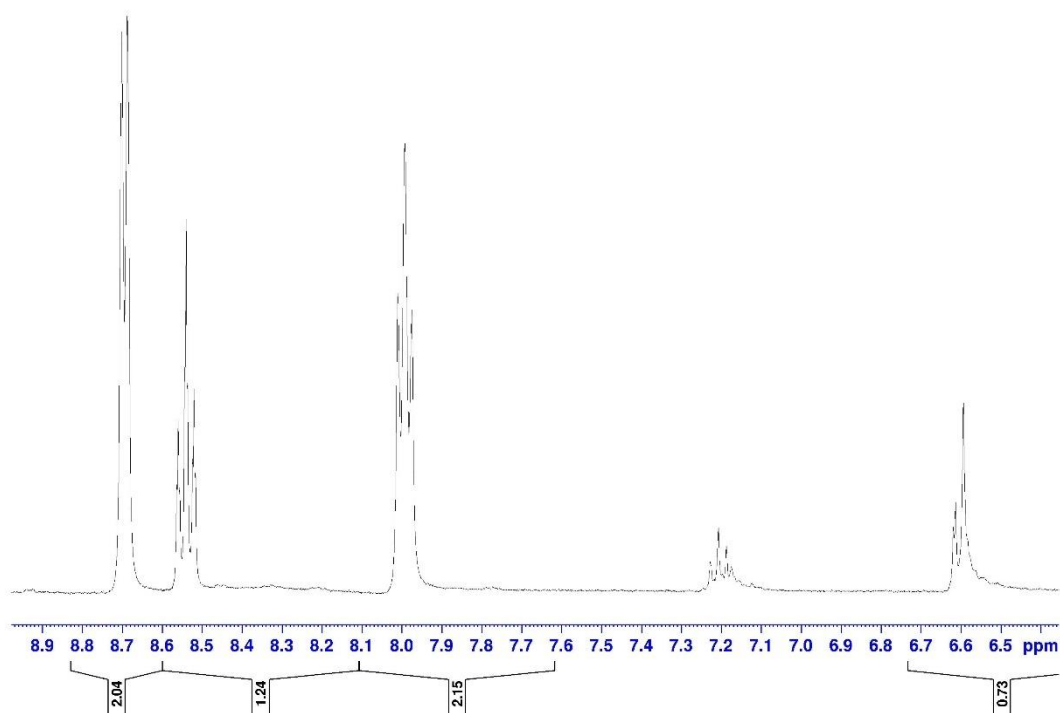


Figure 19: Expanded aromatic region of the reaction using SO$_3$.Py as the sulfating reagent with Et$_3$N as a base.

This difficulty experienced during purification of reaction products could be attributed to a number of mono, di, tri & tetra-sulfated side-products within the reaction mixture. As for reaction not going to completion with only the desired sulfation, this could be due to anion-anion repulsion occurring from the first sulfated site preventing the second, third or fourth sulfation from occurring on the same molecule. Uncompleted reactions leading to a number of products in the reaction mixture after sulfation has been reported by others in the literature (Strätz *et al.*, 2019). However, this theory does not account for why (with the case of the bis-betaaminol with four potential sulfation sites) a fully sulfated molecule with four sulfates on was detected during LC-MS analysis (M-SO$_3$H).

Analysis of the ^{1}H-NMR spectras of some the final compounds showed many merged peaks at around 3.5-4.0ppm, it is expected that these peaks could be a combination of *per*sulfated products in the solution. Sites of sulfation could not be accurately detected with simple 1D-

NMR spectrums. The only information obtained relating to potential sulfation sites is the downfield shifting of the proton(s) adjacent to the *O* & *N*-sulfate groups once sulfation had completed. As compounds could only be assigned with extreme tentativeness with only NMR analysis, further analytical investigation was needed.

Assignment of peaks in both $^{13}$C and $^{1}$H-NMR spectrums for some compounds are unavailable due to compounds not being subsequently purified to assign peaks accurately. These spectra have been included in the supporting information.

Compound 22 had a messy spectrum in the aromatic region, with doublet and doublet-doublet splitting seen. These protons only integrated to around 0.5-0.6, leading the author to believe that this reaction also contained multiple sulfated products which were giving odd splitting patterns (Figure 20).
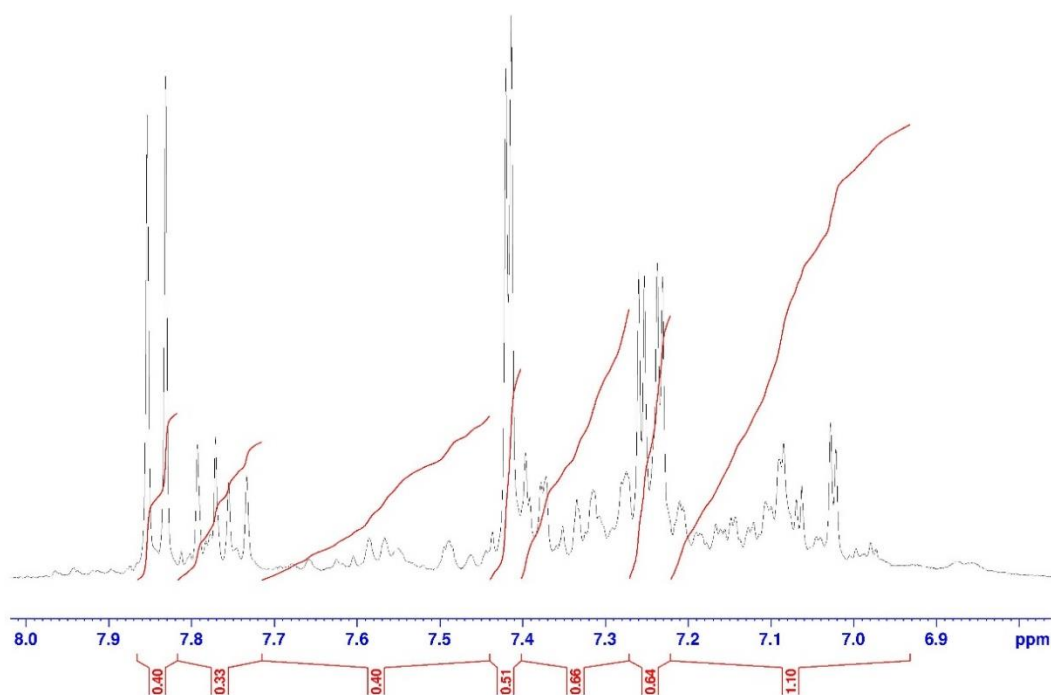


Figure 20: Expanded region of 7.0-8.0 ppm. Integral curves have been included.

The NMR spectra from both the starting material and the sulfation product are visible below in figure 21. This compound could not be accurately assigned with the NMR.
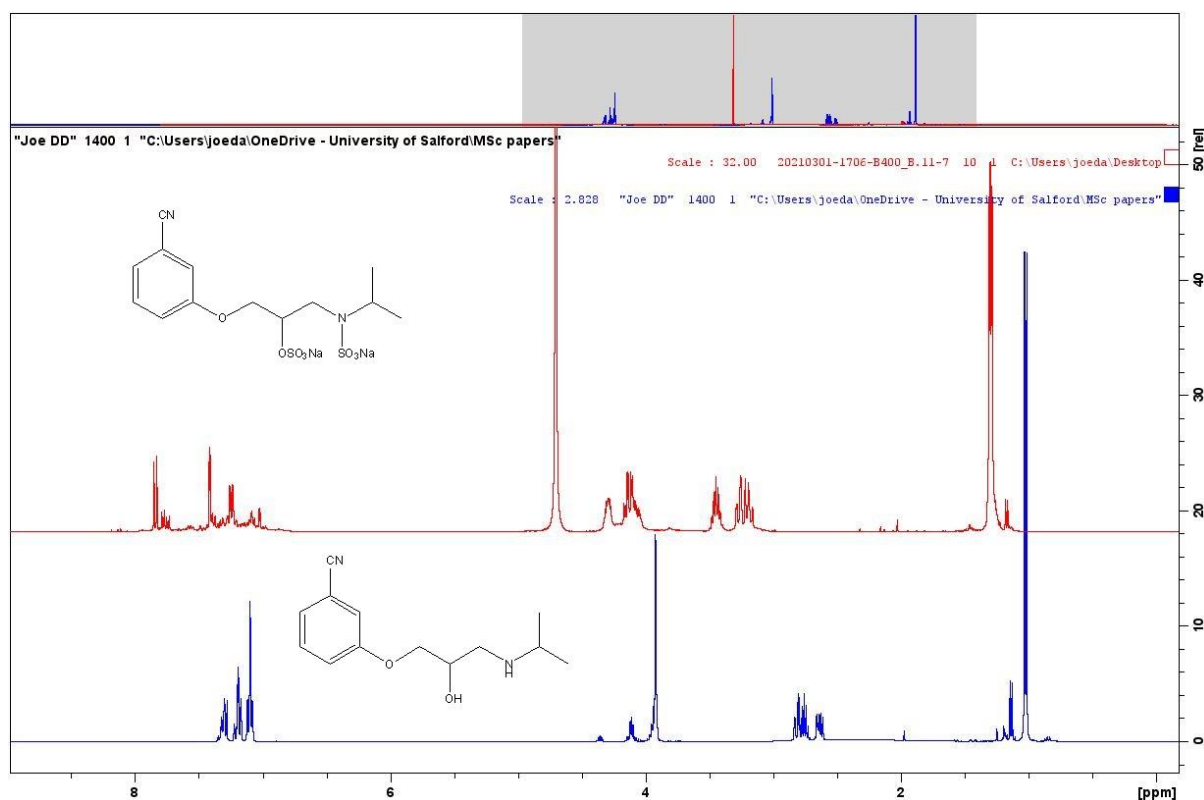
Figure 21: NMR Spectrums for the starting material (blue) & sulfation product (red).

Although NMR is a "gold standard" for analysis by organic chemists, limitations exist for the analysis of our highly sulfated molecules. NMR can give tentative evidence due to upfield shifting of adjacent protons to sulfate groups and sulfate esters. The proton in the -SO₃H group will be labile and will switch out for $^2$D in solution and is therefore not seen and cannot provide any further evidence for sulfation.

LC-MS analysis of the compounds was also very tricky. It was decided to analyse the molecules in both positive ESI & negative ESI mode to gauge which mode would be better for analysis. We decided to use negative ESI mode to see if the M-H or M-SO₃H ion fragments were visible. As high-resolution mass spectrometry or tandem MS/MS was not available at the time, low-resolution MS was the only option. It is worth noting that the Na⁺ atom on certain molecules have been replaced as the H⁺ for the interpretation of the LC-MS spectrum as the instrument was used in negative mode for analysis and any Na⁺ ions will not be seen.

LC-MS analysis was a challenging analytical method for our molecules. At first, it was thought that the MS peaks of [M-SO₃H] might indicate a single sulfation on the molecule

since SO₃H is readily lost during sample fragmentation at the ion source. However, this could not be used for accurately determining all potential sulfations on a persulfated molecule as first though. Due to the highly acidic nature of the -SO₃H group, it is possible that the pKa of the first ionised form of the persulfated molecules could be low enough to prevent ionisation of the second, third or fourth sulfation site. The stability of the sulfate esters in the final molecules are not stable or suitable enough for ESI-MS. Doneanu, Chen & Gebler (2009) also explain that the highly acidic nature of the sulfate groups in heparin sulfate preparations make mass spectrometry of molecules containing sulfate groups a "formidable task".

Conversion of the sulfate from the free acid to the sodium salt enhances stability during electrospray ionisation at the ion source, as ESI sources can cause the formation of multiple ionised species which can decompose to yield a complicated spectra with loss of -SO₃ from the precursor ion. Studies of heparin mixtures via ESI-MS in negative mode have shown that the -SO₃ ion in highly sulfated mixtures of heparin cause an abundance of peaks in the mass spectra that can make fine structure elucidation very difficult (Naggar, Costello & Zaia, 2004)(Zaia & Costello, 2003).

Derivitisation of the sulfate moieties to the corresponding acetyl group have been shown to generate less complicated mass spectrums of chrondroitin sulfate ogliosaccharides during online LC-MS analysis (Huang, Pomin & Sharp, 2011)(Example in figure 22). Although chemical derivitisation would prevent any sulfate loss & can still show exact sulfation patterns based on the positons of the acetyl groups, it is still another synthetic step in the synthesis which may require subsequent purification before analysis.
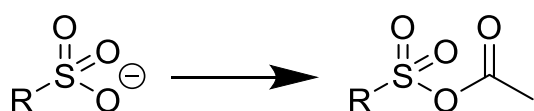


Scheme 36: Chemical derivatisation of the sulfate group to the stable -*sulfoacetyl* group.

Ensuring minimal sulfate loss at the point of ionisation would help to determine the ultimate number of sulfations, fine structural information & a total molecular profile. Minimal sulfation loss is observed when the -SO₃ ion is paired with a metal cation (such as a sodium atom), or when all the -SO₃ groups have been deprotonated.

To look at this phenomenon in different buffer systems, it was decided to swap the buffer from 0.1% formic acid to 0.05% ammonium formate to interpret the differences in spectrums on both mobile phase systems. Peaks of interest remained unchanged for both mobile phase systems but retention time increased when using a basic buffer system. At the time, the only LC-MS system available was an ESI-quadrapole.

Ultimately, the combination of issues with purification & the loss of fine structural information during analysis means we can only tentatively assign these compounds.

## 4.0 - Conclusion:

Chemical sulfation of -OH groups were best carried out using the TBSAB (Bu$_3$NSO$_3$) for column-free purification. Out of all the sulfated molecules successfully synthesised, compound 25 was the purest after work-up and subsequent cation-exchange using sodium-2-ethylhexanoate. TBSAB provides excellent regiochemical control of sulfation, much like other commercially available SO$_3$.Amine complexes. Although this methodology did not transfer across to the sulfation and purification of amine groups, further investigation into the cation-exchange of N-sulfates to the corresponding sodium salts is needed. The electronics of the molecules of interest (and increasing net negative charge with increasing sulfate groups) influences the ability of the sulfate groups to exchange cations.

The synthesis of organosulfate molecules using sulfation protocols for studies in medicinal & biochemistry studies remains an attractive project for many teams working in the field. Although sulfation chemistry is well described and single sulfations can be carried out with ease, sulfating multiple reactive sites on a single molecule whilst ensuring the correct regiospecificity of a reaction is still not well understood. Purification of highly sulfated organic molecules remains a challenge due to the electronics of sulfated molecules. Further investigation into the regiospecificity of sulfation reactions and isolation of organosulfates needs to be explored to produce a reliable protocol for both sufation and isolation of products without the cost of RP-column chromatography. Other useful investigations would include a reliable method for accurate analysis of organosulfates on ESI-MS which can be carried out on a variety of scaffolds.

## 5.0 - Appendices:

### 1-amino-3-phenoxyisopropanol (8):

### FT-IR:
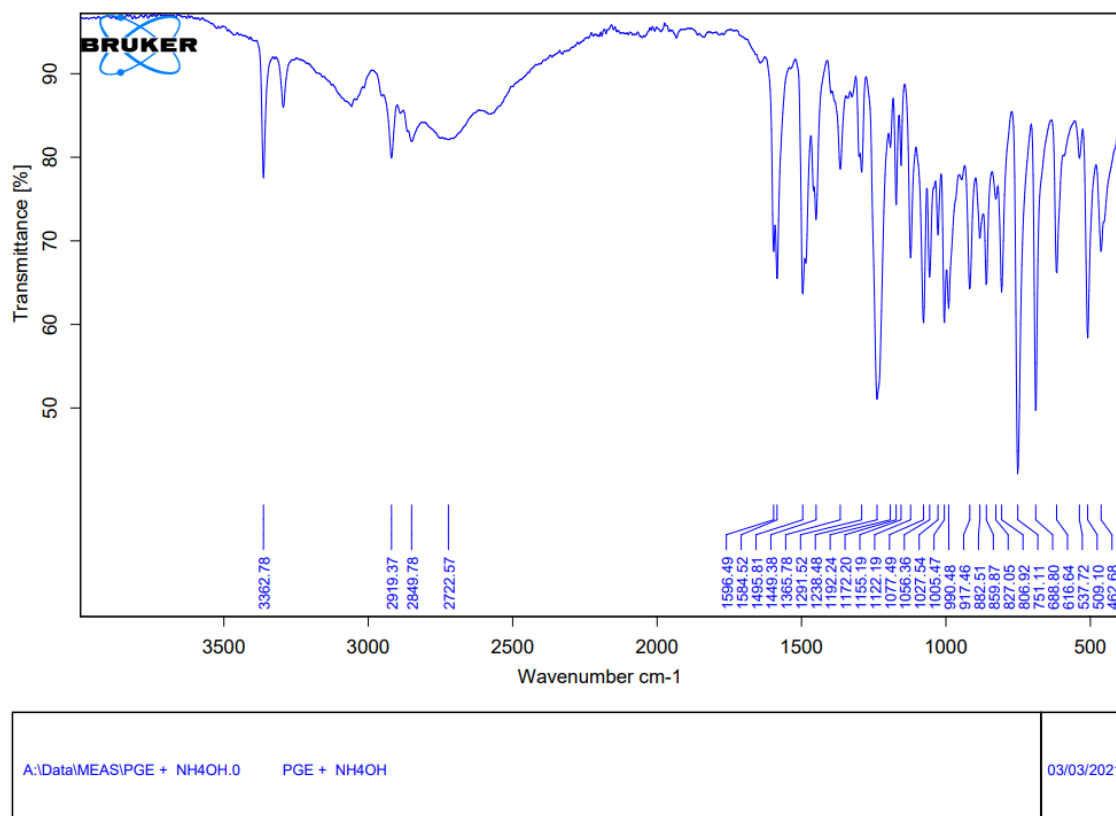


Figure 22a: FT-IR spectrum for compound 8
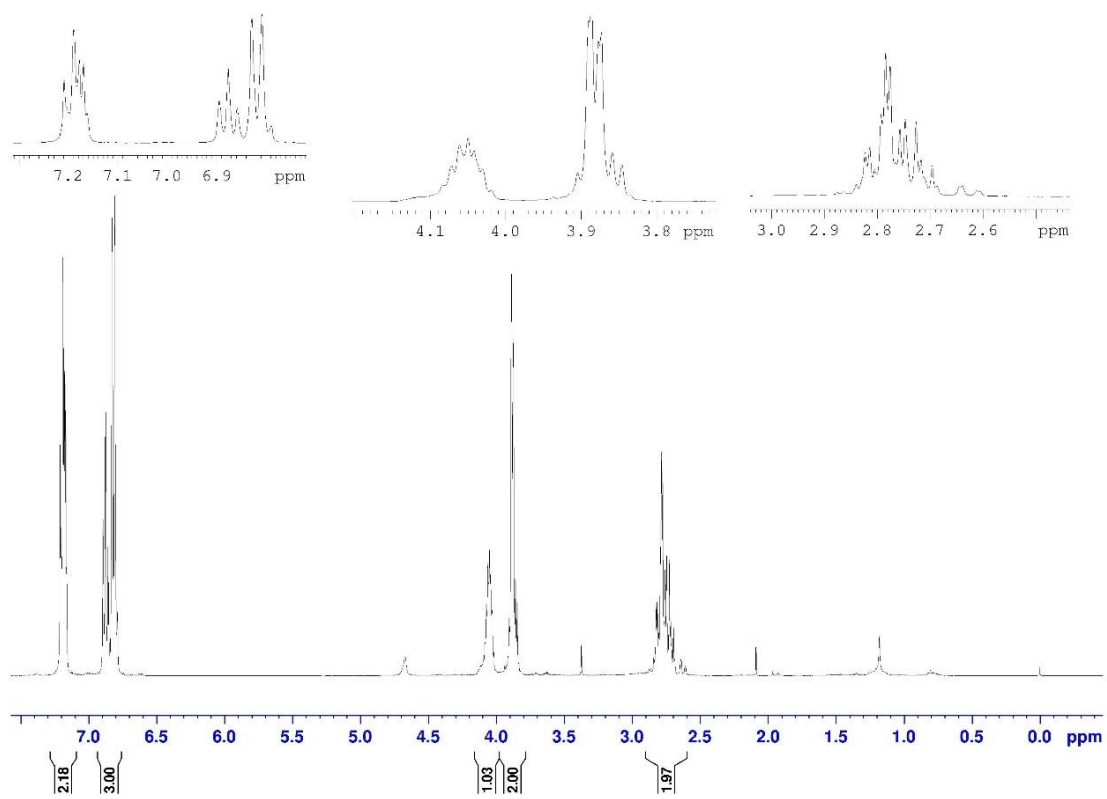
## ¹H-NMR:



Figure 22b: ¹H-NMR spectra for compound 8

**1-Isopropylamino-3-phenoxypropan-2-ol (10):**

**FT-IR:**
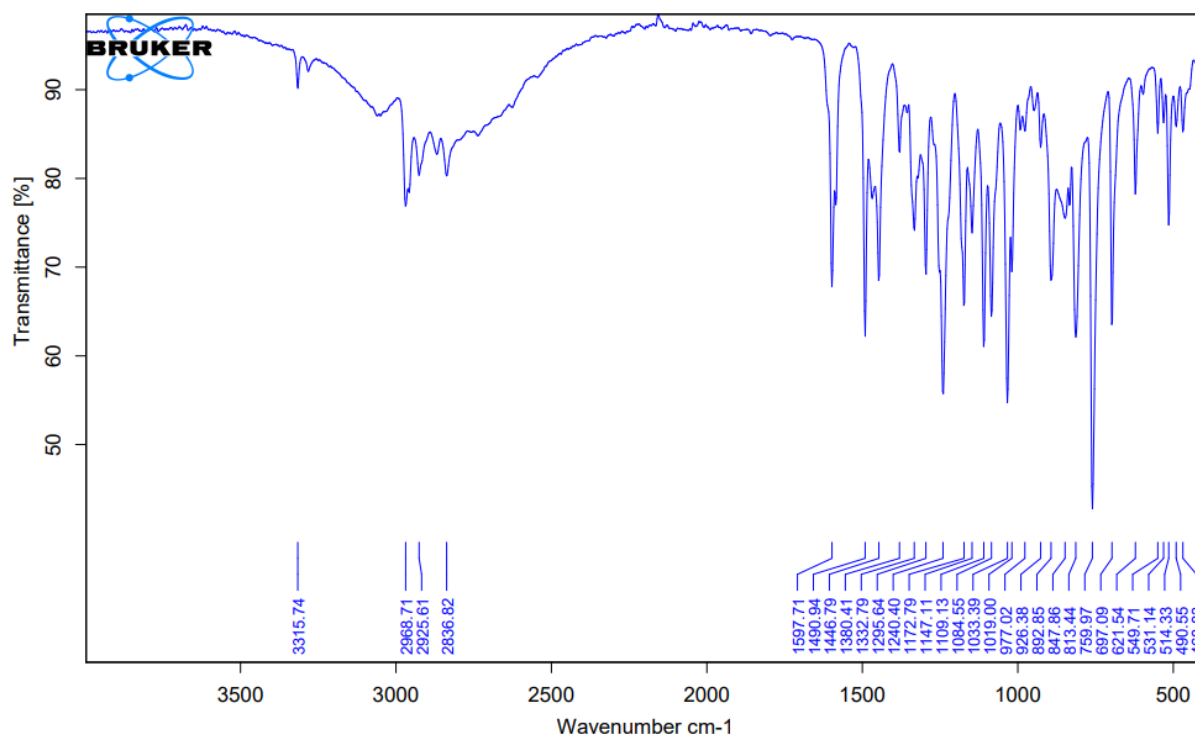
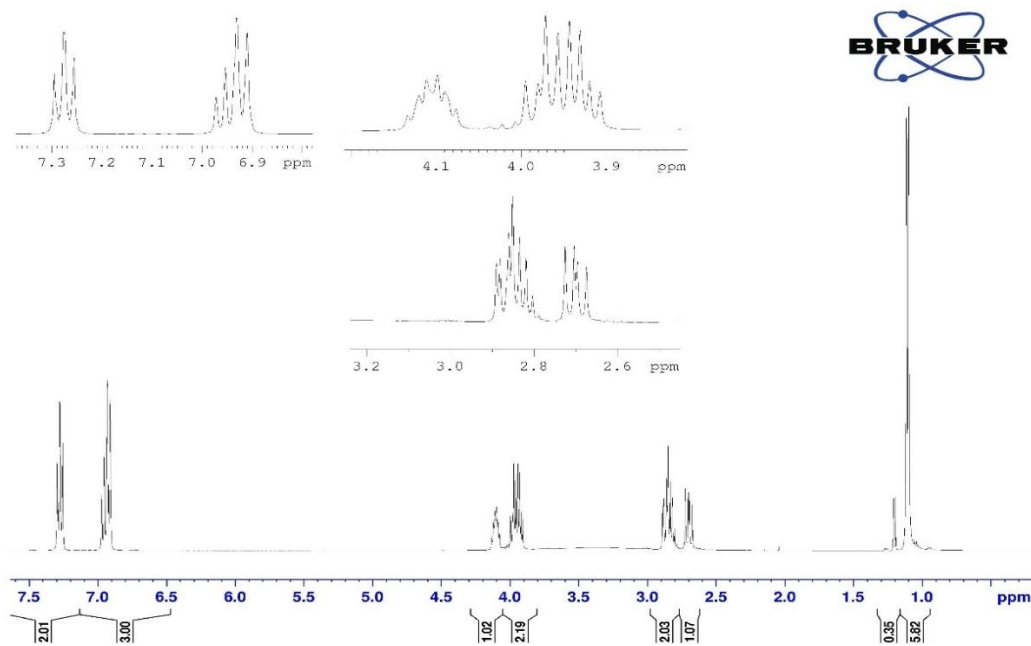

Figure 23: FT-IR of compound 10

**^{1}H-NMR:**



Figure 24: ^{1}H-NMR spectra for compound 10

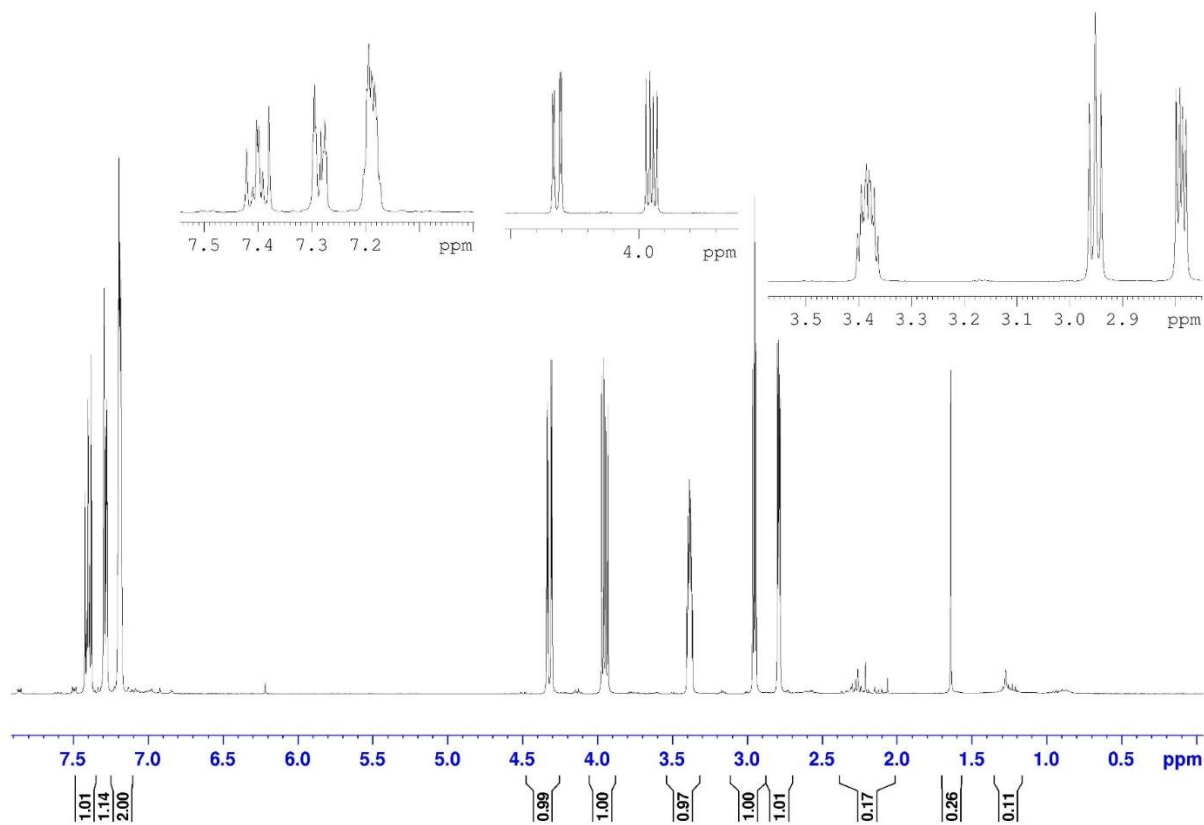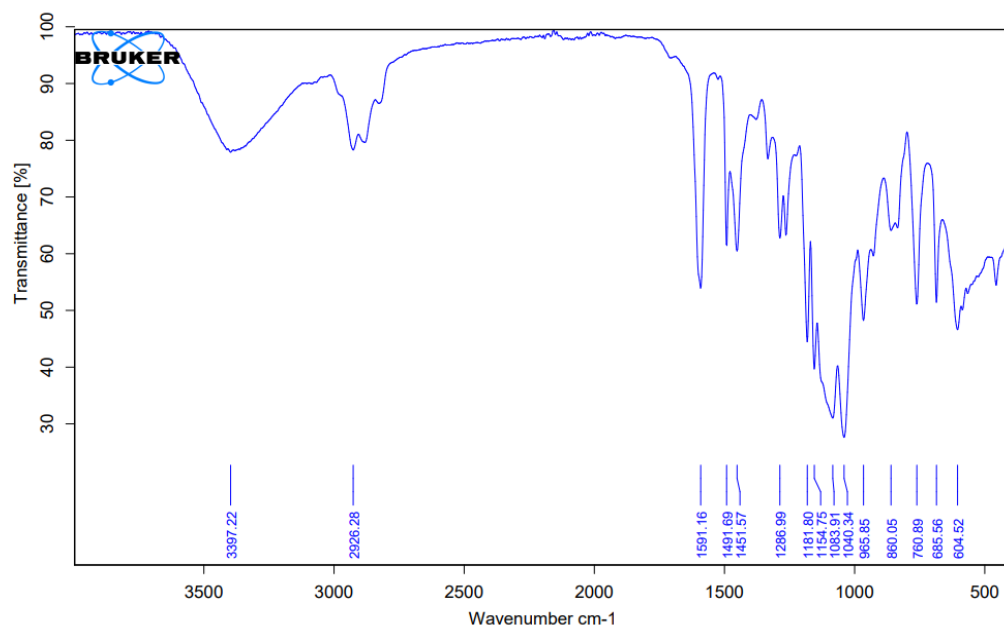**3-Cyanophenyl glycidyl ether (7a):**

**<sup>1</sup>H-NMR:**



Figure 25: <sup>1</sup>H-NMR spectra for 3-Cyanophenyl glycidyl ether

## 1-[3-(2-hydroxy-3-methoxypropoxy)phenoxy]-3-methoxypropan-2-ol (13):

## FT-IR:

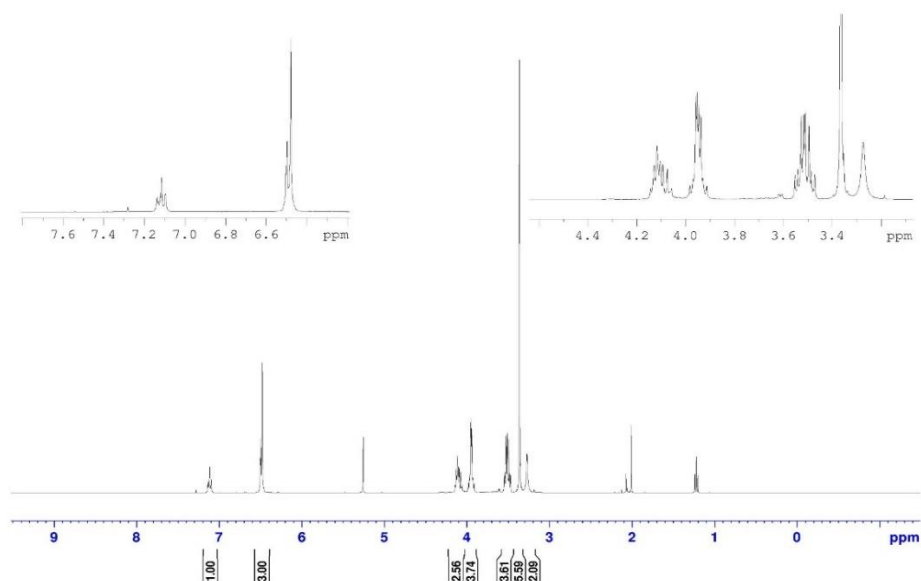

Figure 27: FT-IR spectra for compound 13

## ¹H-NMR:



Figure 28: ¹H-NMR spectra for compound 13

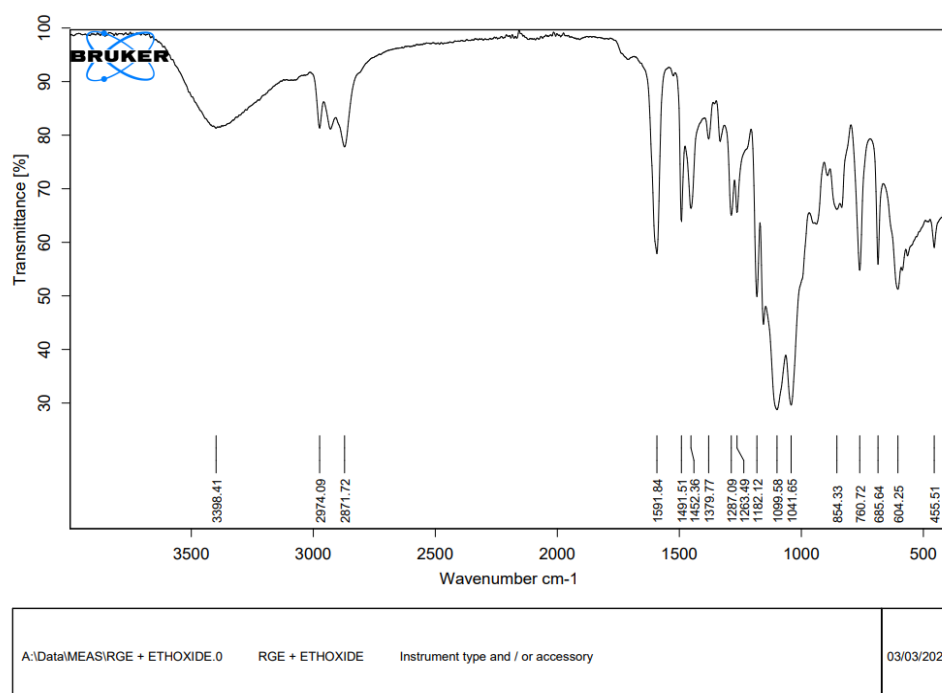## 1-[3-(2-hydroxy-3-ethoxypropoxy)phenoxy]-3-ethoxypropan-2-ol (14):

## FT-IR:



Figure 29: FT-IR spectra for compound 14

**¹H-NMR:**
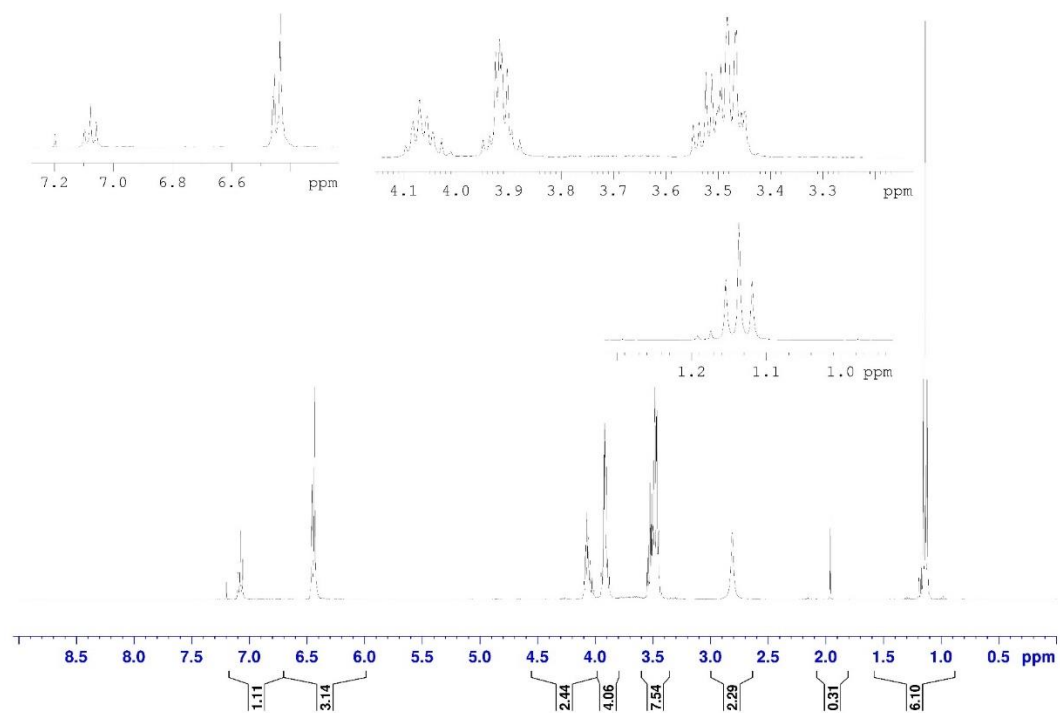


Figure 30: ¹H-NMR spectra for compound 14

## 1,3-Bis-(3-amino-2-hydroxypropyloxy)benzol (15):

### FT-IR:



Figure 32: FT-IR spectra for compound 15

### ¹H-NMR:
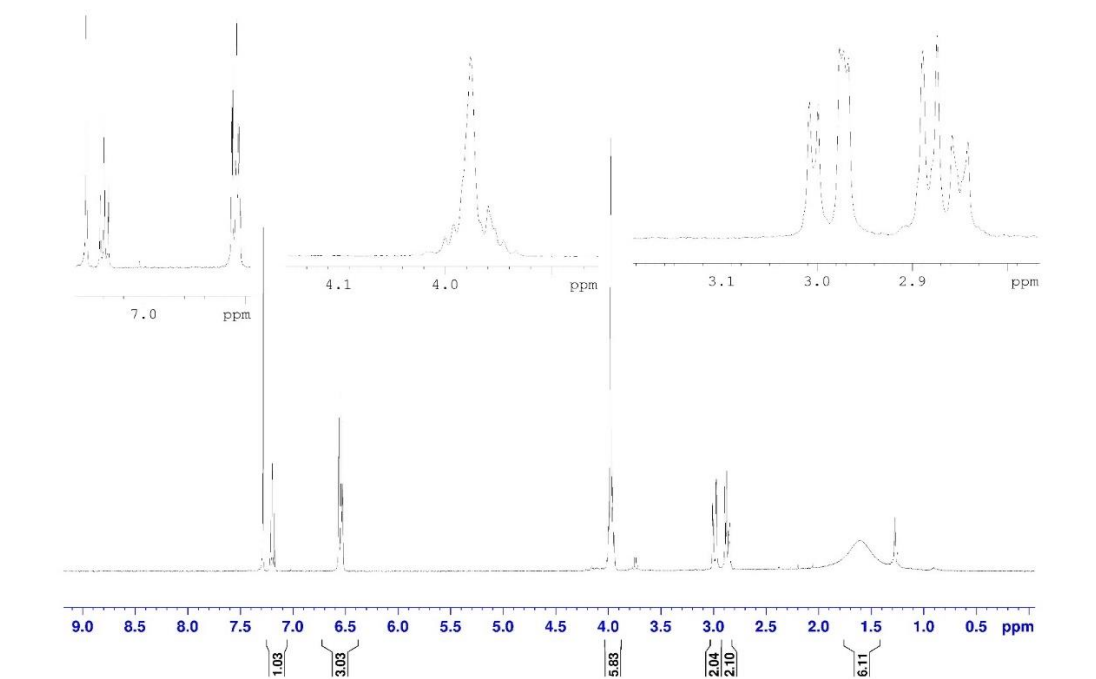
Figure 33: $^1$H-NMR spectra for compound 15

## $^{13}$C-NMR:
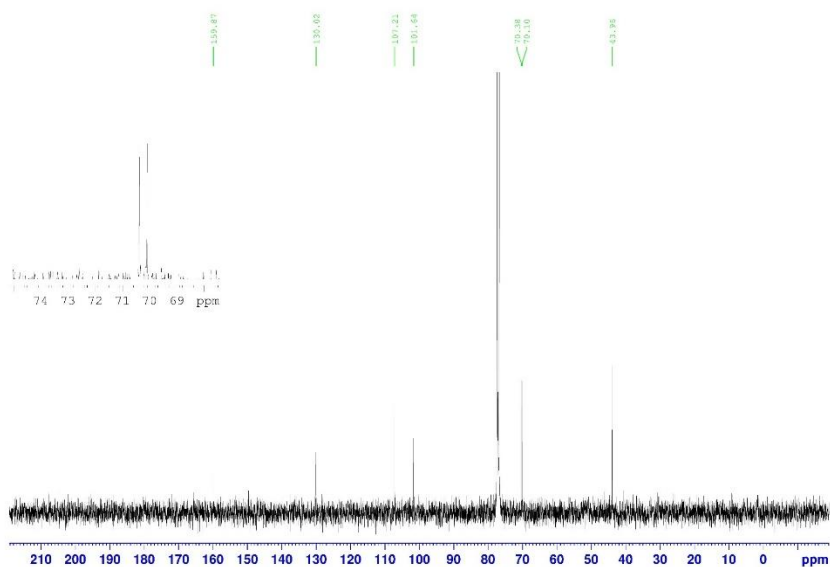


Figure 34: $^{13}$C-NMR spectra for compound 15

## LRMS:
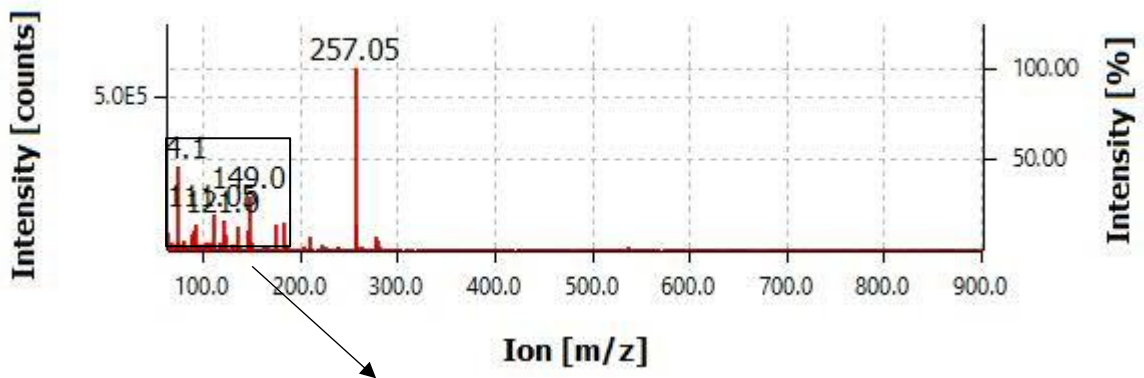
Figure 35: Ion count graph for compound 15 with enhanced zoom region.

## 1,3-Bis-(3-isopropylamino-2-hydroxypropyloxy)benzol (17):

## FT-IR:



Figure 36: FT-IR spectra for compound 17
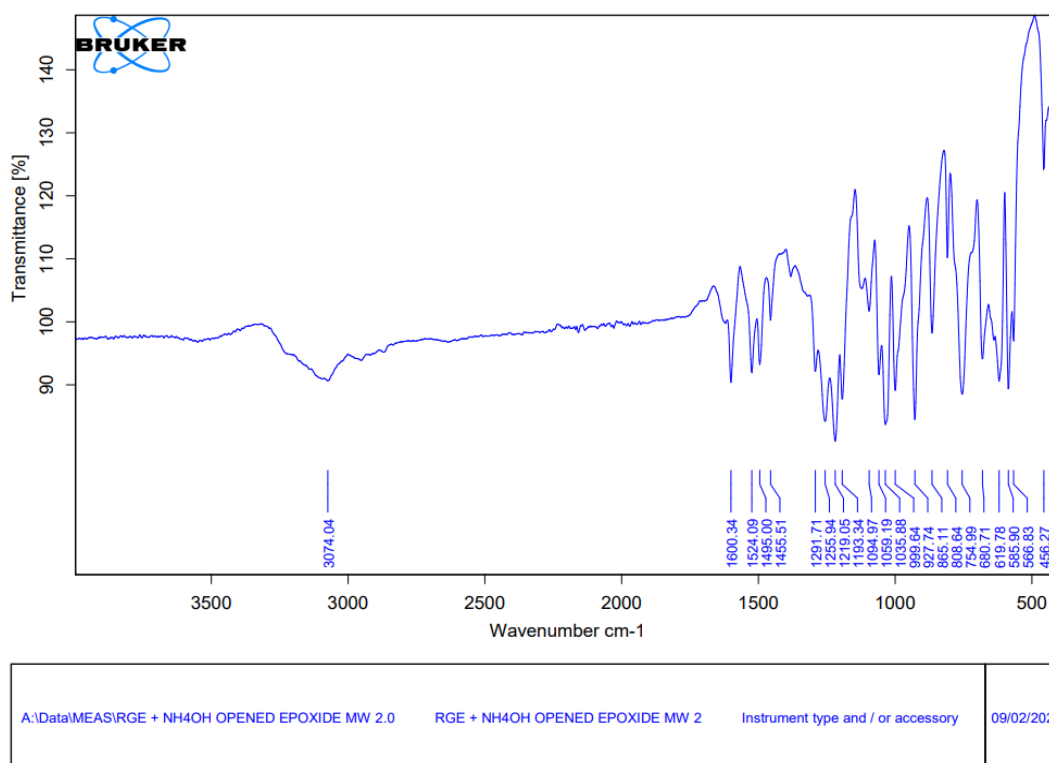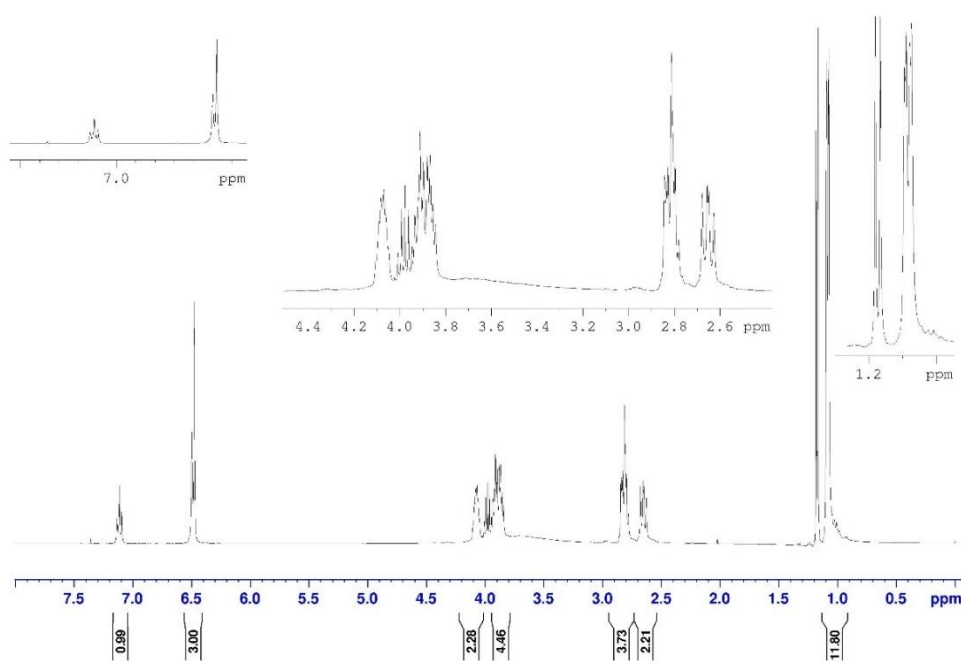
## <sup>1</sup>H-NMR:

**¹H-NMR:**



Figure 37: ¹H-NMR spectra for compound 17

## 1,3-Bis-(3-diisopropylamino-2-hydroxypropyloxy)benzol (18):
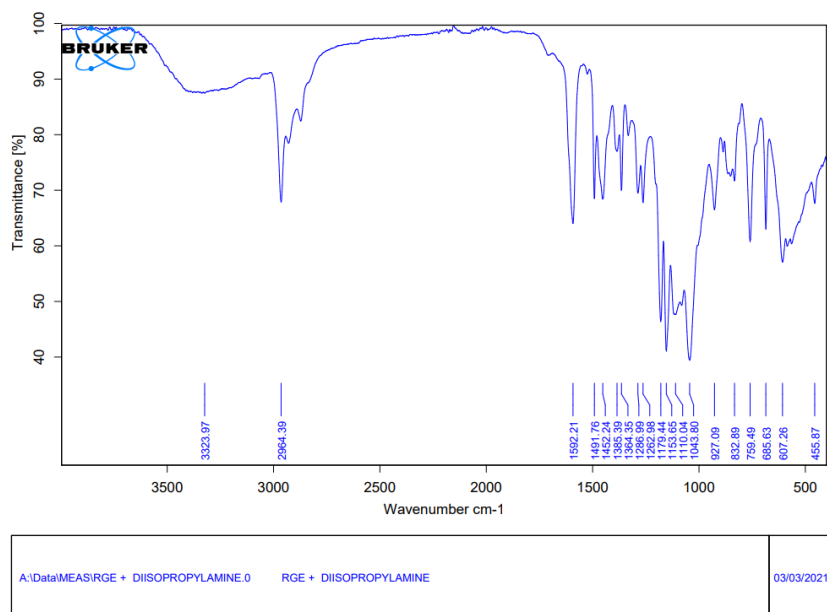
## FT-IR:



Figure 38: FT-IR spectra for compound 18

## ¹H-NMR:



Figure 39: ¹H-NMR spectra for compound 18

**<sup>13</sup>C-NMR:**
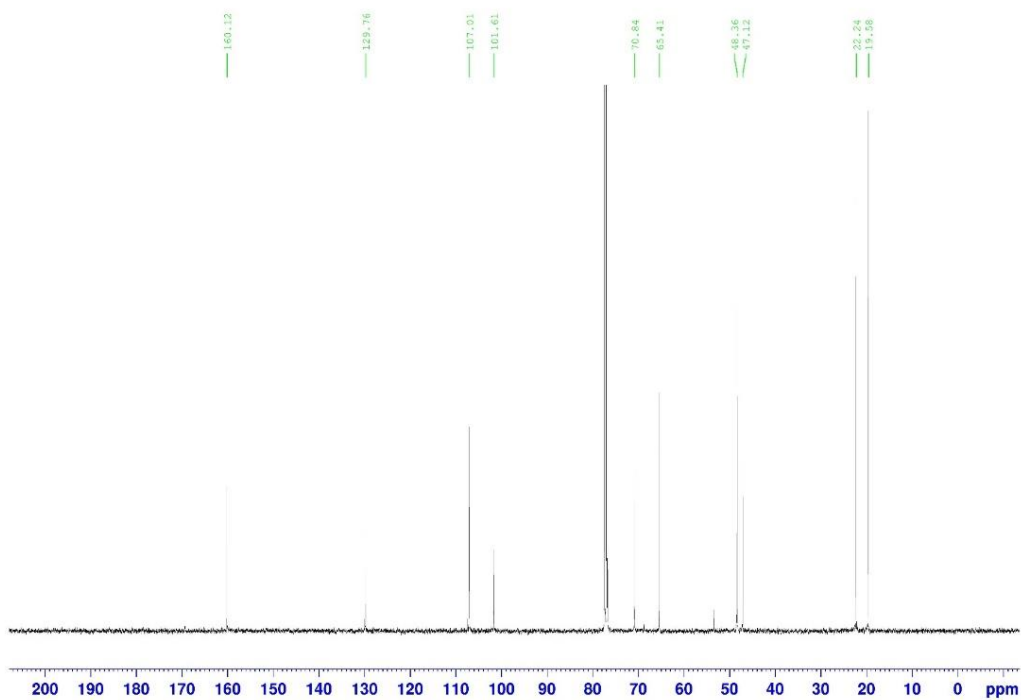


Figure 40: <sup>13</sup>C-NMR spectra for compound 18

**LRMS:**
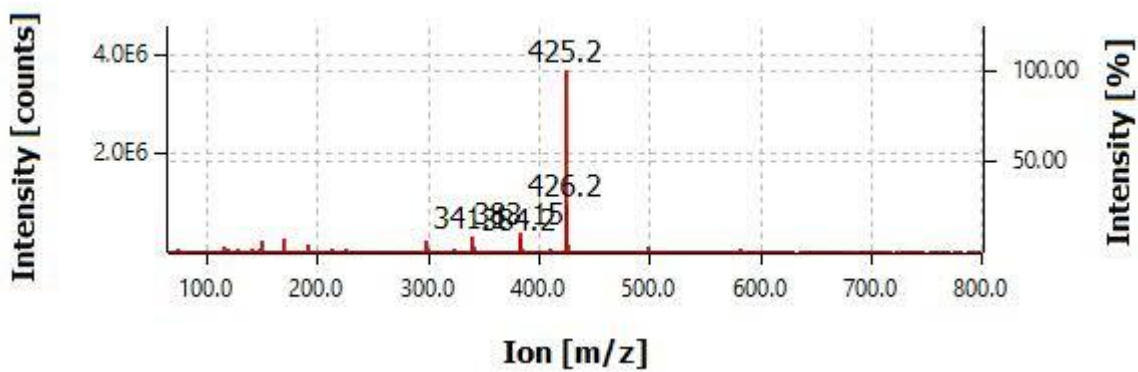


Figure 41: LRMS ion count graph for compound 18

## 1,3-Bis-(3-diethylamino-2-hydroxypropyloxy)benzol (19):
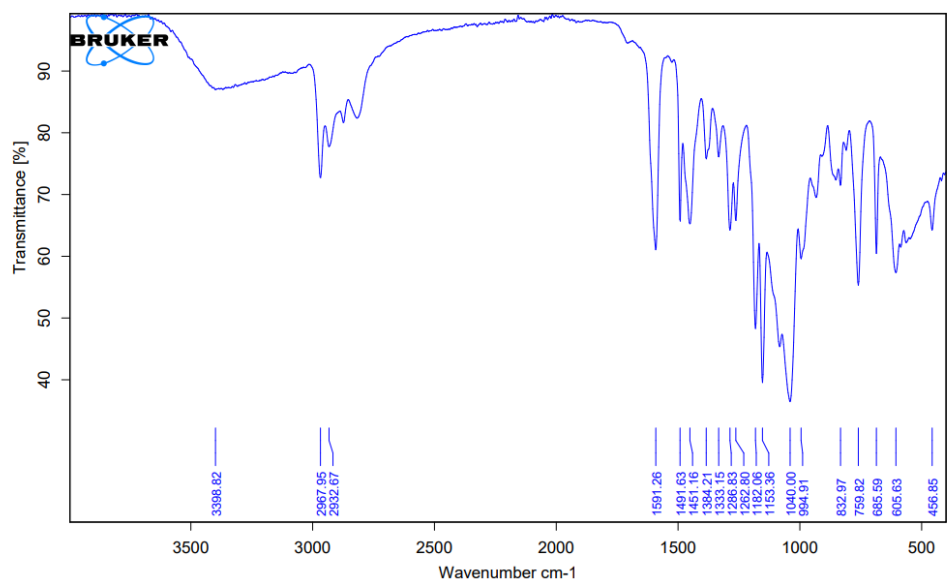
## FT-IR:



Figure 42: FT-IR spectra for compound 19

**¹H-NMR:**
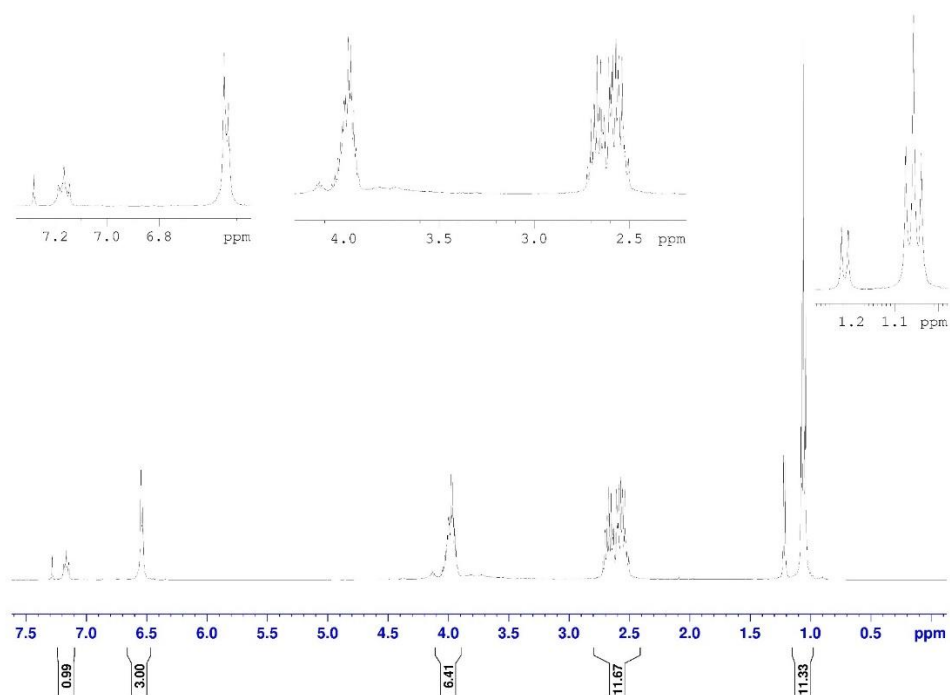


Figure 43: ¹H-NMR spectra for compound 19

**sodium 1-(isopropyl(sulfonato)amino)-3-phenoxypropan-2-yl sulfate (22):**

**FT-IR:**
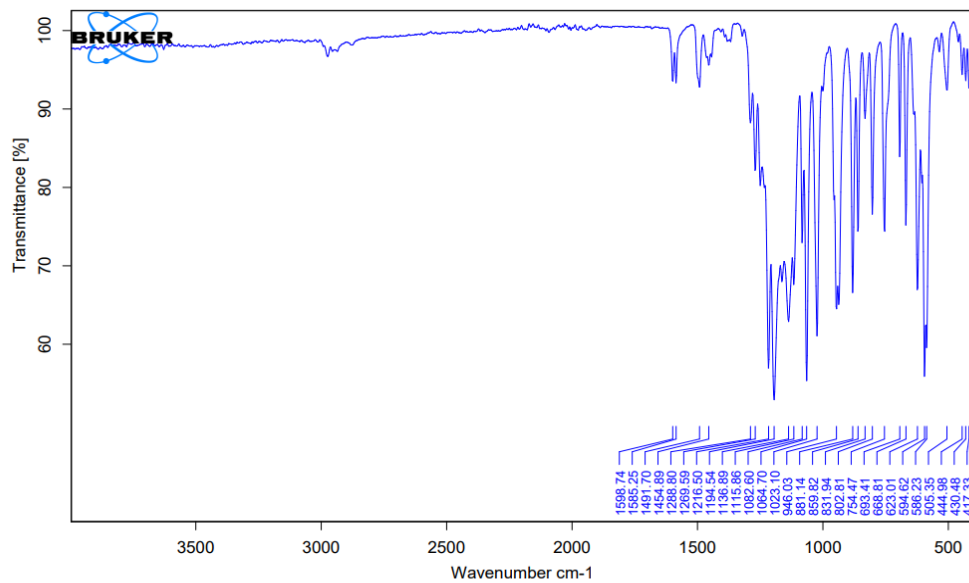


Figure 44: FT-IR spectra for compound 22

**¹H-NMR:**
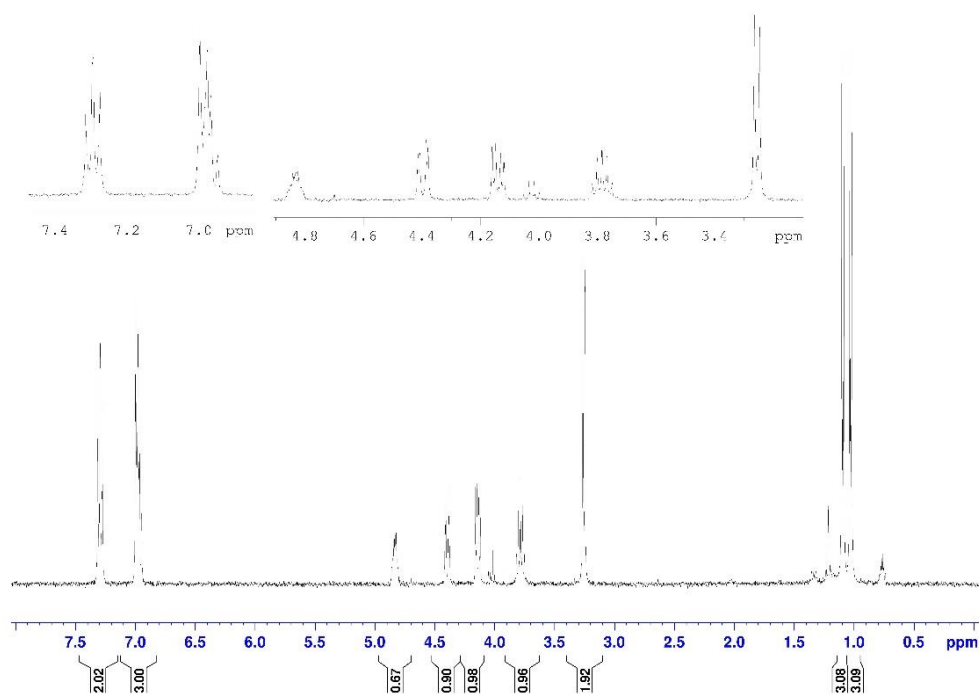


Figure 45: ¹H-NMR spectra for compound 22

**LRMS:**
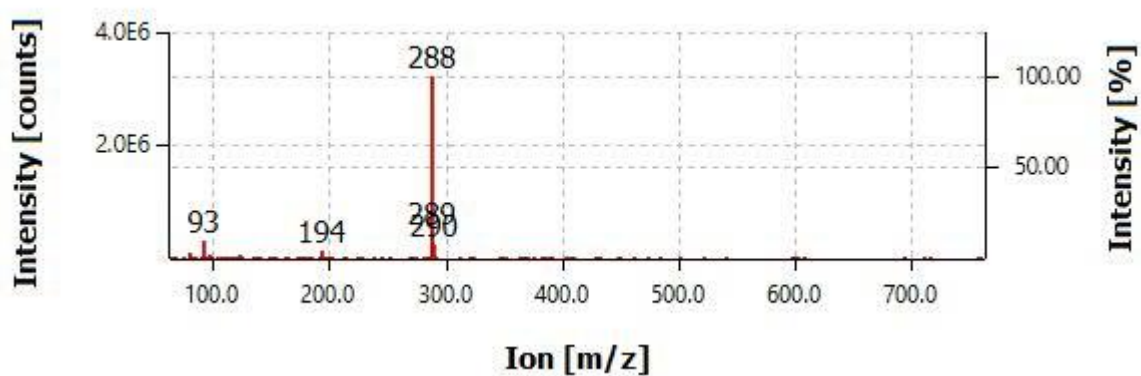


Figure 46: LRMS ion count table for compound 22

**sodium (1,3-phenylenebis(oxy))bis(3-methoxypropane-1,2-diyl) bis(sulfate)(25) :**

**FT-IR:**
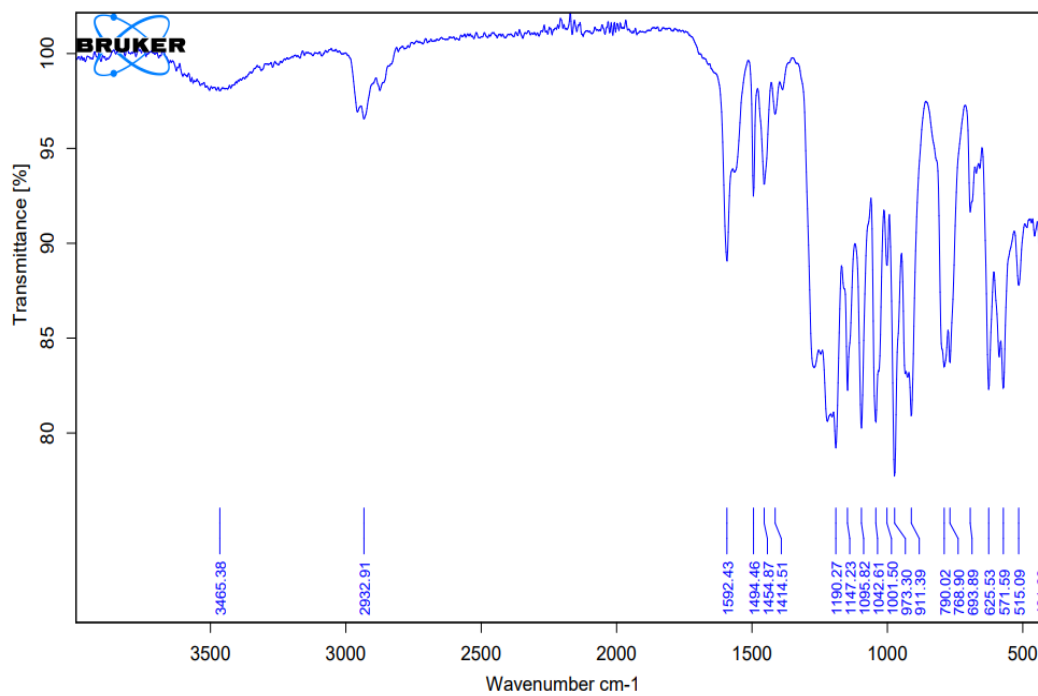


Figure 47: FT-IR spectra for compound 25

**1H-NMR:**
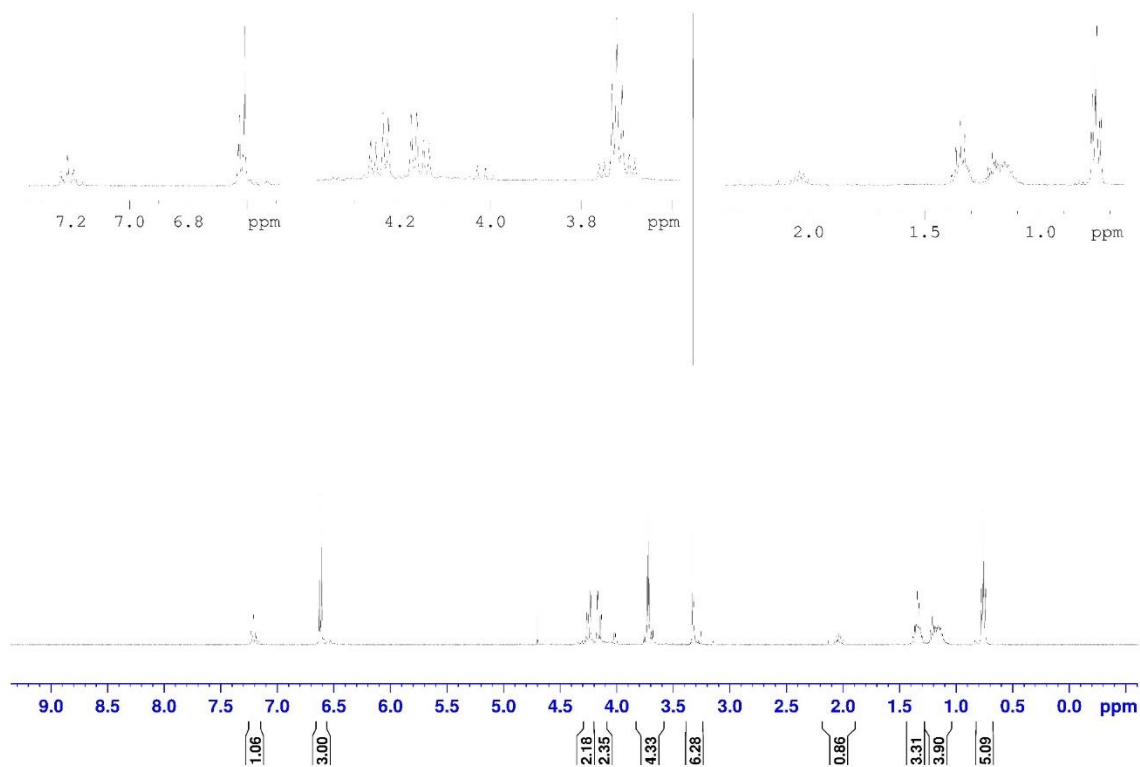


Figure 48: $^1$H-NMR spectra for compound 25

**$^{13}$C-NMR:**
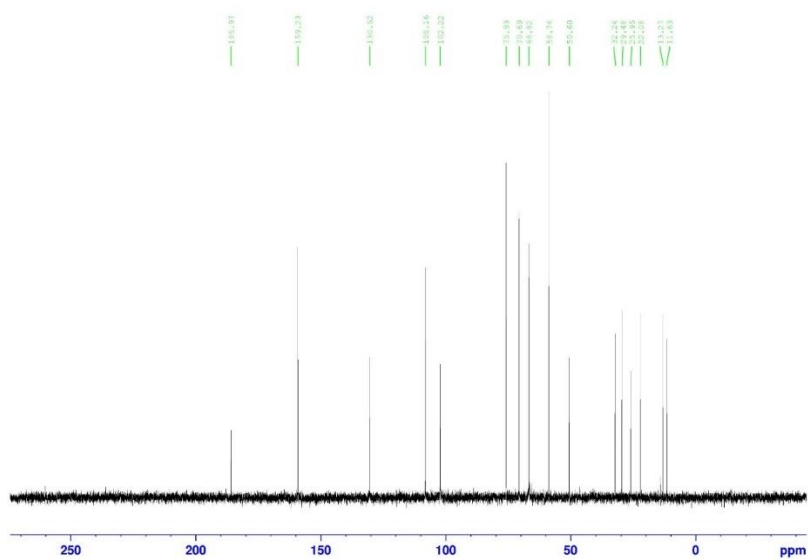


Figure 49: $^{13}$C-NMR spectra for compound 25

**LRMS:**
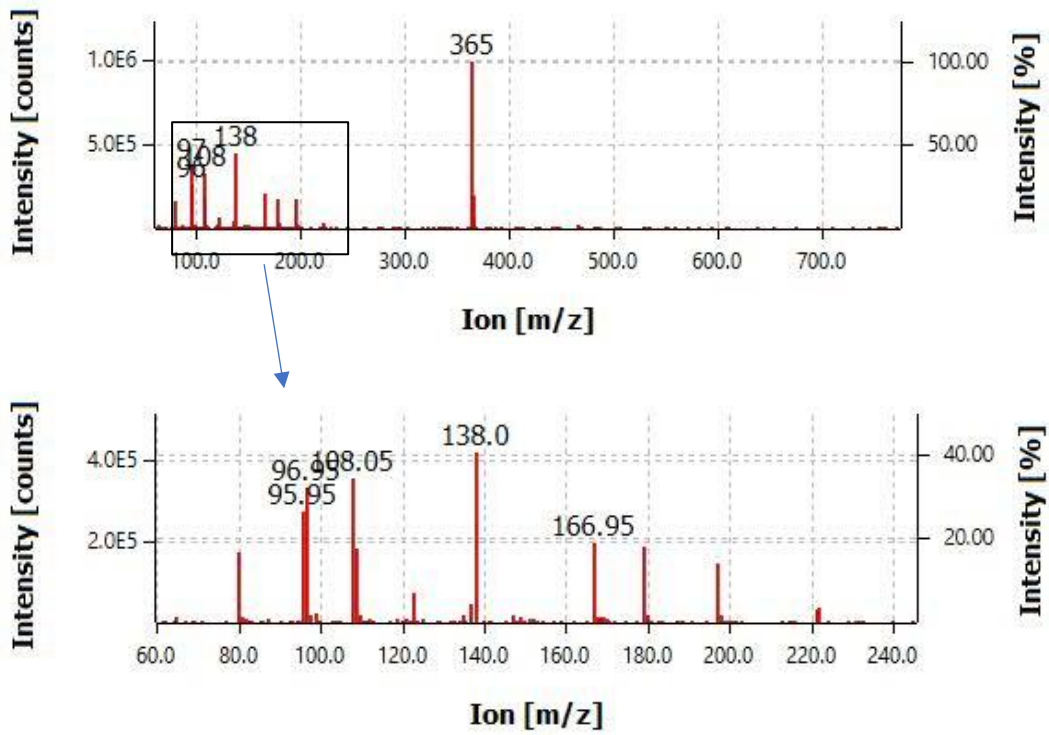


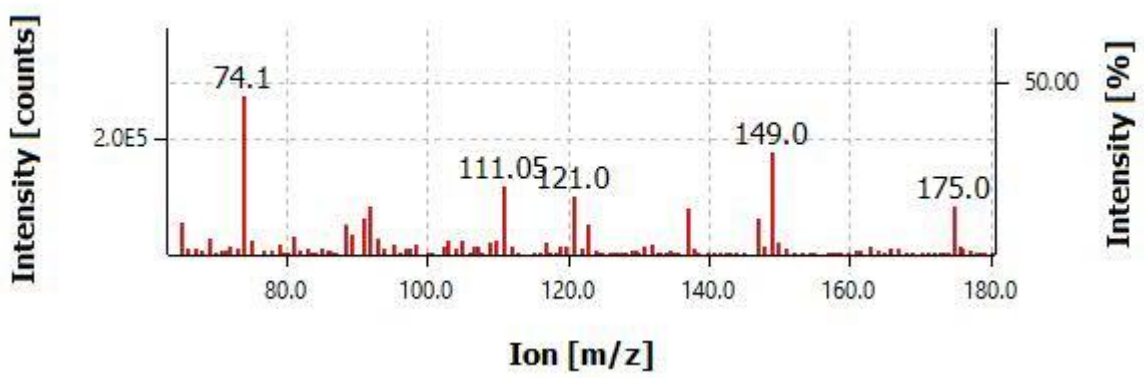Figure 50: LRMS ion count graph for compound 25

## sodium 1-(sulfonatoamino)-3-(4-sulfonatophenoxy)propan-2-yl sulfate (31):

## FT-IR:
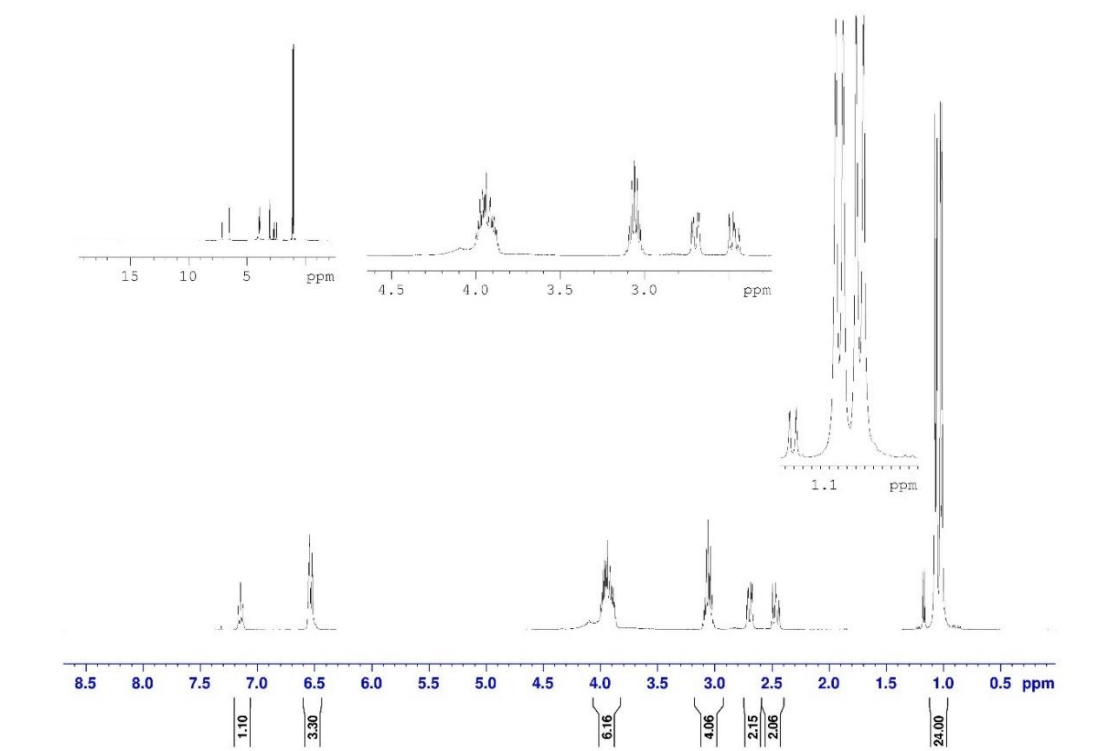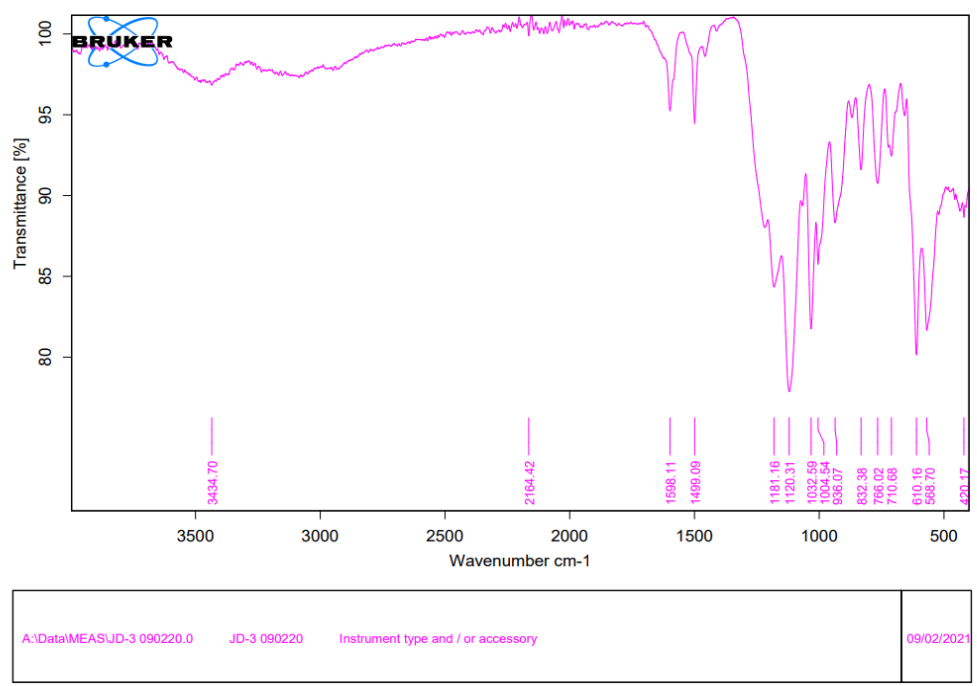


Figure 51: FT-IR spectra for compound 31
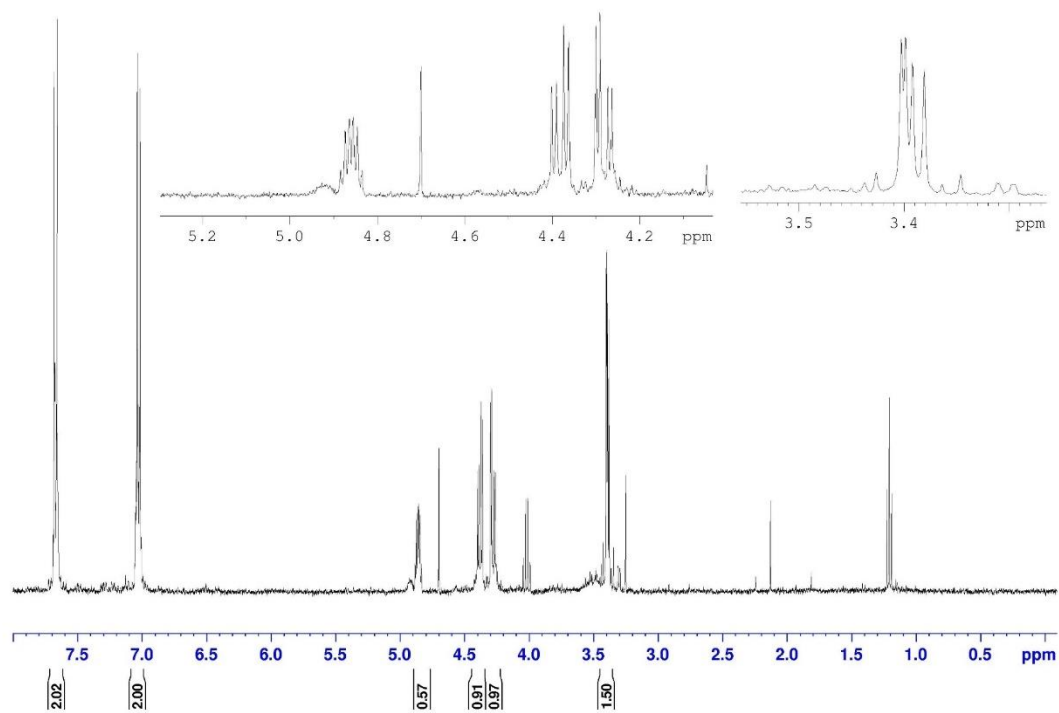
Figure 52: ¹H-NMR spectra for compound 31

**¹³C-NMR:**
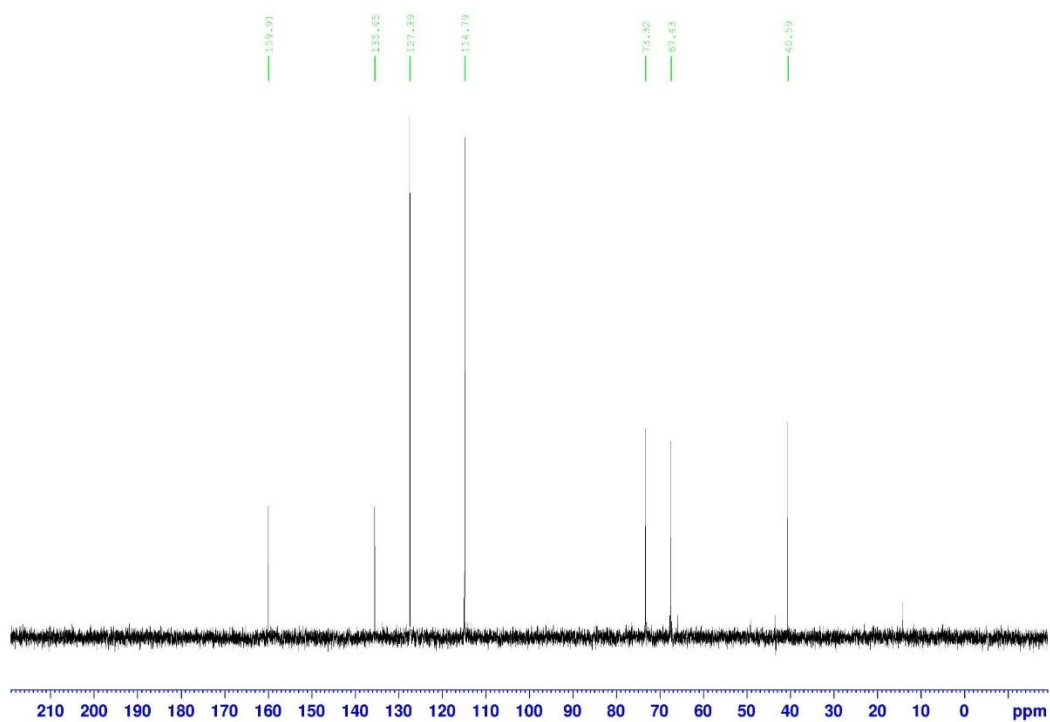


Figure 53: ¹³C-NMR spectra for compound 31

**LRMS:**
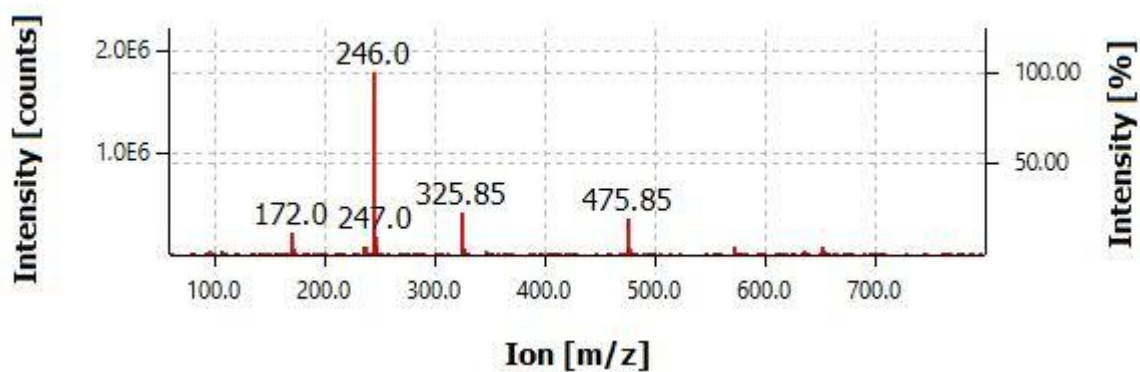


Figure 54: LRMS ion count graph for compound 31

## Sodium 1-(3-cyanophenoxy)-3-(sulfatoamino)propan-2-yl sulfate (33):

FT-IR:
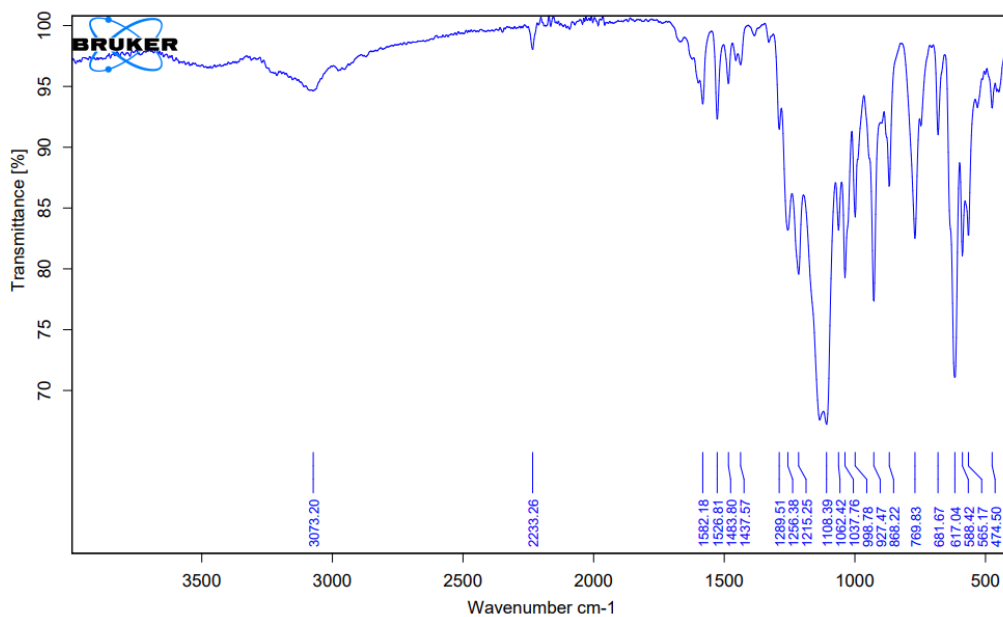


Figure 55: FT-IR spectra for compound 33

**¹H-NMR:**
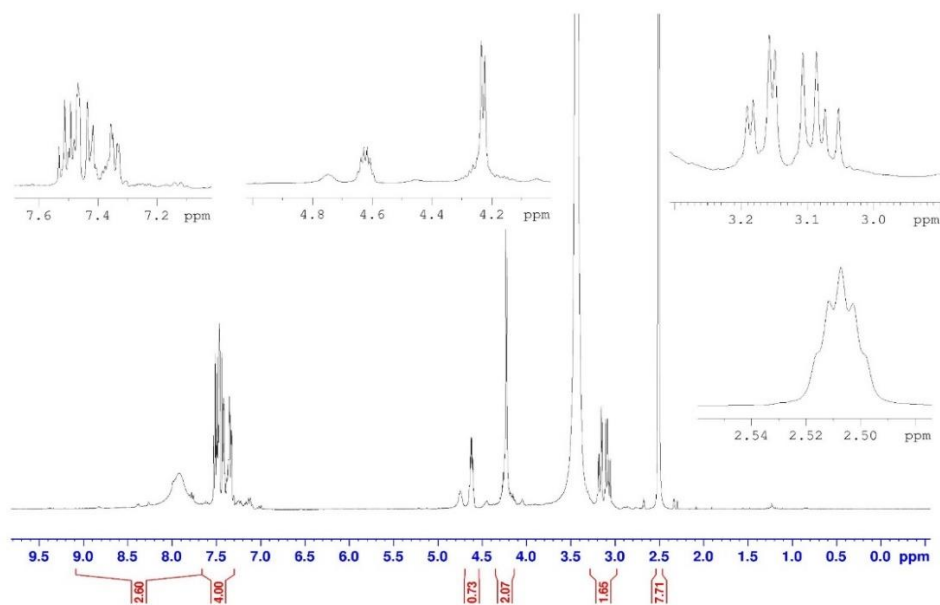


Figure 56: ¹H-NMR spectra for compound 33

**LRMS:**
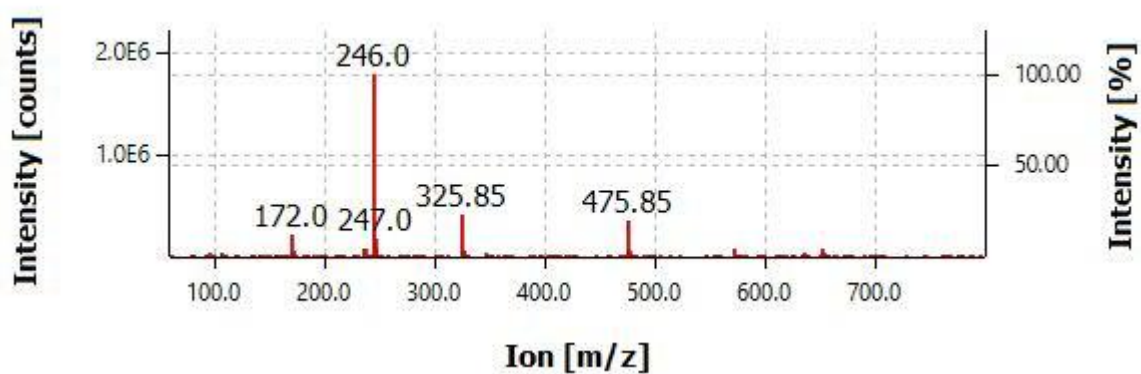


Figure 57: LRMS ion count graph for compound 33

## sodium ((4,6-disulfonato-1,3-phenylene)bis(oxy))bis(3-(isopropyl(sulfonato)amino)propane-1,2-diyl) bis(sulfate) (36):

### ^{1}H-NMR:
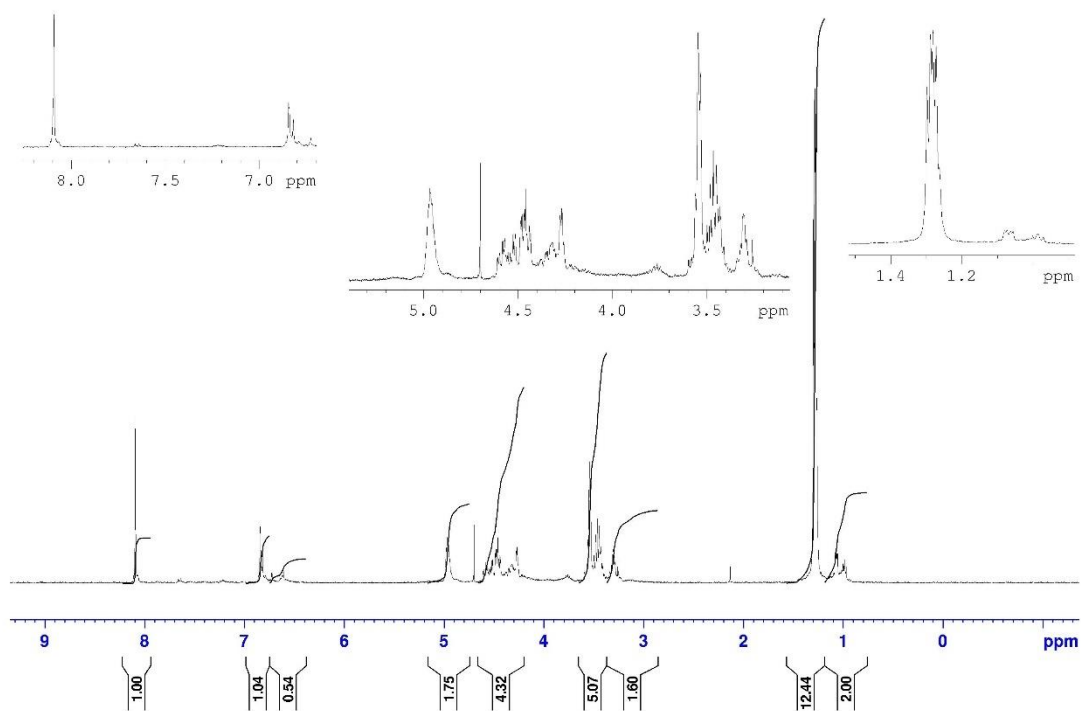


Figure 58: ^{1}H-NMR spectra for compound 36

**Sodium (1,3-phenylenebis(oxy))bis(3-(sulfonatoamino)propane-1,2-diyl) bis(sulfate) (3f -
37):**

**LRMS:**
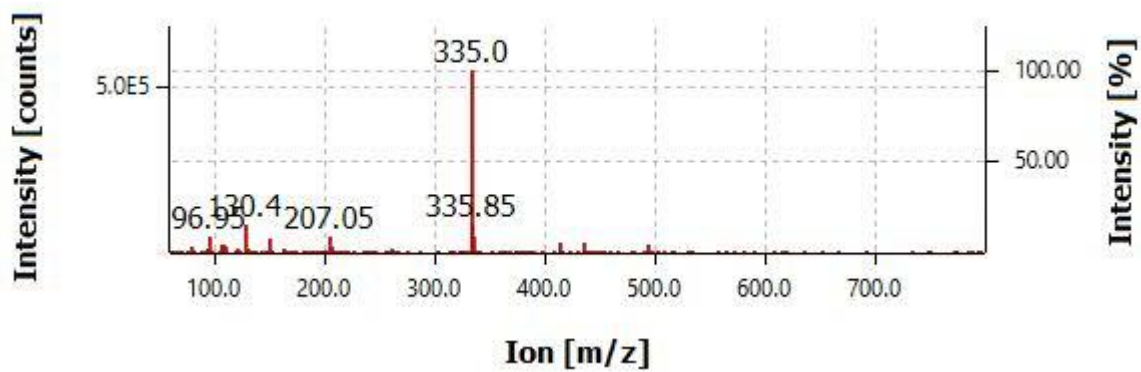


Figure 59: LRMS ion count table for compound 37

## 6.0 - References:

Afosah, D. K., Al-Horani, R. A., Sankaranarayanan, N. V. & Desai, U. R. (2016). Potent, Selective, Allosteric inhibition of human plasmin by sulfated non-saccharide glycosaminoglycan mimetics. *Journal of medicinal chemistry, 60*(2), 641-657. Doi: 10.1021/acs.jmedchem.6b01474

Aikawa, J., Grobe, K., Tsujimoto, M. & Esko, J. D. (2000). Multiple Isozymes of Heparan Sulfate/Heparin GlcNAc N-Deacetylase/GlcN N-Sulfotransferase. *The journal of biological chemistry*, *276*(8), 5876-6882. Doi: 10.1074/jbc.M009606200

Alshehri, J. A., Benedetti, A. M. & Jones, A. M. (2020). A novel exchange method to access sulfated molecules. *Scientific reports*, *10*, 16559. Doi: 10.1038/s41598-020-72500-x

Apparu, M., Tiba, Y. B., Léo, P., Hamman, S. & Coulombeau, C. (2000). Determination of the enantiomeric purity and the confguration of b-aminoalcohols using (R)-2-fluorophenylacetic acid (AFPA) and fluorine-19 NMR: application to b-blockers. *Tetrahedron asymmetry*, *11*(14), 2885-2898. Doi: 10.1016/S0957-4166(00)00254-8

Basilico, C., Arnesano, A., Galluzzo, M., Comoglio, P. M. & Michieli, P. (2008). A High Affinity Hepatocyte Growth Factor-binding Site in the Immunoglobulin-like Region of Met. *The journal of biological chemistry, 283*(30), 21267-21277. Doi: 10.1074/jbc.M800727200

Benedetti, A. M., Gill, D. M., Tsang, C. W. & Jones, A. M. (2019). Chemical methods for N- and O-sulfation of small molecules, amino acids and peptides. *ChemBioChem*, *21*(7), 938-942. Doi: 10.1002/cbic.201900673

Bishop, J. R., Schuksz, M. & Esko, J. D. (2007). Heparan sulphate proteoglycans fine-tune mammalian physiology. *Nature*, *446*, 1030-1037. Doi: 10.1038/nature05817

Bolten, S. N., Rinas, U. & Scheper, T. (2018). Heparin: role in protein purification and substitution with animal-component free material. *Applied microbiology and biotechnology*, *102*(20), 8647-8660. Doi: 10.1007/s00253-018-9263-3

Bonfim-Silva, R., Salomão, K. B., Pimentel, T. V. C. d. A., Menezes, C. C. B. d. O., Palma, P. V. B. & Fontes, A. M. (2019). Biological characterization of the UW402, UW473, ONS-76 and

DAOY pediatric medulloblastoma cell lines. *Cytotechnology 71*, 893–903. Doi:
10.1007/s10616-019-00332-3

Busse, M., Feta, A., Presto, J., Wilén, M., Grønning, M., Kjellén, L. & Kusche-Gullberg, M.
(2007). Contribution of EXT1, EXT2, and EXTL3 to Heparan Sulfate Chain Elongation. *The
journal of biological chemistry. 282*(45). 32802-32810. Doi: 10.1074/jbc.M703560200

Cancer Research UK. (2019). Medullablastoma. Retrieved from
https://www.cancerresearchuk.org/about-cancer/childrens-cancer/brain-
tumours/types/medulloblastoma

Cecchi, F., Rabe, D. C. & Bottaro, D. P. (2012). Targeting the HGF/Met signalling pathway in
cancer therapy. *Expert opinion on therapeutic targets, 16*(6), 553-572. Doi:
10.1517/14728222.2012.680967

Chakraborty, S., Balan, M., Flynn, E., Zurakowski, D., Choueiri, T. K. & Pal, S. (2019).
Activation of c-Met in cancer cells mediates growth-promoting signals against oxidative
stress through Nrf2-HO-1. *Oncogenesis*, *8*, 7. Doi: 10.1038/s41389-018-0116-9


Children with cancer UK. (2021). *About Medulloblastoma*. Retrieved from http://www.
https://www.childrenwithcancer.org.uk/childhood-cancer-info/cancer-
types/medulloblastoma/.

Correia, M. S. P., Lin, W., Aria, A. J., Jain, A. & Globisch, D. (2020). Rapid Preparation of a
Large Sulfated Metabolite Library for Structure Validation in Human Samples. *Metabolites*,
*10*(10), 415. Doi: 10.3390/metabo10100415

Dean, M., Park, M., Le Beau, M. M., Robins, T. S., Diaz, M. O., Rowley, J. D., … Woude, V.
(1985).  The human *met* oncogene is related to the tyrosine kinase oncogenes. *Nature*, *318*,
385-388. Doi: 10.1038/318385a0

Doneanu, C. E., Chen, W. & Gebler, J. C. (2009). Analysis of Oligosaccharides Derived from
Heparin by Ion-Pair Reversed-Phase Chromatography/Mass Spectrometry. *Analytical
chemistry*, *81*(9), 3485-3499. Doi: 10.1021/ac802770r

Engelman, J. A., Zejnullahu, K., Mitsudomi, T., Song, Y., Hyland, C., Park, J. O., … Jänne, P. A. (2007). MET amplification leads to Gefitinib resistance in lung cancer by activating ERBB3 signaling. *Science*, *369*(6509), 1039-1043. Doi: 10.1126/science.1141478

Faria, C., Smith, C. & Rutka, J. (2011). The role of HGF/c-met pathway signalling in human medulloblastoma. Doi: 10.5772/23296

Food and drug administration. (2020). FDA grants accelerated approval to capmatinib for metastatic non-small cell lung cancer, retrieved from https://www.fda.gov/drugs/drug-approvals-and-databases/fda-grants-accelerated-approval-capmatinib-metastatic-non-small-cell-lung-cancer

Fossati, P., Ricardi, U. & Orecchia, R. (2008). Pediatric Medulloblastoma: Toxicity of current treatment and potential role of protontherapy. (2008). *Cancer treatment reviews*, *35*, 79-96. Doi: 10.1016/j.ctrv.2008.09.002

Goodvich, L. V., Milenkovic, L., Higgins, K. M. & Scott, M. P. (1997). Altered neural cell fates and medulloblastoma in mouse *patched* mutants. *Science*, *277*(5329), 1109-1113. Doi: 10.1126/science.277.5329.1109

Gill, D. M., Male, L. & Jones, A. M. (2019). Sulfation made simple: a strategy for synthesising sulfated molecules. *Chemical communications*, *55*, 4319-4322. Doi: 10.1039/C9CC01057B

Hevey, R. (2019). Bioisosteres of carbohydrate functional groups in glycomimetic design. *Biomimetics*, *4*(3), 53. Doi: 10.3390/biomimetics4030053

Hitchcock, A. M., Yates, K. E., Shortkroff, S., Costello, C. E. & Zaia, J. (2006). Optimized extraction of glycosaminoglycans from normal and osteoarthritic cartilage for glycomics profiling. *Glycobiology*, *17*(1), 25-35. Doi: 10.1093/glycob/cw1046

Horner, M. J., Holman, K. T. & Ward, M. D. (2007). Architectural Diversity and Elastic Networks in Hydrogen-Bonded Host Frameworks: From Molecular Jaws to Cylinders. *Journal of the American chemical society*, *129*(47), 14640-14660. Doi: 10.1021/ja0741574

Huang, R., Pomin, V. H. & Sharp, J. S. (2011). LC-$MS_n$ analysis of isomeric chrondroitin sulfate ogliosaccharides using a chemical derivatization strategy. *Journal of the American society for mass spectrometry*. *22*(9), 1577-1587. Doi: 10.1007/s13361-011-0174-0

Ivanov, D. P., Coyle, B., Walker, D. A. & Grabowska, A. M. (2016). *In vitro* models of medulloblastoma: Choosing the right tool for the job. *Journal of biotechnology*, *236*, 10-25. Doi: 10.1016/j.biotec.2016.07.028

Jacobson, P. F., Jenkyn, D. J. & Papadimitriou, J. M. (1985). Establishment of a human medulloblastoma cell line and its heterotransplantation into nude mice. *The Journal of neuropathology & experimental neurology*. *44*(5), 472-485. Doi: 10.1097/00005072-198509000-00003

Juraschka, K. & Taylor, M. D. (2019). Medulloblastoma in the age of molecular subgroups: a review. *Journal of neurosurgery*, *24*(4), 353-363. Doi: 10.3171/2019.5.PEDS18381

Khatua, S., Song, A., Sridhar, D. C. & Mack, S. C. (2018). Childhood medulloblastoma: Current therapies, emerging molecular landscape and therapeutic insights. (2018). *Current neuropharmacology*, *16*(7), 1045-1058. Doi: 10.2174/1570159X15666171129111324

Kongkham, P. N., Onvani, S., Smith, C. A. & Rutka, J. T. (2010). Inhibition of the MET receptor tyrosine kinase as a novel therapeutic strategy in medullablastoma. *Translational oncology*, *3*(6), 336-343. Doi: 10.1593/tlo.10121

Korc, M. & Friesel R. E. (2009). The role of fibroblast growth factors in tumor growth. *Current cancer drug targets*, *9*(5), 639-651. Doi: 10.1274/156800909789057006

Lam, B. Q., Dai, L. & Qin, Z. (2016). The role of HGF/c-Met signalling pathway in lymphoma. *Journal of hematology & oncology*, *9*(1). Doi: 10.1186/s13045-016-0366-

Lanier, J. C. & Abrams, A. N. (2016). Posterior fossa syndrome: Review of the behavioural and emotional aspects in paediatric cancer patients. *Cancer*, *123*(4), 551-559. Doi: 10.1002/cncr.30238

Lee, D., Sing, E, Ahn, J., An, S., Huh, J. & You, W. (2015). Development of antibody-based c-Met inhibitors for targeted cancer therapy. *ImmunoTargets and Therapy*, *4*, 35-44. Doi: 10.2147/ITT.S37409

Li, L., Qiu, D., Shi, J. & Li, Y. (2016). Vicinal diamination of arenes with domino aryne precursors. *Organic letters*, *18*(15), 3726-3729. Doi: 10.1021/acs/orglett.6b01747

Li, X., Chen, N. & Xu, J. (2010). An improved and mild wenker synthesis of aziridines. *Synthesis*, *20*, 3423-3428. Doi: 10.1055/s-0030-1257913

Lidholt, K. (1997). Biosynthesis of glycosaminoglycans in mammalian cells and in bacteria. *Biochemical society transactions*, *25*(3), 866-870. Doi: 10.1042/bst0250866

Lubineau, A. & Lemoine, R. (1994). Regioselective sulfation of galactose derivatives through the stannylene procedure. New synthesis of the 3'-O-sulfated Lewis trisaccharide. *Tetrahedron letters*, *35*(47), 8795-8796. Doi: 10.1016/s0040-4039(00)78500-5

Li, Y., Lal, B., Kwon, S., Fan, X., Saldanha, U., Reznik, T. E., … Abounader, R. (2005). The Scatter Factor/Hepatocyte Growth Factor: c-Met Pathway in Human Embryonal Central Nervous System Tumor Malignancy. *Cancer research*, *65*(20), 9355-6362. Doi: 10.1158/0008-5472.CAN-05-1946

Medeiros, G. F., Mendes, A., Castro, R. A.B., Baú, E. C., Nader, H. B. & Dietrich, C. P. (2000). Distribution of sulfated glycosaminoglycans in the animal kingdom: widespread occurrence of heparin-like compounds in invertebrates. *Biochimica et Biophysica Acta (BBA) – General subjects*, *1475*(3), 287-294. Doi: 10.1016/S0304-4165(00)00079-9

Mahmoud, A. M., Wilkinson, F. L., Jones, A. M., Wilkinson, J. A., Romero, M., Duarte, J. & Alexander, M. Y. (2017). A novel role for small molecule glycomimetics in the protection against lipid-induced endothelial dysfunction: Involvement of Akt/eNOS and Nrf2/ARE signaling. *Biochemica et Biophysica Acta (BBA) – General subjects*, *1861*, 1(A), 3311-3322. Doi: 10.1016/j.bbagen.2016.08.013

Morla, S. (2019). Glycosaminoglycans and glycosaminoglycan mimetics in cancer and inflammation. *International journal of molecular sciences, 20*(8), 1963. Doi: 10.3390/ijms20081963

Moxon-Emre, I., Bouffet, E., Taylor, M. D., Laperriere, N., Scantlebury, N., Law, N., … Mabbott, D. (2014). *Impact of Craniospinal Dose, Boost Volume, and Neurologic Complications on Intellectual Outcome in Patients With Medulloblastoma. Journal of Clinical Oncology, 32(17), 1760–1768.* doi:10.1200/jco.2013.52.3290

Mueller, S. & Chang, S. (2009). Pediatric brain tumors: Current treatment strategies and future therapeutic approaches. *Neurotherapeutics*, *6*, 570-586. Doi: 10.1016/j.nurt.2009.04.006

Mulloy, B., Gray, E. & Barrowcliffe, T. W. (2000). Characterization of unfractioned heparin: comparison of materials from the last 50 years. *Thrombosis and haemostasis*, *84*(12), 1052-1056. Doi: 10.1055/s-0037-1614170

Naggar, E. F., Costello, C. E. & Zaia, J. (2004). Competing Fragmentation Processes in Tandem Mass Spectra of Heparin-Like Glycosaminoglycans. *Journal of the American society for mass spectrometry*, *15*, 1534-1544. Doi: 10.1016/j.jasms.2004.06.019

Nakamura, T., Nawa, K. & Ichihara, A. (1984). Partial purification and characterization of hepatocyte growth factor from serum of hepatectomized rats. *Biochemical and biophysical research communications, 122*(3), 1450-1459. Doi: 10.1016/0006-291x(84)91253-1

Nguyen, P. T., Sharma, R., Rej, R., Carful, C. A De., Roy, R. & Bourgault, S. (2016). Low generation anionic dendrimers modulate islet amyloid polypeptide self-assembly and inhibit pancreatic β-cell toxicity. *RSC Advances*, 6, 76360-76369. Doi: 10.1039/C6RA15373A

Olayioye, M. A., Neve, R. M., Lane, H. A. & Hynes, N. E. (2000). The ErbB signaling network: receptor heterodimerization in development and cancer. *The EMBO journal, 19*(13), 3159-3167. Doi: 10.1093/emboj/19.13.3159

Organ, S. L. & Tsao, MS. (2011). An overview of the c-Met signalling pathway. *Therapeutic advances in medical oncology,* S7-19. Doi: 10.1177/1758834011422556

Packer, R. J., Gajjar, A., Vezina, G., Rorke-Adams, L., Burger, P. C., Robertson, P. L., … Sposto, R. (2006). Phase III Study of Craniospinal Radiation Therapy Followed by Adjuvant Chemotherapy for Newly Diagnosed Average-Risk Medulloblastoma. *Journal of clinical oncology*, *24*(25), 4202-4208. Doi: 10.1200/JCO.2006.06.4980

Page, C. (2013). Heparin and related drugs: beyond anticoagulant activity. *ISRN Pharmacology*, *2013*(6). Doi: 10.1155/2013/910743

Pearce, D. A., Jotterand, N., Carrico, I. S. & Imperiali, B. (2001). Derivatives of 8-Hydroxy-2-methylquinoline are powerful prototypes for zinc sensors in biological systems. *Journal of the American Chemical Society*, *123*(51), 5160-5161. Doi: 10.1021/ja0039839

Provençal, M., Labbé, D., Veitch, R., Boivin, D., Rivard, G, Sartelet, H. … Béliveau, R. (2009). C-Met activation in medulloblastoma induces tissue factor expression and activity: effects on cell migration. *Carcinogenesis*, *30*(7), 1089-1096. Doi: 10.1093/carcin/bgp085

Puccini, A., Marín-Ramos, N. I., Bergamo, F., Schirripa, M., Lonardi, S., Lenz, H., … Battaglin, F. (2019). Safety and tolerability of c-MET inhibitors in cancer. *Drug safety*, *42*, 211-233. Doi: 10.1007/s40264-018-0780-x

Purba, E. R., Saita, E. & Marayuma, I. N. (2017). Activation of the EGF receptor by ligand binding and oncogenic mutations: The "Rotation model". *Cells, 6*(2), 13. Doi: 10.3390/cells6020013

Ragahuraman, A., Riaz, M., Hindle, M. & Desai, U. R. (2007). Rapid and efficient microwave-assisted synthesis of highly sulfated organic scaffolds. *Tetrahedron Letters*, *48*(38), 6754-6758. Doi: 10.1016/j.tetlet.2007.07.100

Raiber, E., Wilkinson, J. A., Manetti, F., Botta, M., Deakin, J., Gallagher, J., … Ducki, S. W. (2007). Novel heparin/heparin sulfate mimics as inhibitors of HGF/SF-induced MET activation. *Bioinorganic & medicinal chemical letters*, *17*(22), 6321-6325. Doi: 10.1016/j.bmcl.2007.08.074

Ritelli, M., Cinquina, V., Giacopuzzi, E., Venturini, M., Chiarelli, N. & Colombi, M. (2019). Further Defining the Phenotypic Spectrum of B3GAT3 Mutations and Literature Review on Linkeropathy Syndromes. *Genes*, *10*(9), 631. Doi: 10.3390/genes10090631

Rong, S., Segal, S., Anver, M., Resau, J. H. & Denver, G. F. V. (1994). Invasiveness and metastasis of NIH 3T3 cells induced by Met-hepatocyte growth factor/scatter factor autocrine stimulation. *Proceedings of the national academy of sciences of the United States of America, 91*(11), 4731-4735. Doi: 10.1073/pnas.91.11.4731

Sarrazin, S., Lamanna, W. C. & Esko, J. D. (2011). Heparan sulfate proteoglycans. *Cold Spring Harbour Perspectives in Biology*. *3*(7), a004952. Doi: 10.1101/cshperspect.a004952

Sierra, J. R. & Tsao, M. (2011). c-MET as a potential therapetutic target and biomarker in cancer. *Therapeutical advances in medical oncology*, *3*(supp1), S21-35. Doi: 10.1177/1758834011422557

Spina, R., Filocamo, G., Iaccino, E., Scicchitano, S., Lupia, M., Chiarella, E. … Morrone, G. (2013). Critical role of zinc finger protein 521 in the control of growth, clonogenicity and tumorigenic potential of medulloblastoma cells. *Oncotarget*, *4*(8), 1280-1292. Doi: 10.18632.oncotarget.1176

Stankevichene, L. M. M., Vizas, V. K., Kost, A. N., Stankevichyus, A. P. & Smailene, R. A. S. (1977). Guanidine analogues of B-adrenergic blockers. I. Synthesis and investigation of aryloxypropanolylguanidines. *Pharmaceutical chemistry journal. 11*, 69-73. Doi: 10.1007/BF00779124.

Strätz, J., Liedmann, A., Heinze, T., Fischer, S. & Groth, T. (2019). Effect of sulfation route and subsequent oxidation on derivatization degree and biocompatibility of cellulose sulfates. *Marcomolecular Bioscience*, *20*(2), 1900413. Doi: 10.1002/mabi.201900403

Sugahara, K. & Kitagawa, H. (2002). Heparin and heparan sulfate biosynthesis. *International union of biochemistry and molecular biology*, *54*(4), 163-175. Doi: 10.1080/15216540214928

Sugahara, K. & Kitagawa, H. (2020). Recent advances in the study and biosynthesis and functions of sulfated glycosaminoglycans. *Current opinion in structural biology*, *10*(5), 518-527. Doi: 10.1016/S0959-440X(00)00125-1

Sun, Y., Wang, Y., Liu, L., Liu, B., Zhang, Q., Wu, D. … Yan, X. (2020). Towards the understanding of acetonitrile suppressing salt precipitation mechanism in a water-in-salt electrolyte for low-temperature supercapacitors. *Journal of Materials chemistry A*, *8*, 17998-18006. Doi: 10.1039/D0TA04538A

Taylor, M. D., Northcott, P. A., Korshunov, A., Remke, M., Cho, Y., Clifford, S. C. … Pfister, S. M. (2012). Molecular subgroups of medulloblastoma: the current consensus. *Acta Neuropathologica*, *123*, 465-472. Doi: 10.1007/s00401-011-0922-z

The Medical Biochemistry Page. (2020). Glycosaminoglycans and Proteoglycans. Retrieved from http://themedicalbiochemistrypage.org/glycosaminoglycans-and-proteoglycans/

Tong, M., Tuk, B., Hekking, I. M., Vermeij, M., Barritault, D., van Neck, J. W. (2009). Stimulated neovascularization, inflammation resolution and collagen maturation in healing rat cutaneous wounds by a heparan sulfate glycosaminoglycan mimetic, OTR4120. *Wound repair and regeneration*, *17*(6), 840-852. Doi: 10.1111/j.1524-475X.2009.00548.x

Tully, S. E., Mabon, R., Gama, C. I., Tsai, S. M., Liu, X. & Hsieh-Wilson, L. C. (2004). A chondroitin sulfate small molecule that stimulates nerve growth. *Journal of the American Chemical Society*, *126*, 7736-7737. Doi: 10.1021/ja0484045

Umrigar, V. M., Chakraborty, M & Parikh, P. A. (2007). Microwave assisted sulfonation of 2-napthol by sulfuric acid: cleaner production of schaeffer's acid. *Industrial & engineering chemical research. 46*(19), 6217-6220. Doi: 10.1021/ie0705352

Waller, C. C. & McLeod, M. D. (2014). A simple method for the small scale synthesis and solid-phase extraction of steroid sulfates. *Steroids*, *92*, 74-80. Doi: 10.1016/j.steroids.2014.09.006

Wen, J., Xiao, J., Rahdar, M., Choudhury, B. P., Cui, J., Taylor, G. S. … Dixon, J. E. (2014). Xylose phosphorylation functions as a molecular switch to regulate proteoglycan biosynthesis. *Proceedings of the national academy of sciences of the United States of America*, *111*(44), 15723-15728. Doi: 10.1073/pnas.1417993111

Wielenga, V. J. M., Voort, R. vd., Taher, T. E. I., Smit, L., Beuling, E. A., Krimpen, C. v. … Pals, S. T. (2000). Expression of c-Met and Heparan sulfate proteoglycan forms of CD44 in colorectal cancer. *American journal of pathology*, *157*(5), 1563-1573. Doi: 10.1016/S0002-9440(10)64793-1

Wingfield, P. T. (2001). Protein precipitation using ammonium sulfate. *Current protocols in protein science*. *13*(1), A.3F.1-A.3F.8. Doi: 10.1002/0471140864.psa03fs13

Xu, P., Laval, S., Guo, Z. & Yu, B. (2015). Microwave-assisted simultaneous O,N-sulfonation in the synthesis of heparin-like ogliosaccharides. *Organic chemistry frontiers*, *3*, 103-109. Doi: 10.1039/C5QO00320B

Yuan, H., Liu, Q., Zhang, L., Hu, S., Chen, T., Li, H., … Lu, T. (2018). Discovery, optimisation and biological evaluation for novel c-met kinase inhibitors. *European journal of medicinal chemistry*, *143*, 491-502. Doi: 10.1016/j.ejmech.2017.11.073

Zaia, J. & Costello, C. E. (2003). Tandem Mass Spectrometry of Sulfated Heparin-Like Glycosaminoglycan Oligosaccharides. *Analytical Chemistry*, *75*(10), 2445-2455. Doi: 10.1021/ac0263418

Zhang, Y., Xia, M., Jin, K., Wang, S., Wei, H., Fan, C., … Xiong, W. (2018). Function of the c-Met receptor tyrosine kinase in carcinogenesis and associated therapeutic opportunities. *Molecular cancer*, *17*(45). Doi: 10.1186/s12943-018-0796-y